A SIMULTANEOUS SOLUTION APPROACH FOR COUPLED SURFACE AND SUBSURFACE FLOW MODELING

by

Orhan Gunduz and Mustafa M. Aral

Multimedia Environmental Simulations Laboratory

School of Civil and Environmental Engineering
Georgia Institute of Technology
Atlanta, GA 30332

MESL-02-03 **April 2003**

A SIMULTANEOUS SOLUTION APPROACH FOR COUPLED SURFACE AND SUBSURFACE FLOW MODELING

by

Orhan Gunduz and Mustafa M. Aral

Multimedia Environmental Simulations Laboratory

School of Civil and Environmental Engineering
Georgia Institute of Technology
Atlanta, GA 30332

The work on which this report is based was supported by the School of Civil and Environmental Engineering, Georgia Institute of Technology, and by the Georgia Sea Grant, National Sea Grant College Program. The project was administered through the Multimedia Environmental Simulations Laboratory of the School of Civil and Environmental Engineering, Georgia Institute of Technology.

MESL-02-03 **April 2003**

Authors

Mr. Orhan Gunduz is a graduate student in the Multimedia Environmental Simulations Laboratory, School of Civil and Environmental Engineering, Georgia Institute of Technology.
Dr. Mustafa M. Aral is a Professor and the Director of Multimedia Environmental Simulations Laboratory in the School of Civil and Environmental Engineering, Georgia Institute of Technology.

Acknowledgements

This report is based on the work conducted in the Multimedia Environmental Simulations Laboratory at the School of Civil and Environmental Engineering, Georgia Institute of Technology. Partial financial support for this work was provided by the Georgia Sea Grant of the National Sea Grant College Program and the Georgia Institute of Technology. Authors are grateful for the continued support of the two institutions in the area of environmental modeling studies. Computational services of this work were provided by the Multimedia Environmental Simulations Laboratory facilities.

Orhan Gunduz and Mustafa M. Aral

A simultaneous solution approach for coupled surface and subsurface flow modeling
Report No.: MESL-02-03; Project No.: E-20-G09; April 2003, 90p.

Keywords – Coupled hydrologic model, simultaneous solution, dynamic wave channel flow, vertically-averaged groundwater flow

Table of Contents

List of Figures

List of Tables

Notation

The following symbols are used in this report:

a	:	Location of sampling point in Gaussian quadrature (-)
A	:	Active cross-sectional area of channel flow (L^2)
A_o	:	Inactive cross-sectional area (off-channel storage) (L^2)
B	:	Active cross-sectional top width (L)
B_o	:	Inactive cross-sectional top width (L)
c_1	:	Unit system dependent constant in Manning's equation (-)
E	:	Dummy parameter (-)
f	:	Function (-)
g	:	Gravitational acceleration (LT^{-2})
g_x	:	The x-coordinate of the parametric equation defining the river in domain (-)
g_y	:	The y-coordinate of the parametric equation defining the river in domain (-)
h_d	:	Downstream boundary condition water surface elevation (L)
h_g	:	Groundwater hydraulic head above a datum (L)
h_{g0}	:	Initial groundwater head (L)
$\hat{h}_g$	:	Approximate groundwater hydraulic head above a datum (L)
$\left(\hat{h}_g\right)_{avg}$	:	Element average approximate groundwater head above a datum (L)
h_r	:	Channel flow water surface elevation (stage) above a datum (L)
h_{r0}	:	Initial water surface elevation in channel (L)
h_T	:	Total headloss in a junction (L)
h_u	:	Upstream boundary condition water surface elevation (L)
H_D	:	Specified head boundary condition value (L)
I	:	Infiltration rate (LT^{-1})

K : Channel conveyance (L^3T^{-1})

K_{ec} : Contraction/expansion coefficient (-)

K_r : Hydraulic conductivity of channel bottom sediment (LT^{-1})

K_x : Hydraulic conductivity in longitudinal direction (LT^{-1})

K_y : Hydraulic conductivity in transverse direction (LT^{-1})

L : Momentum flux due to lateral seepage inflow/outflow (L^3T^{-2})

L_d : Total channel flow domain length (L)

m_r : Channel bed thickness (L)

n_c : Manning's roughness coefficient in channel ($L^{-1/3}T$)

n_w : Number of wells (-)

N : Total number of nodes in the entire channel network or in groundwater flow domain (-)

N_i : i^{th} weighing function (-)

N_j : j^{th} shape function (-)

N_k : Number of nodes in channel k (-)

q_L : Lateral inflow/outflow per channel length (L^2T^{-1})

q_C : Head-dependent boundary condition flux value (L^2T^{-1})

q_N : Specified flux boundary condition value (L^2T^{-1})

Q : Channel discharge (L^3T^{-1})

Q_0 : Initial channel discharge (L^3T^{-1})

Q_d : Downstream boundary condition discharge (L^3T^{-1})

Q_u : Upstream boundary condition discharge (L^3T^{-1})

Q_w : Well discharge (LT^{-1})

R : Residual in the Galerkin method (-)

R_h : Hydraulic radius (L)

s : Scale parameter in underrelaxation coefficient (-)

s_c : Sinuosity factor for continuity equation (-)

s_m : Sinuosity factor for momentum equation (-)

S_e : Contraction/expansion slope (-)

S_f : Channel/floodplain boundary friction slope (-)

S_y : Specific yield of unconfined aquifer (-)

t : Time coordinate (T) and parameter (-)

V : Flow velocity (LT^{-1})

w : Weighing constant in Gaussian quadrature (-)

w_r : Wetted perimeter of channel bed (L)

x : Global longitudinal coordinate (L)

y : Global transverse coordinate (L)

z_b : Top elevation of bottom impervious layer above a datum (L)

z_r : Bottom elevation of channel bed above a datum (L)

α : Time weighing parameter in Galerkin method (-)

α_c : A weighing parameter in Newton-Raphson method used to evaluate the first estimate of the unknown variables (-)

β : Momentum correction coefficient for non-uniform velocity distribution (-)

δ : Dirac delta function (argument^{-1})

γ : Iteration-dependent underrelaxation coefficient (-)

ε : Maximum change in hydraulic head for all nodes between two iterations (L)

η : Local transverse coordinate (L)

θ : Weighing factor for space derivative in the four-point scheme (-)

ξ : Local longitudinal coordinate (L)

Γ : Global groundwater flow domain boundary (L)

Γ_1 : Specified head boundary in groundwater flow model (L)

Γ_2 : Specified flux boundary in groundwater flow model (L)

Γ_3 : Head-dependent boundary in groundwater flow model (L)

ψ : Weighing factor for time derivative in the four-point scheme (-)

Ω : Global groundwater flow domain (L^2)

Ω_e : Local groundwater flow domain (L^2)

A : Global coefficient matrix

B : Global load vector

f : Vector of arbitrary functions

$\mathbf{F}$	:	Load vector
$\hat{\mathbf{h}}_{\mathbf{g}}$	:	Global approximate hydraulic head vector
$\mathbf{J}$	:	Jacobian matrix in Newton-Raphson scheme
$\mathbf{M}$	:	Mass matrix
$\mathbf{n}$	:	Unit normal vector to the boundary
$\mathbf{S}$	:	Stiffness matrix
$\mathbf{x}$	:	Vector of unknown variables

i, j, k, l, m, o	:	Indices

A Simultaneous Solution Approach for Coupled Surface and Subsurface Flow Modeling

Orhan Gunduz and Mustafa M. Aral
Multimedia Environmental Simulations Laboratory
School of Civil and Environmental Engineering
Georgia Institute of Technology
Atlanta, GA 30332

Abstract

Coupled hydrologic modeling of surface and subsurface systems has gained a lot of popularity in the last two decades. Channel flow and groundwater flow models are coupled to obtain a better understanding of these hydrologic pathways in a watershed. In general, this coupling process is done in an iterative fashion until sufficient convergence is achieved for common parameters linking these different domains. In this study, we propose a new solution methodology based on the simultaneous solution of channel and groundwater flow. The method is based on the idea of solving a single global matrix at once rather than solving separate matrices for each flow domain and iteratively improving the solution. This new solution technique is tested by coupling a one-dimensional stream flow model that uses the complete form of the St. Venant equation with a two-dimensional vertically-averaged groundwater flow model. The proposed simultaneous solution approach provides a more efficient solution for this coupled flow problem and is superior to the approximate solution obtained through an iterative approach.

1. Introduction

The movement of water in the hydrologic cycle is a complex phenomenon because of numerous flow pathways and interactions between these pathways. Discrete modeling of these surface and subsurface pathways has been studied extensively and various models of different complexities have been formulated in the past (McDonald and Harbaugh, 1988; Aral, 1990; Fread, 1993). In all of these studies, there is limited or no interaction between different pathways. Even though these models provide good results in simulating the hydrology of their domains, they start to show deviations from observed data when these interactions become considerably important.

This restricted and isolated nature of these models motivated researchers to focus on coupled models. Pinder and Sauer (1971), Smith and Woolhiser (1971) and Freeze (1972) were among the earliest to work with coupled models. More recently, Cunningham and Sinclair (1979), Akan and Yen (1981a), Swain and Wexler (1991), VanderKwaak and

Loague (2001) and Morita and Yen (2002) have all formulated coupled models of various complexities to simulate the interactions of surface and subsurface systems. The level of complexity is generally determined by the number of dimensions included in the model as well as the inclusion of all possible physical phenomena. In this regard, the most advanced model would involve a three-dimensional surface flow component based on the complete Navier-Stokes equations and a three-dimensional variably saturated subsurface flow component. Currently, no such model exists in the hydrologic literature due to the inevitable drawbacks of (i) insufficient computational power (i.e., storage capacity and processing speed); and, (ii) insufficient calibration and verification data.

Because of these limitations, it is still very tempting for the hydrologic modeler to use approximate models over large scale applications. In this research area, the works of Vanderkwaak and Loague (2001) and Morita and Yen (2002) both include a three-dimensional variably saturated subsurface flow component and two-dimensional non-inertia wave surface flow component. It must be noted that even with this fairly complex approximate formulation, these models can only be operated on test or small scale applications. In order to perform practical simulations of larger scale domains, it is necessary to make further simplifications in the formulation of the physical system. One such approximate formulation of coupled surface/subsurface flows involves the use of a one-dimensional approach for the surface flow in streams and rivers and a two-dimensional vertically averaged approach for the subsurface flow in the saturated zone.

Regardless of the level of complexity, the coupling process in all models is based on the idea of solving for the common parameters linking the surface and subsurface components. This solution can be done in an iterative or non-iterative fashion. The non-iterative technique involves a one-time solution of surface and subsurface flow equations and is also known as “external” coupling. On the other hand, the iterative technique involves numerous solutions of both surface and subsurface equations until the outcome of subsequent solutions become less than a tolerance criterion. Iterative coupling is sometimes known as “internal” coupling. Because of the fact that iterative coupling algorithms involve numerous solutions of surface and subsurface flow equations within a time step, they require more computational time as opposed to external coupling algorithms. On the other hand, this iterative improvement of the solution generally provides more accurate results and thus it is generally proved to be superior over external coupling.

In this study, a new solution technique is proposed for the coupled solution of surface and subsurface flows. In this approach, the surface and subsurface flow equations are solved simultaneously within the same global matrix structure and, hence, this new method is called the “simultaneous solution” approach to differentiate it from internal and external coupling methods. Since this new approach eliminates the need for iterative solution of the governing equations, it is comparably faster than the iterative coupling algorithm. Furthermore, as there is no necessity to check for the convergence of an iterative solution, and thus it yields a more accurate solution than iterative coupling approach. To test the applicability of this approach, a one-dimensional stream flow model based on the dynamic wave form of the St Venant equations is coupled with a two-dimensional vertically

averaged saturated groundwater flow model to simulate surface/subsurface interactions along the river bed.

The mathematical background of the coupled model is given in the second section of this report where the governing partial differential equations of the channel flow and saturated groundwater flow models are presented together with the accompanying initial and boundary conditions. In the third section, the numerical solution methodology for the coupled model is presented where spatial and temporal discretization of the equations is given and the simultaneous solution methodology is explained. The new approach is first applied to two hypothetical domains to test its capabilities and limitations and finally to a watershed in southern Georgia for real-time modeling.

2. Mathematical Model

The coupled model is a combination of a one-dimensional channel flow model and a two-dimensional groundwater flow model (Figure 1). The channel flow model is based on the dynamic wave form of the St. Venant equations and the groundwater flow model is based on the vertically-averaged mass conservation equation of groundwater flow. The link between the two models is provided via the lateral flow term at the river-bottom interface using the relative values of the river water surface elevation and the groundwater head.

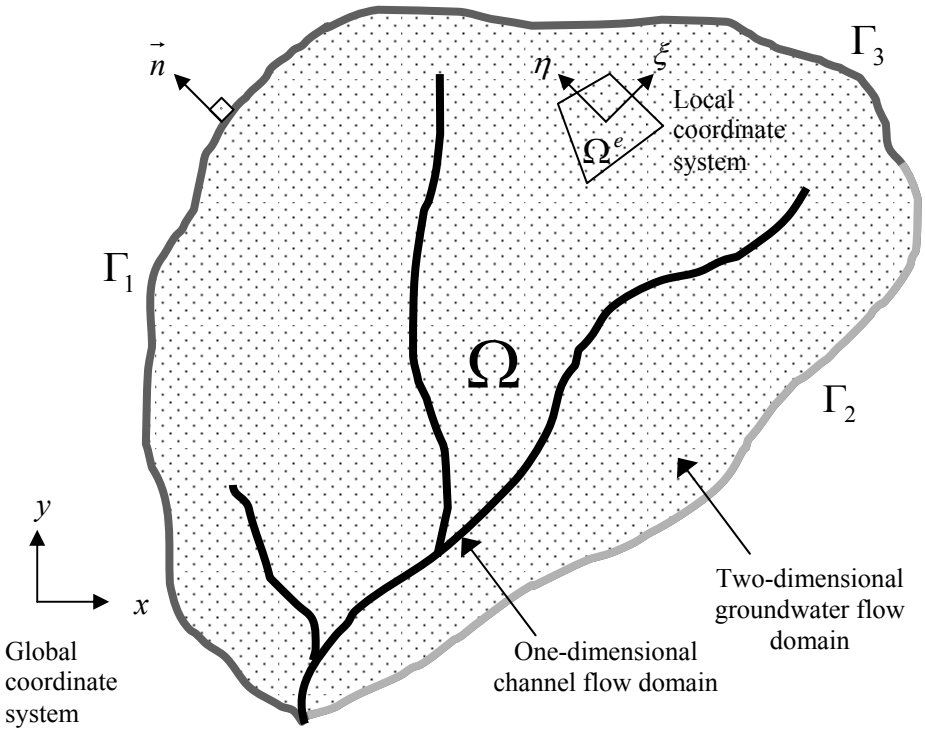

Figure 1. Coupled modeling domain

2.1. Channel Flow Model

2.1.1. Governing Equations

The governing equations of the one-dimensional channel flow model are given by the continuity and momentum equations modified to include the effects of natural channel geometry and characteristics. The momentum equation is based on the complete dynamic wave form of the unsteady non-uniform St. Venant equations (Fread, 1993):

$$\frac{\partial s_c (A + A_o)}{\partial t} + \frac{\partial Q}{\partial x} - q_L = 0 \tag{1}$$

$$\frac{\partial s_m Q}{\partial t} + \frac{\partial (\beta Q^2 / A)}{\partial x} + gA\left(\frac{\partial h_r}{\partial x} + S_f + S_e \right) + L = 0 \tag{2}$$

where s_c and s_m are sinuosity factors for continuity and momentum equations, A is the active cross-sectional area of flow, A_o is the inactive (off-channel storage) cross-sectional area, Q is the discharge, t is the time, x is the longitudinal distance along the channel/flood plain, q_L is the lateral flow per channel length that provides the link with the groundwater flow model (positive for inflow and negative for outflow), β is the momentum coefficient for velocity distribution, g is the gravitational acceleration, h_r is the water surface elevation in the stream (i.e., stage), L is the momentum flux due to lateral seepage inflow/outflow, S_f and S_e are channel/flood plain boundary friction slope and contraction/expansion slope, respectively. The momentum flux due to seepage inflow/outflow, channel/flood plain boundary friction slope and contraction/expansion slope are evaluated as:

$$L = \begin{cases} 0 & \text{for inflow} \\ -\dfrac{Q q_L}{2A} & \text{for outflow} \end{cases} \tag{3}$$

$$S_e = \frac{K_{ec} \Delta (Q / A)^2}{2g\Delta x} \tag{4}$$

$$S_f = \frac{n_c^2 |Q| Q}{c_1^{\,2} A^2 R_h^{\,4/3}} = \frac{|Q| Q}{K^2} \tag{5}$$

where K_{ec} is the expansion/contraction coefficient, Δx is the reach length, c_1 is the unit system dependent constant, n_c is the Manning's roughness coefficient, K is the flow conveyance factor and R_h is the hydraulic radius. The hydraulic radius is defined as the

ratio of cross-section area to wetted perimeter but can be approximated as the ratio of cross-section area to top width for large rivers. It is important to note that the momentum influx due to seepage inflow is assumed to be negligible and is not considered in the model. The lateral flow that provides the link between the channel flow model and the groundwater flow model is defined as:

$$q_L = \begin{cases} -K_r w_r \dfrac{h_r - h_g}{m_r} & h_g > (z_r - m_r) \\ -K_r w_r \dfrac{h_r - (z_r - m_r)}{m_r} & h_g \le (z_r - m_r) \end{cases} \tag{6}$$

where K_r is the river bottom sediment conductivity, m_r is the river bed thickness, z_r is the river bottom elevation and w_r is the wetted perimeter of the river bed as shown in Figure 2. It can be seen from the expression given in Equation (6) that lateral flow is a function of water surface elevation and groundwater head, and provides the coupling mechanism between the surface and subsurface flow systems. The coupling term is explicitly embedded in the governing equation for the channel flow model.

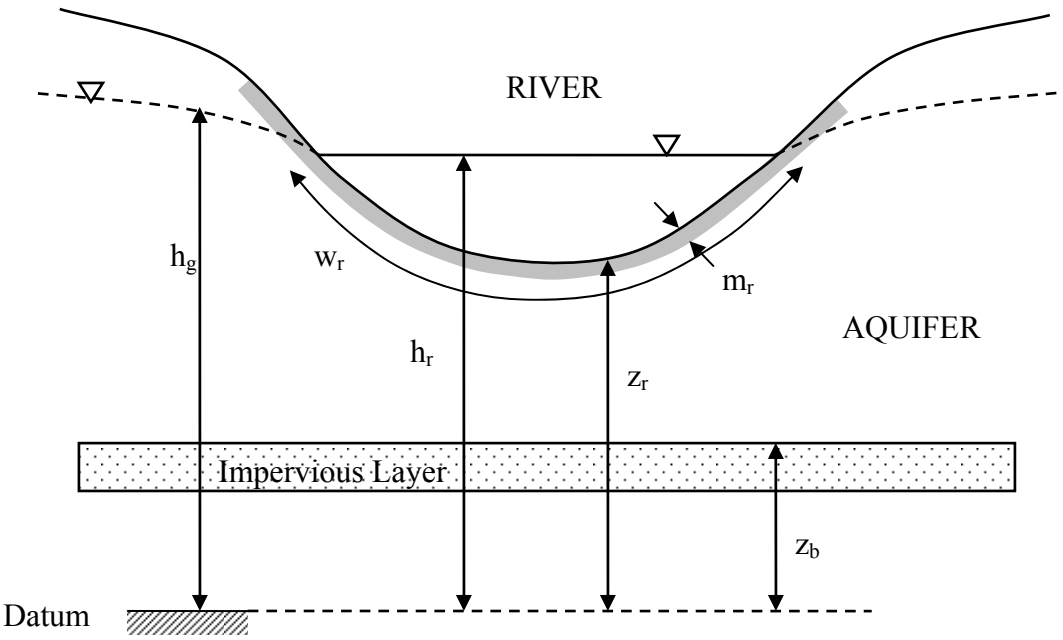

Figure 2. Channel flow / groundwater flow interaction (Gunduz and Aral, 2003)

2.1.2. Initial Conditions

In order to start the transient solution, initial values of the model unknowns (i.e., discharge and water surface elevation) are to be specified along the one-dimensional stream domain. The initial conditions can be obtained from: (i) field data; (ii) a previous unsteady model solution; or, (iii) solution of steady, non-uniform flow equation. In any case, the initial conditions are given as:

$$Q(x,0) = Q_0(x) \tag{7}$$

$$h_r(x,0) = h_{r0}(x) \tag{8}$$

where Q_0 and h_{r0} represent the discharge and water surface elevation in the channel at the beginning of the simulation, respectively.

2.1.3. Boundary Conditions

In the one-dimensional channel flow model, there are two different types of boundary conditions specified at (i) external; and, (ii) internal boundaries of the domain. The external boundary conditions are given at the most upstream and downstream points of the channel network where as the internal boundary conditions are specified at internal junction points of the channel network.

2.1.3.1. External Boundary Conditions

The proposed model is capable of modeling a network of river channels. The network is generally composed of several upstream and internal channels and a single downstream channel. Therefore, the model can accommodate several upstream boundary conditions and a single downstream boundary condition. At any upstream boundary, a discharge or a stage hydrograph can be used as the boundary condition. These conditions are expressed as discharge and stage time series and are given as:

$$Q(0,t) = Q_u(t) \tag{9}$$

$$h_r(0,t) = h_u(t) \tag{10}$$

where Q_u and h_u represent upstream boundary discharge and water surface elevation values, respectively. Similarly, the boundary condition at the downstream boundary can also be defined as a discharge or a stage hydrograph and specified as:

$$Q(L_d,t) = Q_d(t) \tag{11}$$

$$h_r(L_d, t) = h_d(t) \tag{12}$$

where Q_d and h_d represent downstream boundary discharge and water surface elevation values, and L_d is the total domain length. Moreover, it is also possible to define the downstream boundary condition as a single-valued rating curve, a looped rating curve or a critical depth section. The single-valued rating curve maps a particular stage value to a corresponding discharge value and can be expressed by using linear interpolation within a table of stage-discharge data:

$$Q(L_d, t) = Q^k + \frac{Q^{k+1} - Q^k}{h_r^{k+1} - h_r^k}\left(h_d - h^k\right) \tag{13}$$

where Q^k, Q^{k+1}, h^k and h^{k+1} are consecutive tabular data sets of the rating curve and h_d is the stage at the downstream boundary. A looped rating curve, on the other hand, maps a stage value to several possible discharge values depending on the hydraulic conditions of the channel and can be expressed using the Manning's equation:

$$Q(L_d, t) = \frac{c_1}{n_c} A R_h^{2/3} S_f^{1/2} \tag{14}$$

where S_f is given by the modified momentum equation as:

$$S_f = -\frac{1}{gA}\frac{\partial Q}{\partial t} - \frac{1}{gA}\frac{\partial (Q^2 / A)}{\partial x} - \frac{\partial h_r}{\partial x} \tag{15}$$

Finally, it is also possible to use a critical depth section as the downstream boundary condition when the most downstream point of the modeling domain is a controlled structure such as a weir. In this particular case, the critical depth is mapped to the critical discharge via the following equation:

$$Q(L_d, t) = \sqrt{\frac{g}{B}} A^{3/2} \tag{16}$$

where B is the cross-sectional top width of the channel.

2.1.3.2. Internal Boundary Conditions

Any two or more channels intersecting within a channel network forms a junction where internal boundary conditions are specified to satisfy the mass and energy balance. The proposed model does not allow for looped networks and require that there is always a single outflow channel from a junction. The mass balance equation at a junction can be specified as:

$$\sum_{k=1}^{m} Q_k - Q_o = \frac{dS}{dt} \tag{17}$$

where m is the total number of inflowing channels to the junction, Q_k is the discharge at the end of the k^{th} inflowing channel to the junction, Q_o represents the discharge at the beginning of the outflowing channel from the junction, and dS/dt corresponds to the change in storage within the junction. For many modeling applications, it is a common practice to assume that the change in storage within a junction is negligible compared to the change in storage within in a channel (Akan and Yen, 1981b; Fread, 1993; Jha et al., 2000). Consequently, the mass balance equation reduces to a simple continuity equation. On the other hand, the energy equation is written as:

$$(h_r)_k + \frac{V_k^2}{2g} = (h_r)_o + \frac{V_o^2}{2g} + h_T \qquad k = 1,2,\ldots,m \tag{18}$$

where $(h_r)_k$ and V_k are the stage and flow velocity at the end of the k^{th} inflowing channel to the junction, $(h_r)_o$ and V_o are the stage and flow velocity at the beginning of the outflowing channel from the junction and h_T is the total headloss in the junction. When all the flows in all the branches joining a junction are subcritical and the head lost in the junction is negligible, the equation simplifies to:

$$(h_r)_k = (h_r)_o \qquad k = 1,2,\ldots,m \tag{19}$$

2.2. Groundwater Flow Model

2.2.1. Governing Equations

The governing equation of two-dimensional groundwater flow in an anisotropic, non-homogeneous unconfined aquifer with principle permeability directions not matching the coordinate directions is given by:

$$\frac{\partial}{\partial x}\left[\left(h_g - z_b\right)K_{xx}\frac{\partial h_g}{\partial x} + \left(h_g - z_b\right)K_{xy}\frac{\partial h_g}{\partial y}\right] + \frac{\partial}{\partial y}\left[\left(h_g - z_b\right)K_{yx}\frac{\partial h_g}{\partial x} + \left(h_g - z_b\right)K_{yy}\frac{\partial h_g}{\partial y}\right] + \sum_{k=1}^{n_w}\left[Q_{w_k}(x,y,t)\delta(x - x_k)\delta(y - y_k)\right] + \sum_{m=1}^{n_r}\left[\int_0^1 q_{Lm}(x,y,t)\sqrt{\left(\frac{dg_{xm}}{dt}\right)^2 + \left(\frac{dg_{ym}}{dt}\right)^2}\,\delta\left(x - g_{xm}(t)\right)\delta\left(y - g_{ym}(t)\right)dt\right] + I = S_y\frac{\partial h_g}{\partial t} \tag{20}$$

where h_g is the vertically averaged hydraulic head, z_b is the top elevation of bottom impervious layer, K_{xx}, K_{xy}, K_{xy} and K_{yy} are anisotropic saturated hydraulic conductivities, Q_w is the flow rate of the kth well located at point (x_k, y_k) in the domain (i.e., positive for an injecting well and negative for a discharging well), n_w is the number of wells in the domain, δ is the Dirac delta function, q_L is the lateral flow at the river-bottom interface defined by Equation (6) (i.e., positive for lateral inflow and negative for lateral outflow), g_x and g_y are the Cartesian coordinate components of the parametric equation of the mth river in the domain, n_r is the number of rivers in the domain, t is the parameter, I is the infiltration rate and S_y is the specific yield of the aquifer.

2.2.2. Initial Conditions

The initial values of the hydraulic head, h_{go}, are specified as the initial conditions of the groundwater flow model:

$$h_g(x,y,0) = h_{g0}(x,y) \tag{21}$$

2.2.3. Boundary Conditions

Three different types of boundary conditions can be specified along different external boundaries of the groundwater flow domain. Type-1 or specified head boundary conditions are used to model boundaries with known hydraulic head values. It is also known as a Dirichlet boundary condition and is given as:

$$h_g(x,y,t) = H_D(x,y) \tag{22}$$

where H_D is the known hydraulic head value. Type-2 or specified flux boundary conditions are used to model boundaries with known flux values. It is also known as a Neumann boundary condition and is given as:

$$q_N = -\mathbf{n}\cdot\left(\left(h_g - z_b\right)\mathbf{K}\cdot\nabla h_g\right) \tag{23}$$

where q_N is the known flux value and **n** is the unit normal to the boundary. Finally, type-3 or head-dependent boundary conditions are used to model boundaries on which the conditions depend on the changing hydraulic head such as streams and rivers at the external boundaries of the domain. It is also known as a Cauchy boundary condition and is given as:

$$q_C = -\mathbf{n} \cdot \left(\left(h_g - z_b \right) \mathbf{K} \cdot \nabla h_g \right) = q_L = \begin{cases} -K_r w_r \dfrac{h_r - h_g}{m_r} & h_g > \left(z_r - m_r \right) \\ -K_r w_r \dfrac{h_r - \left(z_r - m_r \right)}{m_r} & h_g \le \left(z_r - m_r \right) \end{cases} \tag{24}$$

where q_C is the head-dependent flux value that is also equal to the lateral flow between the two systems. It must be noted, however, that the lateral flow is no longer a head-dependent flux when the second condition applies in Equation (24) since (z_r - m_r) term becomes constant when the hydraulic head falls below the bottom elevation of river sediments. In this particular case, the head-dependent flux is treated as a constant flux condition. The coupling term is now implicitly embedded in the boundary condition term for the groundwater flow model.

2.3. Coupling of Models

The coupling of the channel flow and groundwater flow models is provided via lateral inflow/outflow. The lateral inflow/outflow term appears as a source/sink term both in the channel flow model and in the groundwater flow model. In its current state, the coupled model does not allow any other lateral inflow/outflow to the channel flow model such as overland flow, precipitation and evaporation. Therefore, the following coupling mechanism is assumed to be valid in the channel flow model:

- $h_r > h_g$

  Seepage occurs from the channel to the groundwater flow domain. Hence, it becomes a lateral outflow for the channel flow model and a lateral inflow for the groundwater flow model.

- $h_r = h_g$

  No seepage occurs between the two domains. Hence, the lateral inflow/outflow term in equations (1) and (20) becomes zero representing a no flux condition for both models.

- $h_r < h_g$

  Seepage occurs from the groundwater flow domain to the channel. Hence, it becomes a lateral inflow for the channel flow model and a lateral outflow for the groundwater flow model.

3. Numerical Solution

3.1. Channel Flow Model

In general, the available numerical techniques for the solution of expanded Saint-Venant equations can be given as: (i) method of characteristics; (ii) finite difference methods; and, (iii) finite element methods. Of these methods, the finite element method is rarely used when flow is approximated as one-dimensional such as in the case of Saint-Venant equations. The other two methods have been commonly applied for the numerical solution of one-dimensional unsteady flow since 1960s. The finite difference methods can further be classified as explicit and implicit techniques, each of which holds distinct numerical characteristics. A major advantage of the implicit finite difference method over the method of characteristic and the explicit finite difference technique is its inherent stability without the requirement to satisfy the Courant condition, which sets the criteria for the maximum allowable time step. This requirement to satisfy Courant condition often makes the method of characteristics and explicit techniques very inefficient in terms of the use of computer time. Furthermore, certain implicit schemes such as the one proposed by Preissmann (1961) allow the use of variable time and spatial steps, which make the method extremely convenient for applications in routing of flood hydrographs in river systems (Sturm, 2001). Considering these advantages, the implicit finite difference technique is used to solve the channel flow equations given by Equations (1) and (2).

Of the various implicit schemes that have been developed, the "weighted four-point" scheme of Preissmann is very advantageous since it can readily be used with unequal distance steps that becomes particularly important for natural waterways where channel characteristics are highly variable even in short distances. Similarly, the applicability of unequal time steps is another important characteristic of this technique for hydrograph routing where floodwaters would generally rise relatively quickly and recess gradually in time.

The finite difference counterparts of the continuity, momentum and boundary condition equations are derived in Appendix 1. In a channel network, the discretized forms of Equations (1) and (2) form the core of the channel flow model. These equations are written for each channel in the network, and supplemented by the discretized forms of the boundary condition equations. For each channel, the final form of the continuity equation is written as:

$$\theta\left[Q_{i+1}^{j+1}-Q_i^{j+1}-\Delta x_i\left[\left(-\frac{K_r w_r}{m_r}\right)_{i+1/2}^{j+1}\left(h_{r\,i+1/2}^{\;j+1}-h_{g\,i+1/2}^{\;j+1}\right)\right]\right]+$$

$$(1-\theta)\left[Q_{i+1}^{j}-Q_i^{j}-\Delta x_i\left[\left(-\frac{K_r w_r}{m_r}\right)_{i+1/2}^{j}\left(h_{r\,i+1/2}^{\;j}-h_{g\,i+1/2}^{\;j}\right)\right]\right]+ \qquad (25)$$

$$\frac{\Delta x_i}{2\Delta t^j}\begin{bmatrix} s_{c\,i+1/2}^{\;j+1}\left(A+A_o\right)_{i+1}^{j+1}+s_{c\,i+1/2}^{\;j+1}\left(A+A_o\right)_i^{j+1} \\ -s_{c\,i+1/2}^{\;j}\left(A+A_o\right)_{i+1}^{j}-s_{c\,i+1/2}^{\;j}\left(A+A_o\right)_i^{j}\end{bmatrix}=0$$

The final form of the momentum equation is written differently for lateral inflow and outflow. It is important to note that the lateral inflow has no contribution to the momentum balance, and therefore, the terms associated with the lateral flow drop out from the difference equation. For the case of lateral outflow, the finite difference form of the momentum equation is written as:

$$\frac{\Delta x_i}{2\Delta t^j}\left[s_{m\,i+1/2}^{\;j+1}Q_{i+1}^{j+1}+s_{m\,i+1/2}^{\;j+1}Q_i^{j+1}-s_{m\,i+1/2}^{\;j}Q_{i+1}^{j}-s_{m\,i+1/2}^{\;j}Q_i^{j}\right]+$$

$$\theta\begin{bmatrix}\left(\beta Q^2/A\right)_{i+1}^{j+1}-\left(\beta Q^2/A\right)_i^{j+1}+ \\ gA_{i+1/2}^{j+1}\left[h_{r\,i+1}^{\;j+1}-h_{r\,i}^{\;j+1}+\Delta x_i S_{f\,i+1/2}^{\;j+1}+\Delta x_i S_{e\,i+1/2}^{\;j+1}\right]+ \\ \Delta x_i\left(-\frac{Q_{i+1/2}^{j+1}}{2A_{i+1/2}^{j+1}}\right)\left[\left(-\frac{K_r w_r}{m_r}\right)_{i+1/2}^{j+1}\left(h_{r\,i+1/2}^{\;j+1}-h_{g\,i+1/2}^{\;j+1}\right)\right]\end{bmatrix}+$$

$$(1-\theta)\begin{bmatrix}\left(\beta Q^2/A\right)_{i+1}^{j}-\left(\beta Q^2/A\right)_i^{j}+ \\ gA_{i+1/2}^{j}\left(h_{r\,i+1}^{\;j}-h_{r\,i}^{\;j}+\Delta x_i S_{f\,i+1/2}^{\;j}+\Delta x_i S_{e\,i+1/2}^{\;j}\right)+ \\ \Delta x_i\left(-\frac{Q_{i+1/2}^{j}}{2A_{i+1/2}^{j}}\right)\left[\left(-\frac{K_r w_r}{m_r}\right)_{i+1/2}^{j}\left(h_{r\,i+1/2}^{\;j}-h_{g\,i+1/2}^{\;j}\right)\right]\end{bmatrix}=0 \qquad (26)$$

In Equations (25) and (26), subscripts (*i*) and (*j*) represent the spatial and temporal indices, respectively. The terms with subscript (*j*) are known either from initial conditions or from the solution of Saint-Venant equations at the previous time line. Since cross sectional area and channel top width are functions of water surface elevation, the only unknown terms in these equations are discharge and water surface elevation at the $(j+1)^{th}$ time line at nodes (*i*) and (*i+1*). Therefore, there are only four unknowns in these equations. All remaining terms

are either constants or are functions of these unknowns. The resulting two algebraic equations obtained by the application of the weighted four-point scheme are nonlinear and an iterative solution technique is required. When the finite difference forms of continuity and momentum equations are solved for each grid shown in Appendix 1, a system of $2(N_k-1)$ equations are formed for one time-line between the upstream and downstream boundary of channel k, where N_k represents the number of nodes in channel k. The two unknowns in each of these equations yield a total of $2N_k$ unknowns for each time line. The system of $2(N_k-1)$ equations with $2N_k$ unknowns requires two additional equations for the closure of the system. These two additional equations are supplied by the upstream and downstream boundary conditions of the channel. When this procedure is repeated for each channel of the network, a total of $\Sigma(2N_k)=2N$ equations are formed, where k runs from 1 to the number of channels in the network, and N represents the total number of nodes in the entire system. The resulting system of $2N$ non-linear equations with $2N$ unknowns is solved by a suitable matrix solution algorithm such as the Newton-Raphson iterative technique.

Of all the non-linear solution procedures, the Newton-Raphson method is one of the most common iterative techniques used for the solution of a system of non-linear equations. It provides an efficient means of converging to a root given a sufficiently good initial guess. For any channel network application, the system of equations can be denoted as $2N$ functional relations to be zeroed that involves variables Q and h_r represented by x_k for $k=1,2,...,2N$:

$$f_k(x_1, x_2, x_3, ..., x_{2N}) = 0 \tag{27}$$

If $\mathbf{x}$ denotes the entire vector of unknown variables x_k and $\mathbf{f}$ denotes the entire vector of functions f_i, each of the functions f_i can be expanded as a Taylor series expansion in the neighborhood of $\mathbf{x}$:

$$f_k(\mathbf{x}+\delta\mathbf{x}) = f_k(\mathbf{x}) + \sum_{m=1}^{2N} \frac{\partial f_k}{\partial x_m} \delta x_m + O(\delta\mathbf{x}^2) \tag{28}$$

where the matrix of first partial derivatives is called the Jacobian matrix, $\mathbf{J}$. The elements of the Jacobian matrix for 2N unknowns are evaluated in Appendix 2. In matrix notation, one can rewrite Equation (28) as:

$$\mathbf{f}(\mathbf{x}+\delta\mathbf{x}) = \mathbf{f}(\mathbf{x}) + \mathbf{J}\cdot\delta\mathbf{x} + O(\delta\mathbf{x}^2) \tag{29}$$

Neglecting the higher order terms and setting the left hand-side equal to zero, one can obtain a set of linear equations that are solved for the corrections $\delta\mathbf{x}$:

$$\mathbf{J}\cdot\delta\mathbf{x} = -\mathbf{f} \tag{30}$$

This matrix equation is solved by a matrix solver such as Gaussian elimination or LU decomposition for the unknown $\delta\mathbf{x}$, and an improved estimate of solution is obtained by:

$$\mathbf{x}^{j+1,k+1} = \mathbf{x}^{j+1,k} + \delta\mathbf{x}^{j+1,k} \tag{31}$$

where superscript k represents the level of iteration at the unknown time line. The iterative solution is tracked by finding the values of the unknowns Q and h_r so that the residuals given in Equation (31) are forced to zero or very close to zero. It must be noted that the convergence process depends on a good first estimate for the unknown variables. Fread (1985) states that a reasonably good estimate for the first time step is to use the initial condition of discharge and water surface elevation. For all other time steps, the first estimates of the unknown variables can be obtained by using the linearly extrapolated values from solutions at previous time steps according to the algorithm given below:

$$\mathbf{x}^{j+1,1} = \mathbf{x}^{j} + \alpha_c\left(\mathbf{x}^{j} - \mathbf{x}^{j-1}\right)\frac{\Delta t^{j+1}}{\Delta t^{j}} \qquad \text{j} \neq 1 \tag{32}$$

where $\mathbf{x}^{j+1,1}$ is the first estimate of unknown variables at $(j+1)^{\text{th}}$ time line, $\mathbf{x}^{j}$ is the solution vector of Q and h_r values from previous time step, $\mathbf{x}^{j-1}$ is the solution vector of Q and h_r values from two previous time steps, α_c is a weighing factor from 0 to 1 and Δt^{j+1} and Δt^{j} are the two consecutive time step sizes.

3.2. Groundwater Flow Model

In groundwater flow modeling literature, there exist numerous models implementing different numerical solution procedures. The most common of these procedures are the finite difference and finite element methods (McDonald and Harbaugh, 1988; Aral, 1990). The finite element method became a popular method due to the flexibility it offers in simulating aquifer domains with irregular boundaries as well as heterogeneous aquifer properties. In this regard, the Galerkin finite element method based on the method of weighted residuals is used in the numerical solution of the groundwater flow component of the proposed coupled model.

The numerical procedure starts with the idealization of the solution domain by a finite number of distinct, non-overlapping regions, called the finite elements, over which the unknown variables are to be interpolated. In any idealization, the elements are selected such that the material properties of the domain, such as hydraulic conductivity and specific yield, are retained in individual elements. In two-dimensional finite element analysis, families of triangular and/or quadrilateral elements are generally used to discretize the analysis domain. Although these elements can be linear, quadratic or cubic, using simple linear elements provides sufficient accuracy and a better solution strategy. Quadrilateral elements are superior as opposed to triangular elements due to the fact that they are computationally more efficient and they simplify the task of tiling the problem domain without introducing

any bias that the triangular elements possess. For these reasons, linear irregular quadrilateral elements with four nodes are selected to discretize the domain and develop basis functions in the proposed model (Figure 1). The details associated with the basis functions are given in Appendix 3.

Following the idealization of domain and selection of the interpolating functions, an appropriate weak form of the problem is developed. Using the Galerkin weighted residual method, a weak form of the groundwater flow equation is derived in Appendix 4 by using standard steps of writing the weighted residual, integration by parts and incorporating the natural boundary conditions. The resulting finite element matrix equation obtained by applying the Galerkin procedure is given as:

$$\mathbf{S} \cdot \hat{\mathbf{h}}_{\mathbf{g}} + \mathbf{M} \cdot \frac{d\,\hat{\mathbf{h}}_{\mathbf{g}}}{dt} = \mathbf{F} \tag{33}$$

where **S**, **M** and **F** stand for global stiffness matrix, global mass matrix and global load vector, respectively, and $\hat{\mathbf{h}}_{\mathbf{g}}$ is the approximate hydraulic head vector. These global matrices and vectors are obtained by tiling their element counterparts according to the connectivity of elements within the solution domain. The explicit formulas of element matrices and vectors are derived in Appendix 5. At this point, it is clearly seen that these element integrals are generally complex and can not be integrated analytically. Hence, a numerical integration scheme is required to evaluate these element integrals. In the proposed model, a two-dimensional Gaussian quadrature technique is implemented to evaluate these integrals numerically. The details of this technique are discussed in Appendix 6.

The ordinary differential Equation (33) obtained as a result of finite element discretization can be solved using a number of techniques including the one-step finite difference approximations. Since the hydraulic head is a function of time, it is possible to define two positions, *j* and *j+1*, representing the known and unknown time lines, respectively. If one defines an intermediate point between the known and the unknown time line (i.e., $j+\alpha$ where $0 \le \alpha \le 1.0$), then the corresponding head could be calculated as a weighted average:

$$\hat{\mathbf{h}}_{\mathbf{g}}{}^{j+\alpha} = \alpha \hat{\mathbf{h}}_{\mathbf{g}}{}^{j+1} + (1-\alpha)\hat{\mathbf{h}}_{\mathbf{g}}{}^{j} \tag{34}$$

such that if the intermediate point is selected as the mid point between the two time lines (i.e., $\alpha=0.5$), the head becomes an arithmetic average of the two heads at two ends. Using the Taylor series expansion of the hydraulic head around the intermediate point using the points *j* and *j+1*, one would obtain:

$$\hat{\mathbf{h}}_{\mathbf{g}}{}^{j+(1-\alpha)} = \hat{\mathbf{h}}_{\mathbf{g}}{}^{j} + \frac{(1-\alpha)\Delta t}{1!}\frac{\partial \hat{\mathbf{h}}_{\mathbf{g}}{}^{j}}{\partial t} + \frac{(1-\alpha)^2 \Delta t^2}{2!}\frac{\partial^2 \hat{\mathbf{h}}_{\mathbf{g}}{}^{j}}{\partial t^2} + O\left(\Delta t^3\right) \tag{35}$$

$$\hat{\mathbf{h}}_{\mathbf{g}}{}^{j+(1-\alpha)} = \hat{\mathbf{h}}_{\mathbf{g}}{}^{j+1} - \frac{\alpha\Delta t}{1!}\frac{\partial \hat{\mathbf{h}}_{\mathbf{g}}{}^{j+1}}{\partial t} + \frac{\alpha^2\Delta t^2}{2!}\frac{\partial^2 \hat{\mathbf{h}}_{\mathbf{g}}{}^{j+1}}{\partial t^2} - O\left(\Delta t^3\right) \tag{36}$$

Neglecting the terms equal to or higher than second order and subtracting the second equation from the first yields:

$$0 = \hat{\mathbf{h}}_{\mathbf{g}}{}^{j} - \hat{\mathbf{h}}_{\mathbf{g}}{}^{j+1} + \frac{(1-\alpha)\Delta t}{1!}\frac{\partial \hat{\mathbf{h}}_{\mathbf{g}}{}^{j}}{\partial t} + \frac{\alpha\Delta t}{1!}\frac{\partial \hat{\mathbf{h}}_{\mathbf{g}}{}^{j+1}}{\partial t} \tag{37}$$

and after rearranging, reduces to:

$$\frac{\hat{\mathbf{h}}_{\mathbf{g}}{}^{j+1} - \hat{\mathbf{h}}_{\mathbf{g}}{}^{j}}{\Delta t} = (1-\alpha)\frac{\partial \hat{\mathbf{h}}_{\mathbf{g}}{}^{j}}{\partial t} + \alpha\frac{\partial \hat{\mathbf{h}}_{\mathbf{g}}{}^{j+1}}{\partial t} \tag{38}$$

Since it is always possible to write the ordinary differential equation for a particular time line, one would obtain the following equations for the two time lines:

$$\mathbf{S}^{j} \cdot \hat{\mathbf{h}}_{\mathbf{g}}{}^{j} + \mathbf{M}^{j} \cdot \frac{d\,\hat{\mathbf{h}}_{\mathbf{g}}{}^{j}}{dt} = \mathbf{F}^{j} \tag{39}$$

$$\mathbf{S}^{j+1} \cdot \hat{\mathbf{h}}_{\mathbf{g}}{}^{j+1} + \mathbf{M}^{j+1} \cdot \frac{d\,\hat{\mathbf{h}}_{\mathbf{g}}{}^{j+1}}{dt} = \mathbf{F}^{j+1} \tag{40}$$

When these equations are multiplied by the weighing parameters (*1-*α) and α, respectively and added together, one would obtain:

$$\alpha\mathbf{S}^{j+1} \cdot \hat{\mathbf{h}}_{\mathbf{g}}{}^{j+1} + (1-\alpha)\mathbf{S}^{j} \cdot \hat{\mathbf{h}}_{\mathbf{g}}{}^{j} + \alpha\mathbf{M}^{j+1} \cdot \frac{d\hat{\mathbf{h}}_{\mathbf{g}}{}^{j+1}}{dt} + (1-\alpha)\mathbf{M}^{j} \cdot \frac{d\hat{\mathbf{h}}_{\mathbf{g}}{}^{j}}{dt} = \alpha\mathbf{F}^{j+1} + (1-\alpha)\mathbf{F}^{j} \tag{41}$$

It must be noted that in saturated unconfined aquifer flow, the mass matrix, **M**, is a constant matrix which is not a function of hydraulic head and takes the same values for all time steps. Therefore, the above formulation can be simplified as:

$$\alpha\mathbf{S}^{j+1} \cdot \hat{\mathbf{h}}_{\mathbf{g}}{}^{j+1} + (1-\alpha)\mathbf{S}^{j} \cdot \hat{\mathbf{h}}_{\mathbf{g}}{}^{j} + \mathbf{M} \cdot \left(\alpha\frac{d\hat{\mathbf{h}}_{\mathbf{g}}{}^{j+1}}{dt} + (1-\alpha)\frac{d\hat{\mathbf{h}}_{\mathbf{g}}{}^{j}}{dt} \right) = \alpha\mathbf{F}^{j+1} + (1-\alpha)\mathbf{F}^{j} \tag{42}$$

It is now possible to substitute for the weighted averaged derivative terms given in Equation (38) for the term in the parenthesis to obtain:

$$\alpha \mathbf{S}^{j+1} \cdot \hat{\mathbf{h}}_{\mathbf{g}}{}^{j+1} + (1-\alpha)\mathbf{S}^{j} \cdot \hat{\mathbf{h}}_{\mathbf{g}}{}^{j} + \mathbf{M} \cdot \left(\frac{\hat{\mathbf{h}}_{\mathbf{g}}{}^{j+1} - \hat{\mathbf{h}}_{\mathbf{g}}{}^{j}}{\Delta t} \right) = \alpha \mathbf{F}^{j+1} + (1-\alpha)\mathbf{F}^{j} \tag{43}$$

After rearrangement, the equation takes the following final from:

$$\left(\alpha \mathbf{S}^{j+1} + \frac{\mathbf{M}}{\Delta t} \right) \cdot \hat{\mathbf{h}}_{\mathbf{g}}{}^{j+1} = \alpha \mathbf{F}^{j+1} + (1-\alpha)\mathbf{F}^{j} - \left((1-\alpha)\mathbf{S}^{j} - \frac{\mathbf{M}}{\Delta t} \right) \cdot \hat{\mathbf{h}}_{\mathbf{g}}{}^{j} \tag{44}$$

It is now possible to obtain different time integration schemes depending on the value of the time weighing parameter. Even though infinitely many values of the weighing parameter are possible, several of these are particularly important and have significant properties With $\alpha=0$, the equation becomes an explicit scheme and it does not require the solution of any system of equations in order to advance the solution across the time. However, explicit schemes often encounter numerical instabilities if the time step is taken too large. When $\alpha=0.5$, the scheme becomes the so-called Crank-Nicholson method, which implements a central-difference approximation between two time lines. It is known that this choice of the time weighing factor corresponds to the optimal sampling of the first temporal derivative over the time step. If the data of the problem have sufficient continuity, this scheme exhibits its optimal accuracy properties and results in a very efficient method for handling the time-dependence of the transient problem. Unfortunately, presence of any discontinuity in the data might lead to spurious oscillations of the computed solution. If $\alpha=1$, the scheme becomes a fully-implicit scheme and resists the development of solution oscillations better than any other one-step method. Therefore, it is commonly used for most difficult problems. However, it should be noted that this scheme is not fully accurate or especially efficient but it will dampen spurious high-frequency effects more strongly than the other schemes. The proposed model generally uses a time-weighing parameter of 0.5.

Due to the non-linearity of the governing equation of unconfined aquifer flow, a suitable iterative scheme is implemented to solve the system of non-linear equations. Common non-linear solution techniques such as Newton-Raphson method or successive substitution (Picard) iteration method can be applied in this solution. Although the Newton-Raphson method is faster in convergence, it requires the computation of partial derivatives that is rather costly in finite element framework. Hence, the relatively simple Picard iteration technique is applied in the solution of the groundwater flow model. The Picard method is a very simple technique and is based on successively substituting the latest values of the hydraulic head to compute new values until sufficient convergence is achieved. When Picard method is applied, the discretized groundwater flow equation can be written as:

$$\left(\alpha \mathbf{S}^{j+1,k} + \frac{\mathbf{M}}{\Delta t} \right) \cdot \hat{\mathbf{h}}_{\mathbf{g}}{}^{j+1,k+1} = \alpha \mathbf{F}^{j+1,k} + (1-\alpha)\mathbf{F}^{j} - \left((1-\alpha)\mathbf{S}^{j} - \frac{\mathbf{M}}{\Delta t} \right) \cdot \hat{\mathbf{h}}_{\mathbf{g}}{}^{j} \tag{45}$$

where superscripts k and $k+1$ represent previous and current iteration values of hydraulic head at the unknown time level. For all iterations, most recent values of the hydraulic heads are used to obtain an improved estimate of the heads at the unknown time level according to the following formula:

$$\hat{\mathbf{h}}_{\mathbf{g}}^{\,j+1,k+1} = \gamma \hat{\mathbf{h}}_{\mathbf{g}}^{\,j+1,k+1} + (1-\gamma)\hat{\mathbf{h}}_{\mathbf{g}}^{\,j+1,k} \tag{46}$$

where γ is an iteration-dependent underrelaxation coefficient (or a damping parameter) taking values between 0 and 1. The left hand-side value at $(k+1)^{th}$ iteration represents the improved estimate to be used in next iteration. For very non-linear problems, head change in iterations might be large enough to cause the solution to oscillate. In such cases, a damping parameter can be used to restrict the head change from one iteration cycle to the next (Huyakorn *et al*, 1986). In each iteration cycle, the value of damping parameter is computed according to the following procedure:

$$\gamma = \begin{cases} \dfrac{3+s}{3+|s|} & s \geq -1 \\ \dfrac{1}{2|s|} & s < -1 \end{cases} \tag{47}$$

where s is a scale parameter evaluated according to the following rule:

$$s = \begin{cases} 1 & k = 1 \\ \dfrac{\varepsilon_{k+1}}{\gamma_{old}\varepsilon_k} & k > 1 \end{cases} \tag{48}$$

where ε_{k+1} and ε_k represent the hydraulic head change for iteration $k+1$ and k, respectively, that is largest in absolute value and γ_{old} is the value of damping parameter at the previous iteration.

3.3. Simultaneous Solution of the Coupled Model

The initial step for the numerical solution of the coupled model is discretizing the analysis domain. In this procedure, the channel network is discretized first considering the stability requirements of the channel flow model. Then, the groundwater flow domain is discretized considering the heterogeneity of the aquifer. During the discretization of the groundwater flow domain, each node of the channel flow model is selected such that it coincides with a node in the groundwater flow model as seen in Figure 3. This one-to-one correspondence of the nodes along the channel network is essential for the simultaneous solution of the coupled model. If there is a requirement for finer discretization of the groundwater flow domain at any point along the channel network due to highly variable aquifer properties,

the discretization of the channel flow model must also be modified to satisfy the one-to-one correspondence of the nodes. In this regard, the simultaneous solution of the coupled model is always based on finest discretized domain that either model enforces along the channel network. For any other point in the analysis domain, the discretization is solely based on the requirements of the groundwater flow model.

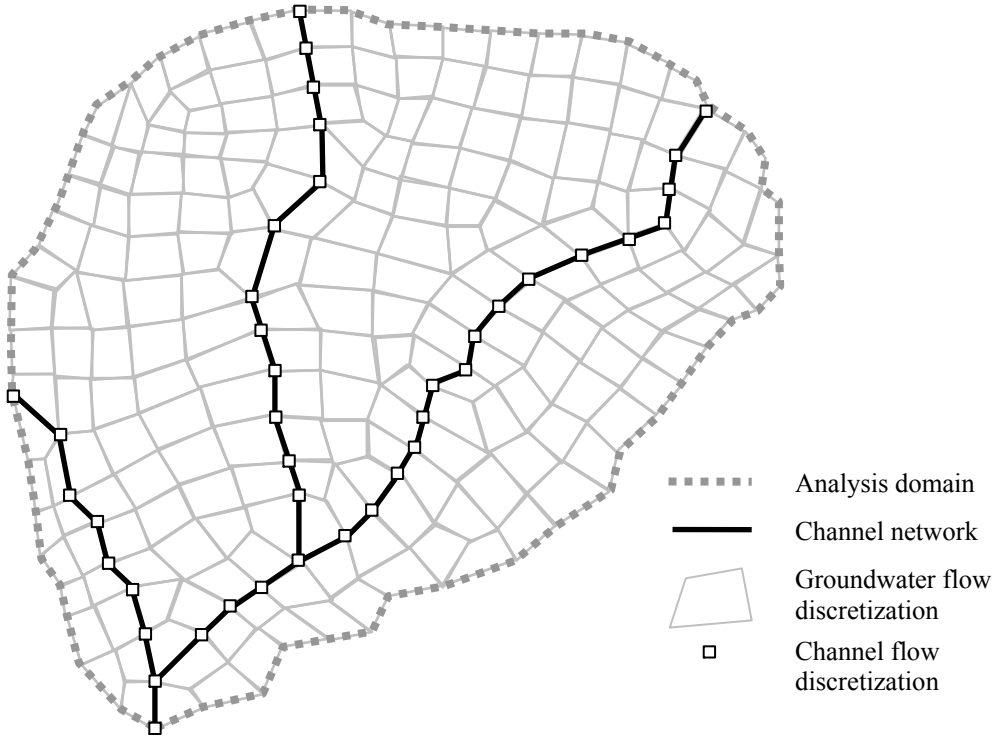

Figure 3. Discretization of the domain

The only exception to the one-to-one correspondence of nodes is observed at the channel junction points. At any junction with k inflowing channels and one outflowing channel, the numerical discretization of the channel flow model require that $k+1$ nodes are used to properly represent the k downstream boundary nodes of the inflowing channels and one upstream boundary node of the outflowing channel. Since all $k+1$ nodes physically represent the same junction point, they all correspond to a single point in the groundwater flow model. Therefore, at junction points, $k+1$ nodes of the channel flow model corresponds to one node of the groundwater flow model.

The second step of the simultaneous solution of the coupled model is to write discretized equations of channel and groundwater flow equations. These are given in Equations (30) and (45), respectively. When these equations are written for all nodes of channel and groundwater flow domains, a system of equations is obtained for both channel and groundwater flow system. At this point, these systems of equations are assembled together

within a single system so that they can be solved together in a simultaneous manner. The assembled final matrix equation is shown in Figure 4.

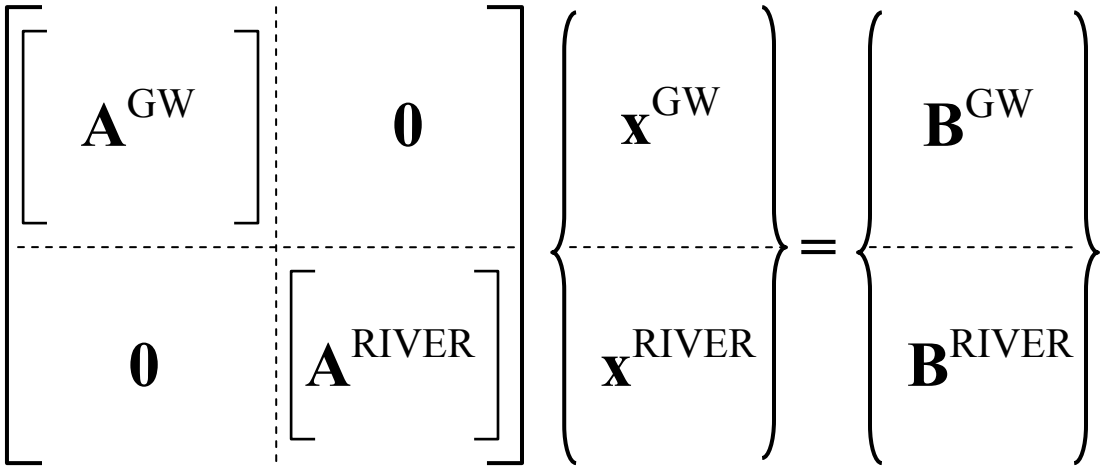

Figure 4. Global matrix equation and component blocks

In the assembled global matrix equation, ***A*** is the global coefficient matrix, ***B*** is the global load vector and ***x*** is the global unknown vector. As seen from Figure 4, the global matrix and vectors are obtained by combining their separate blocks obtained from channel and groundwater flow model. These separate blocks are written as:

$$\mathbf{A}^{GW} = \alpha \mathbf{S}^{j+1,k} + (1/\Delta t)\mathbf{M} \tag{49}$$

$$\mathbf{A}^{RIVER} = \mathbf{J}^{j+1,k} \tag{50}$$

$$\mathbf{B}^{GW} = \alpha \mathbf{F}^{j+1,k} + (1-\alpha)\mathbf{F}^{j} - \left((1-\alpha)\mathbf{S}^{j} - (1/\Delta t)\mathbf{M}\right)\cdot \hat{\mathbf{h}}_{\mathbf{g}}{}^{j} \tag{51}$$

$$\mathbf{B}^{RIVER} = -\mathbf{f}^{j+1,k} \tag{52}$$

$$\mathbf{x}^{GW} = \hat{\mathbf{h}}_{\mathbf{g}}{}^{j+1,k+1} \tag{53}$$

$$\mathbf{x}^{RIVER} = \delta \mathbf{x}^{j+1,k+1} \tag{54}$$

Although the global matrix is shown in full-matrix format, the calculations are performed using a banded matrix structure to reduce computer memory required to store and solve the system. The total bandwidth of the global matrix depends on the relative magnitudes of the bandwidths of channel flow and groundwater flow models. Therefore, the size of the global

matrix is determined by the size of the bigger bandwidth. In general, the bandwidth of the groundwater flow model is bigger than the bandwidth of the channel flow model.

It is important to note that since the global system is non-linear and time dependent, it is solved several times for each time step until sufficient convergence is achieved for the unknown parameters. Hence, the global matrix solution involves an iterative portion to handle the non-linearity of the governing equations of both models. However, this iterative non-linear solution does not affect the simultaneous solution of the overall coupled system. The iterative solution is only used in the solution of the non-linearity in the two sub-systems. The convergence of the non-linear solution is checked using two separate criteria for channel flow and groundwater flow components. Therefore, although the systems are solved together, the convergence of the solution is tested with different criteria since the degree of the non-linearity in channel flow is generally much higher than the degree of non-linearity in groundwater flow. Typically, 2 to 3 iterations are found to be sufficient for the convergence of two sub-domain models.

Even though the two hydrologic systems coupled in this model may have significantly different time scales, their simultaneous solution, unlike an iterative solution, requires a common time step in numerical discretization. Particularly, the behavior of a channel flow model is generally more dynamic than the overall response of a groundwater model. This constraint could occasionally create long simulation periods with the proposed algorithm but is always faster than the iterative solution approach that utilizes the same time step size.

4. Application

Three sets of simulations are made using the proposed model and the solution algorithm. In the first application, a hypothetical test case is simulated to test the model's capabilities and limitations with a rectangular groundwater flow domain and an overlying single channel domain. In the second application, the same hypothetical test case is modified to analyze the model's response with the presence of a channel network. Finally, the third application is based on simulating a real system from southern Georgia.

4.1. Hypothetical Case: Single Channel

The coupled channel/groundwater flow model is first applied to a hypothetical stream-aquifer system to demonstrate the performance of the proposed simultaneous solution algorithm. The physical setup of the hypothetical domain is shown in Figure 5. In this application, the stream is a 30m wide 10km long uniform rectangular channel with a constant slope of 0.0001m/m and divides the aquifer into two equal domains of 2000m wide on each side of the channel. The Manning's roughness coefficient of the stream is uniform through out the channel and has a value of 0.025. At steady flow conditions, the channel carries $100m^3/s$ discharge at the uniform flow depth of 3.56m. The thickness of the sediments at the bottom of the channel is 0.3m and the hydraulic conductivity of the

deposits is 1.0E-6m/s. The channel bottom elevation at the most upstream point is given as 30m above mean sea level. To visualize results easily, the 10km long and 4 km wide unconfined aquifer is assumed to have a uniform and isotropic hydraulic conductivity of 1.0E-3m/s and the aquifer base is set at mean sea level. The stream flow model is discretized by 100m long elements giving a total of 101 nodes. The groundwater flow model domain is discretized by square elements with a side length of 100m giving a total of 4141 nodes and 4000 square elements. Furthermore, a constant time step of 1hr is used in simulations.

In the channel flow model, the upstream boundary condition for the channel is given by a trapezoidal discharge hydrograph with a base discharge of $100m^3/s$, a peak discharge of $350m^3/s$ and a time to peak of 10 days (Figure 6). The downstream boundary condition is given by a single-valued rating curve that maps the discharge to its normal depth. In the groundwater flow model, the boundaries parallel to the stream are specified as constant head condition and the boundaries perpendicular to the stream are specified as no-flux condition. Moreover, the internal boundary, where the stream runs through, is specified as a head-dependent line source. The initial conditions in the stream flow model is given as uniform flow conditions (i.e., $100m^3/s$ of discharge and a corresponding 3.56m of depth) at all nodes. In the groundwater flow model, two different sets of initial hydraulic head surfaces are used. In the first simulation, the initial groundwater head in the aquifer is chosen to be at 32m at all nodes. This simulation illustrates a condition where lateral inflow occurs from the stream to the aquifer. In the second simulation, the opposite scenario is simulated and the initial groundwater head in the aquifer is chosen to be 35m, illustrating a condition where the lateral inflow occurs from the aquifer to the stream. These two simulations of Problem-1 are referred to as Scenario-1 and Scenario-2, respectively and are abbreviated as P1-S1 and P1-S2 in the following discussion.

In both scenarios, the point comparisons of groundwater head and stream stage are presented in figures 6 and 8 at the mid point of the analysis domain (i.e., 5000m from the upper boundary of the aquifer, which also corresponds to the mid point of the stream). A spatial distribution of groundwater heads are also presented in figures 7 and 9 along the line ($-2000m \leq x \leq 2000m$; $y = 5000m$). Analysis of groundwater head time series in figures 6 and 8 reveals that the passage of the flood wave creates an increase in the groundwater heads by creating a mound near the river as long as the stream stages are higher than the groundwater heads for a sufficiently long period of time. This mound is the result of lateral inflow to the aquifer (Figure 7). It is also seen that the mound subsides and the bank storage is drained back to the stream when the stream stage falls below the groundwater heads. It is also seen from figures 6 and 8 that there is a lag between the peak values of the hydraulic head and the stream stage which clearly represents the dynamic behavior of the stream flow as opposed to the groundwater flow.

The response of the coupled system to a flood wave is directly related to the initial conditions in the stream and the aquifer. A comparison of figures 7 and 9 demonstrate the effect of initial groundwater head in the aquifer and its position relative to the stage in the stream. When the hydraulic head in the aquifer is higher than the stream stage (Figure 9), a

discharge from bank storage occurs in the first 5 days of the simulation creating a drawdown near the stream. During the second 5 day period, stream stages increases due to the arrival of the flood peak and this creates a flow reversal towards the aquifer (Figure 9).

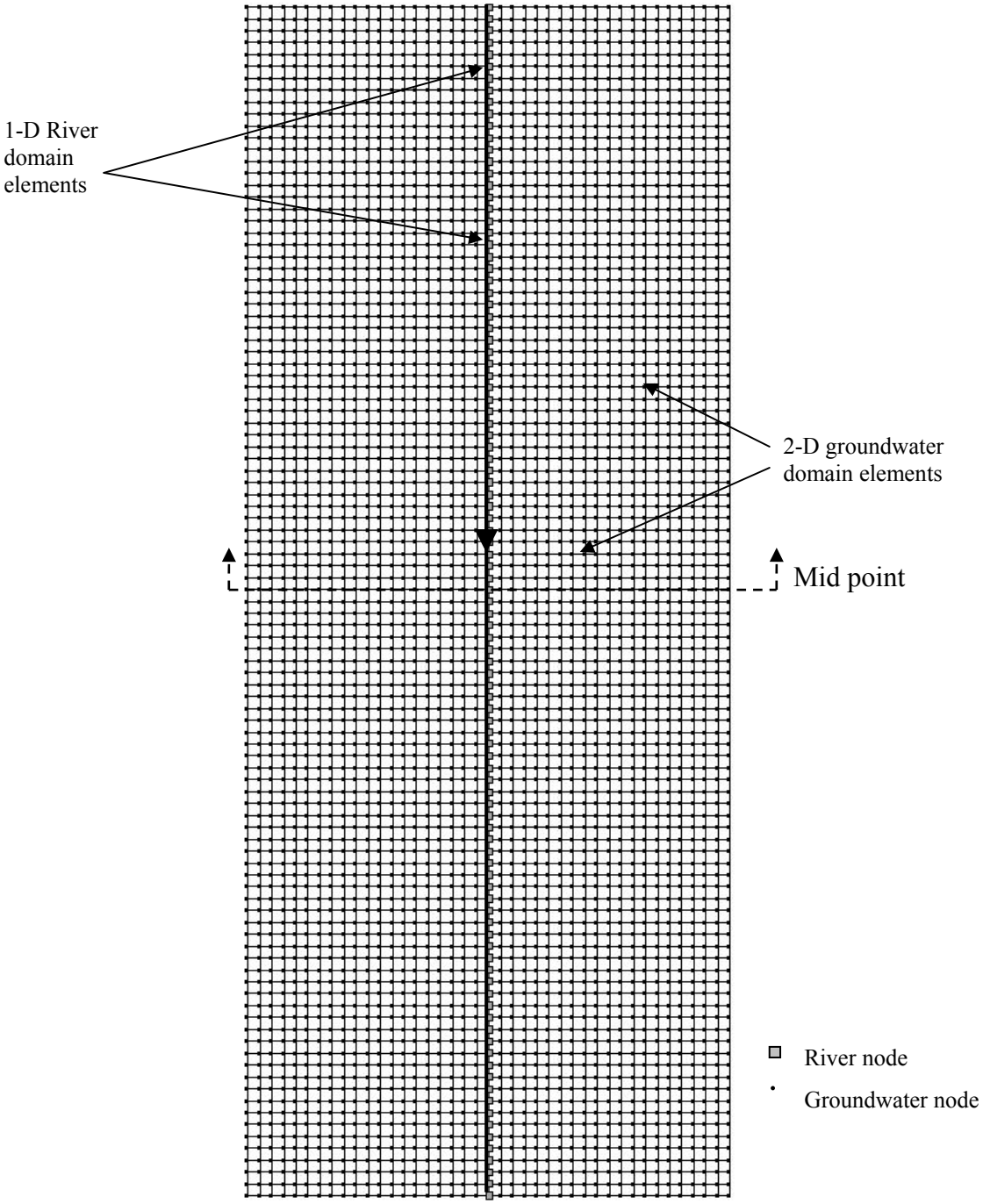

Figure 5. Physical setup of hypothetical domain, single channel

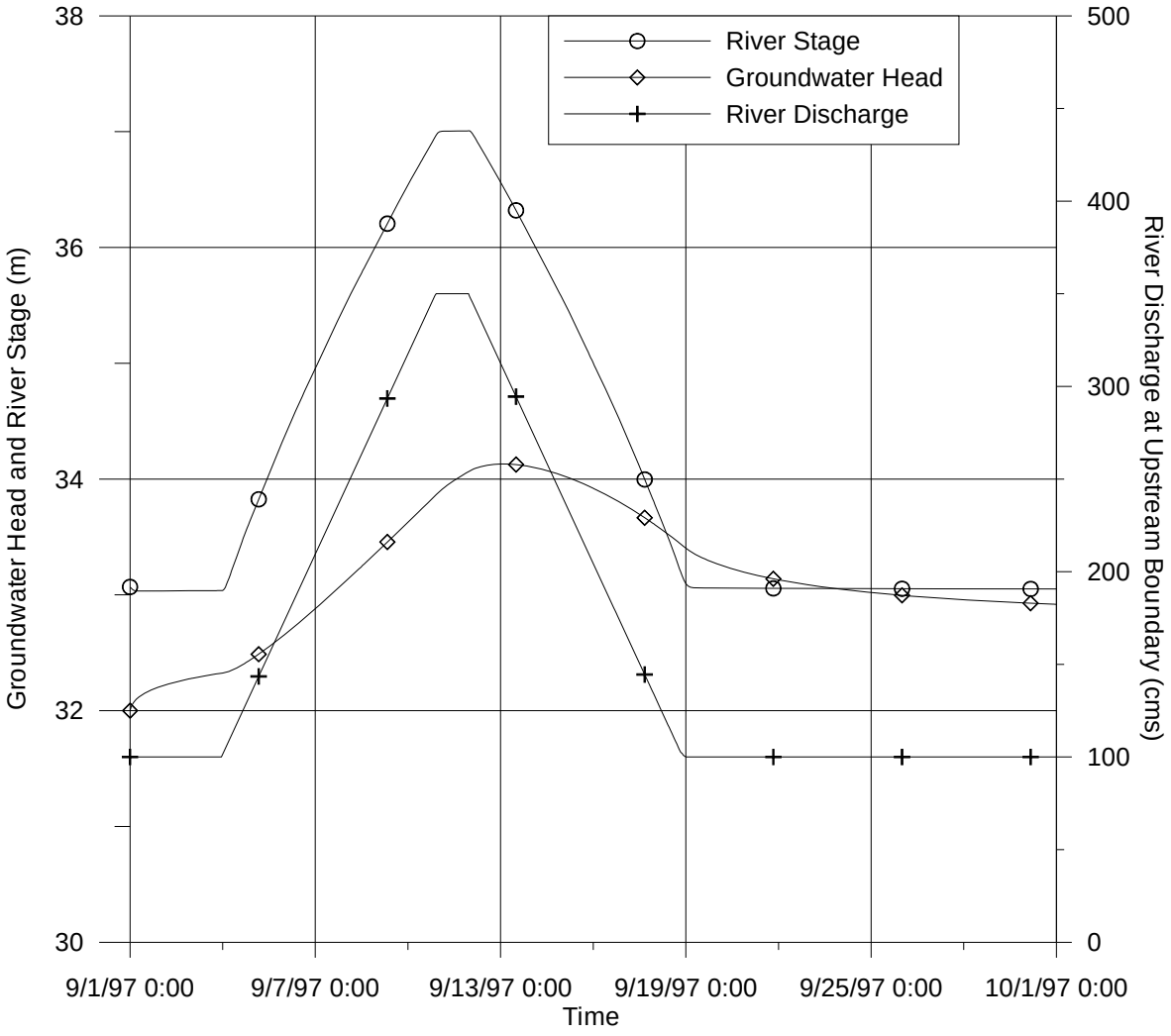

Figure 6. Groundwater head and river stage at the mid point and river discharge at the upstream boundary (P1-S1)

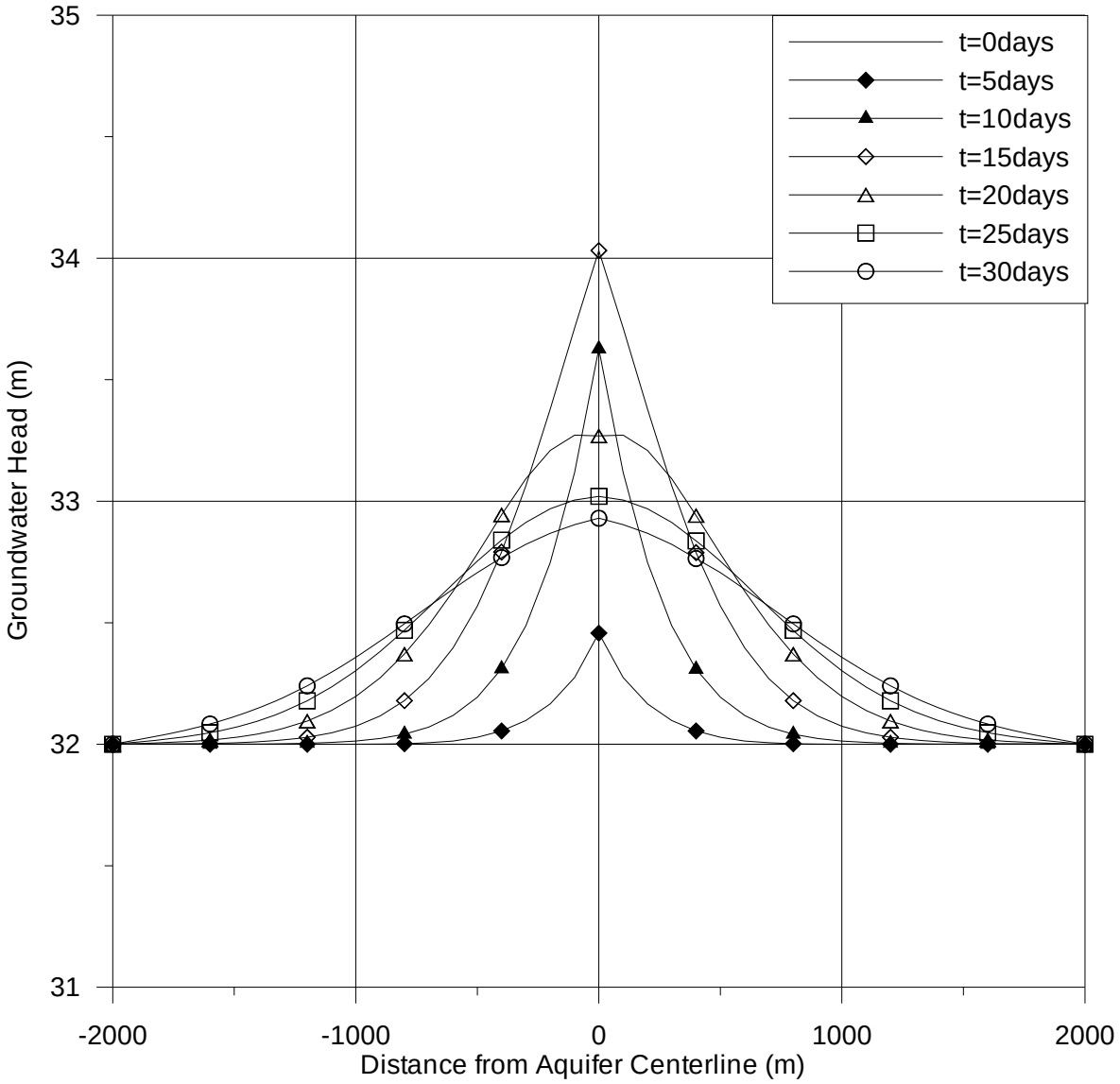

Figure 7. Groundwater head profile at various times along the mid point (P1-S1)

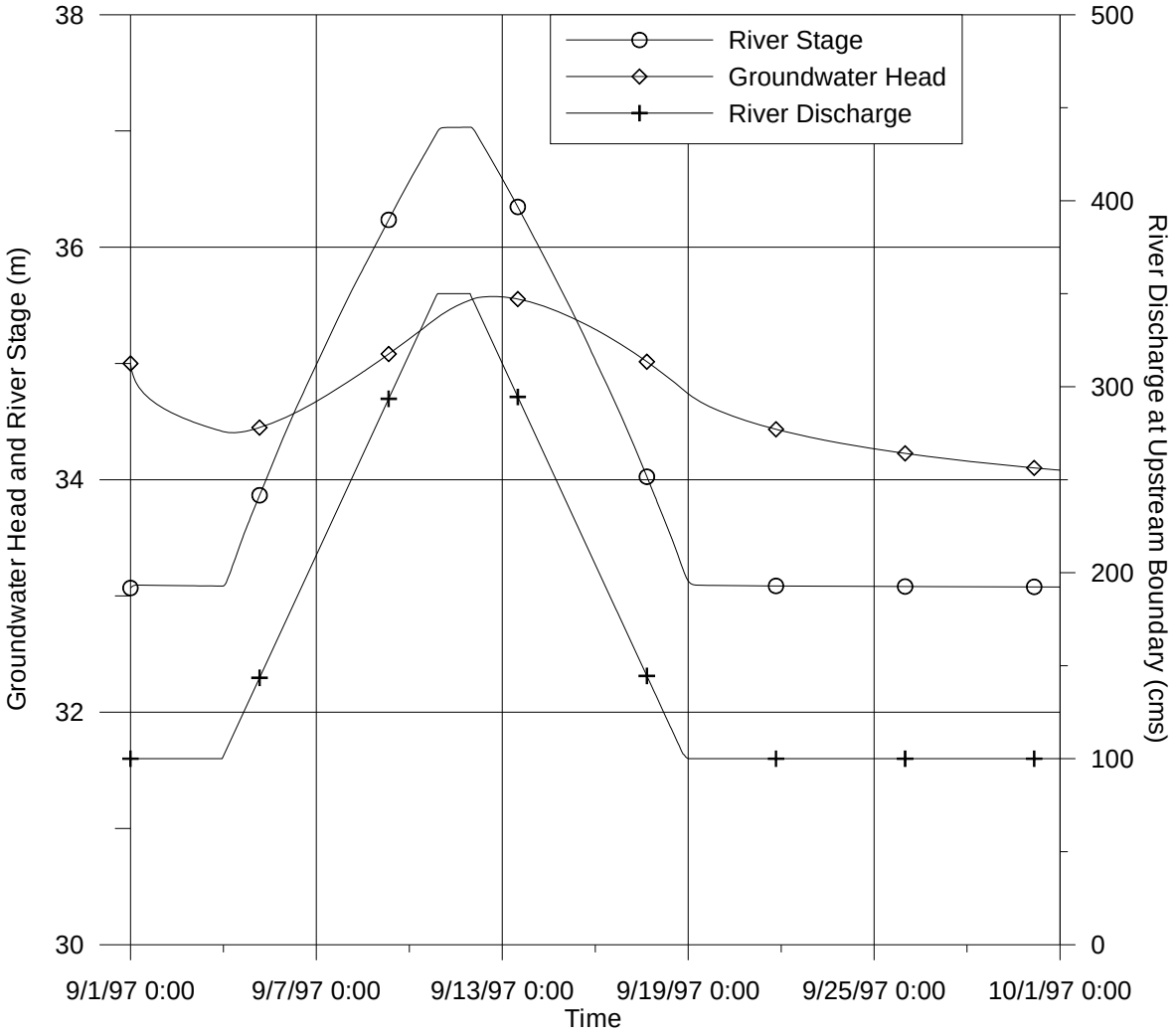

Figure 8. Groundwater head and river stage at the mid point and river discharge at the upstream boundary (P1-S2)

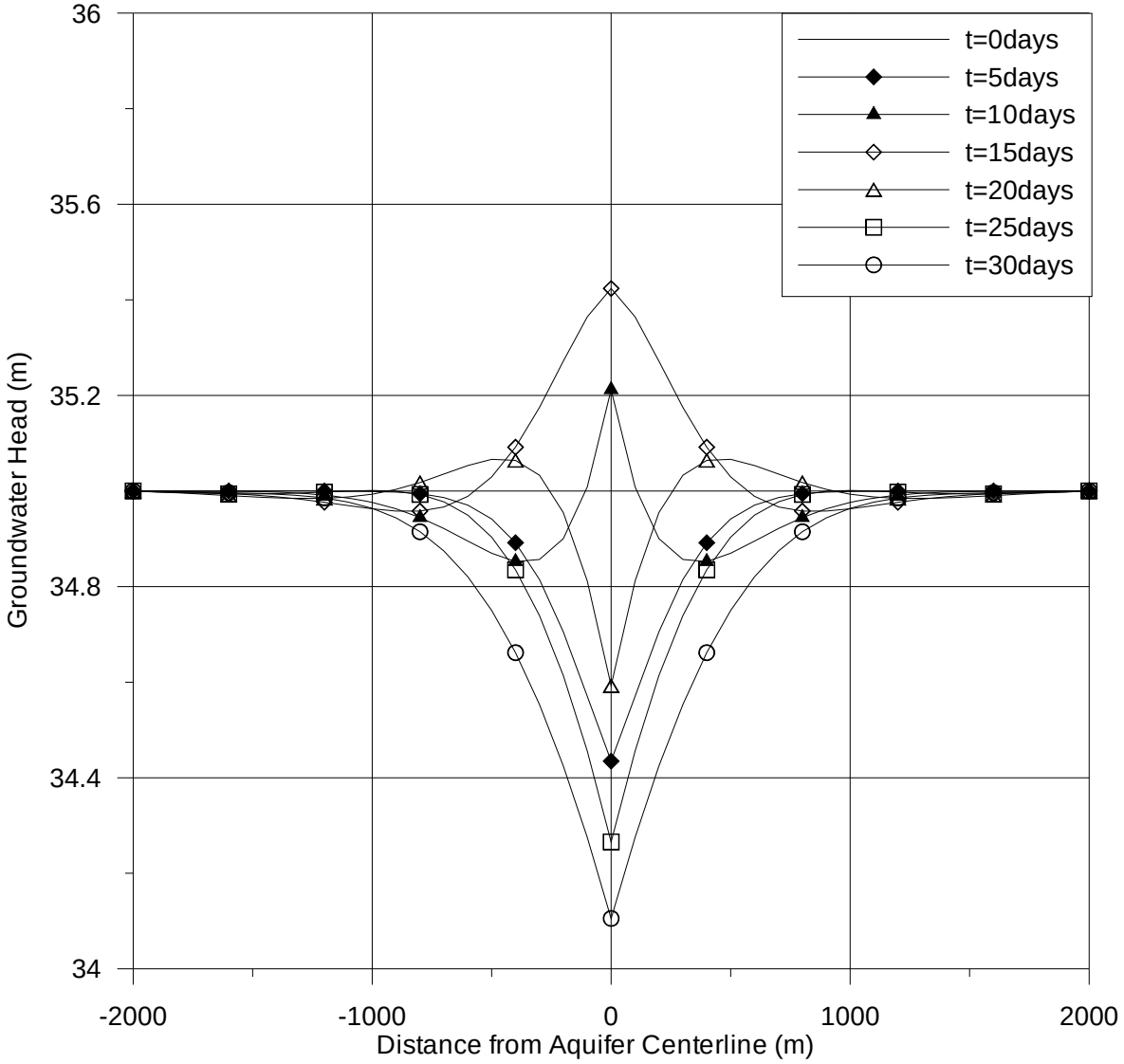

Figure 9. Groundwater head profile at various times along the mid point (P1-S2)

4.2. Hypothetical Case: Channel Network

In the second application, the coupled channel/groundwater flow model is applied to a hypothetical stream network-aquifer system to demonstrate the performance of the proposed simultaneous solution algorithm to multiple channel applications. The physical setup of the hypothetical domain is shown in Figure 10. In this application, two stream channels (i.e., channels 1 and 2) meet and form a larger channel (i.e., channel 3) at the junction point shown in Figure 10. The two upstream tributaries are 30m wide and 7071m long uniform rectangular channels with a constant slope of 0.00015m/m. The downstream stream is 45m wide and 5000m long uniform rectangular channel with a constant slope of 0.0001m/m. The two upstream channels confluence at the mid-point of the domain and creates the junction. The Manning's roughness coefficients of all channels are uniform through out the domain and have a value of 0.025. At steady flow conditions, the two upstream channels carry $100m^3/s$ whereas the downstream channel carries $200m^3/s$. The thickness of the sediments at the bottom of the channel is 0.3m and the hydraulic conductivity of the deposits is 1.0E-6m/s. To visualize results easily, the 10km long and 4 km wide unconfined aquifer is assumed to have a uniform and isotropic hydraulic conductivity of 1.0E-3m/s and the aquifer base is set at mean sea level. The stream flow model is discretized by variable length elements giving a total of 155 nodes. The groundwater flow model domain is discretized by quadrilateral elements with variable side lengths giving a total of 4161 nodes and 4022 elements. A constant time step of 1hr is used in simulations.

In the channel flow model, the upstream boundary conditions are given by a trapezoidal discharge hydrograph with a base discharge of $100m^3/s$, a peak discharge of $350m^3/s$ and a time to peak of 10 days (Figure 11). The downstream boundary condition is given by a single-valued rating curve that maps the discharge to its normal depth. In the groundwater flow model, the boundaries parallel to the stream are specified as constant head condition and the boundaries perpendicular to the stream are specified as no-flux condition. Moreover, the internal boundary, where the stream runs through, is specified as a head-dependent line source. The initial conditions in the stream flow model are given as uniform flow conditions at all nodes. In the groundwater flow model, two different sets of initial hydraulic head surfaces are used. In the first simulation, the initial groundwater head in the aquifer is chosen to be at 32m at all nodes. This simulation illustrates a condition where lateral inflow occurs from the stream to the aquifer. In the second simulation, the opposite scenario is simulated and the initial groundwater head in the aquifer is chosen to be 35m, illustrating a condition where the lateral inflow occurs from the aquifer to the stream. These two simulations of Problem-2 are referred to as Scenario-1 and Scenario-2, respectively and are abbreviated as P2-S1 and P2-S2 in the following discussion.

In both scenarios, the point comparisons of groundwater head and stream stage are presented in figures 11 and 15 at three points in the analysis domain. These points are shown in Figure 10. Of these three points, points 1 and 2 are on the left upstream channel and are situated 1745m and 4537m from the most upstream point of channel 1. On the other

hand, point 3 is on the downstream channel and is situated at the mid point between the junction and the channel's most downstream point (i.e., 2500m from the junction). These three points are also positioned on the three transects depicted in Figure 10 (i.e., 1600m, 4200m, and 7500m from the upper boundary of the aquifer). These transects are used to present the spatial distributions of groundwater heads along the aquifer.

Analysis of groundwater head time series in figures 12 through 14 and 16 through 18 reveal that the passage of the flood wave creates an increase in the groundwater heads by creating a mound near the river as long as the stream stages are higher than the groundwater heads for a sufficiently long period of time. This mound is the result of lateral inflow to the aquifer. It is also seen that the mound subsides and the bank storage is drained back to the stream when the stream stage falls below the groundwater heads. The spatial distribution of groundwater heads in transects 1 and 2 illustrate a symmetric response behavior since the physical characteristics of the upstream channels and their boundary conditions are exactly identical as a function of time. Any difference between these characteristics would clearly create an asymmetric hydraulic head distribution in the upper half of the aquifer.

In P2-S1, the initial groundwater head in all three transects are below the initial river stages. This situation creates a lateral outflow from stream channels towards the groundwater domain, creating an increase in groundwater heads as seen in figures 12, 13 and 14. Then, the flood wave arrives and this increase is even more pronounced. Once the flood wave starts receding, the groundwater heads start falling. Since the water surface elevation decrease in channel is much more dynamic than the groundwater head decrease, a flow reversal is observed creating a lateral inflow to stream channels from the groundwater domain. This behavior is present in all transects after 09/15/1997 in figures 12, 13 and 14. In P2-S2, however, the initial groundwater head in all three transects are above the initial river stages. Hence, an immediate lateral inflow to the stream channels starts to develop. In the absence of a flood wave, this situation creates a decrease in groundwater heads in the immediate vicinity of the channels. Therefore, it is possible to observe the drawdown associated with this behavior in all transects till 09/05/1997 in figures 16, 17 and 18. After 09/05/97, the arrival of the flood wave forces an increase in the groundwater heads due to lateral outflow from the channel.

It is important to mention the fact that a relatively high hydraulic conductivity value and a relatively smoothly-increasing upstream discharge hydrograph are used to promote a rapid response behavior so that the results could be analyzed in a simpler and idealized fashion. In real time simulations, however, the aquifer conductivity values are generally much smaller and the hydrographs are commonly much steeper on the rising limb. Such a situation is presented in the next application of the model.

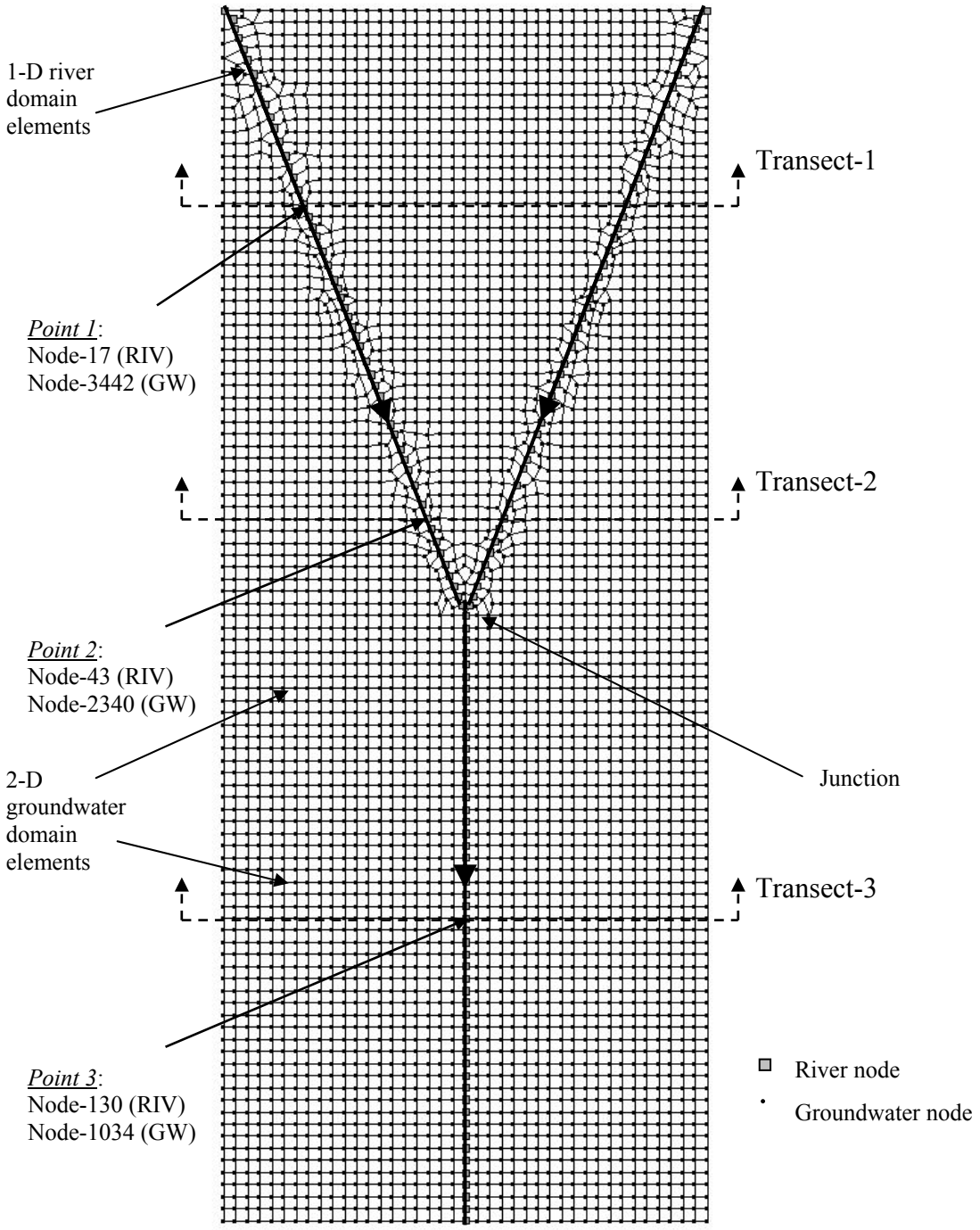

Figure 10. Physical setup of hypothetical domain, channel network

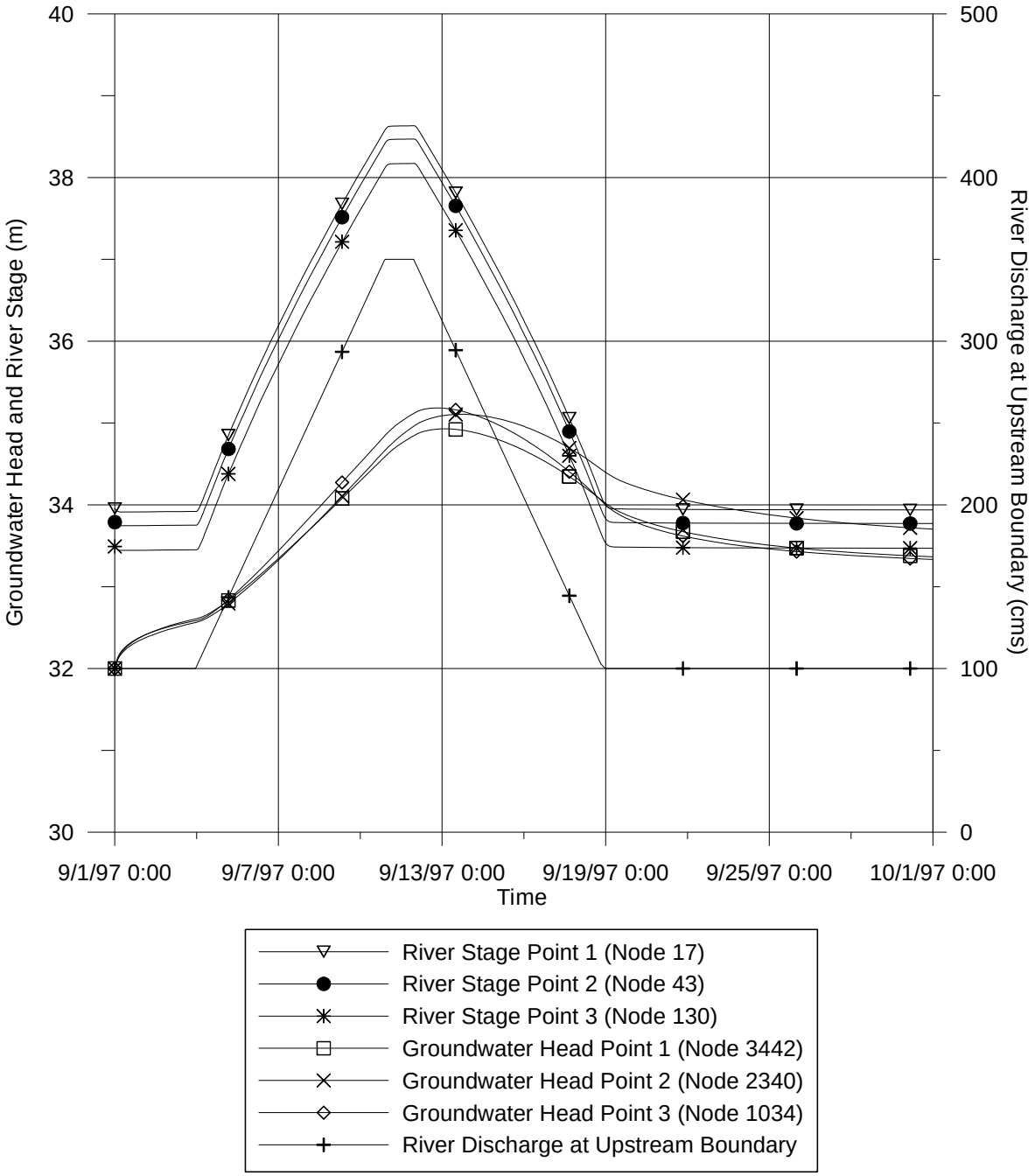

Figure 11. Groundwater head and river stage at various points in domain and river discharge at the upstream boundary (P2-S1)

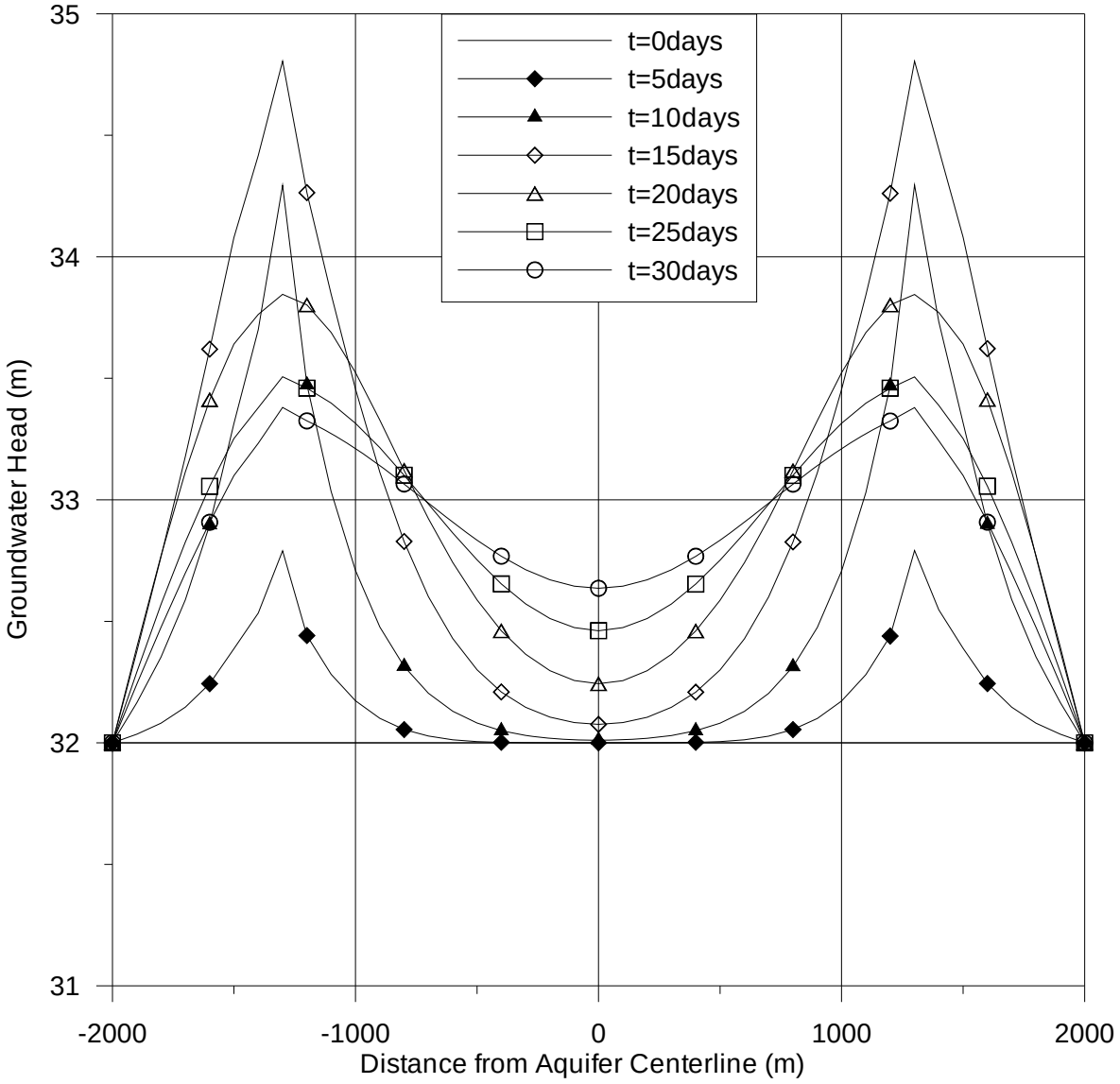

Figure 12. Groundwater head profile at various times along the transect-1 (P2-S1)

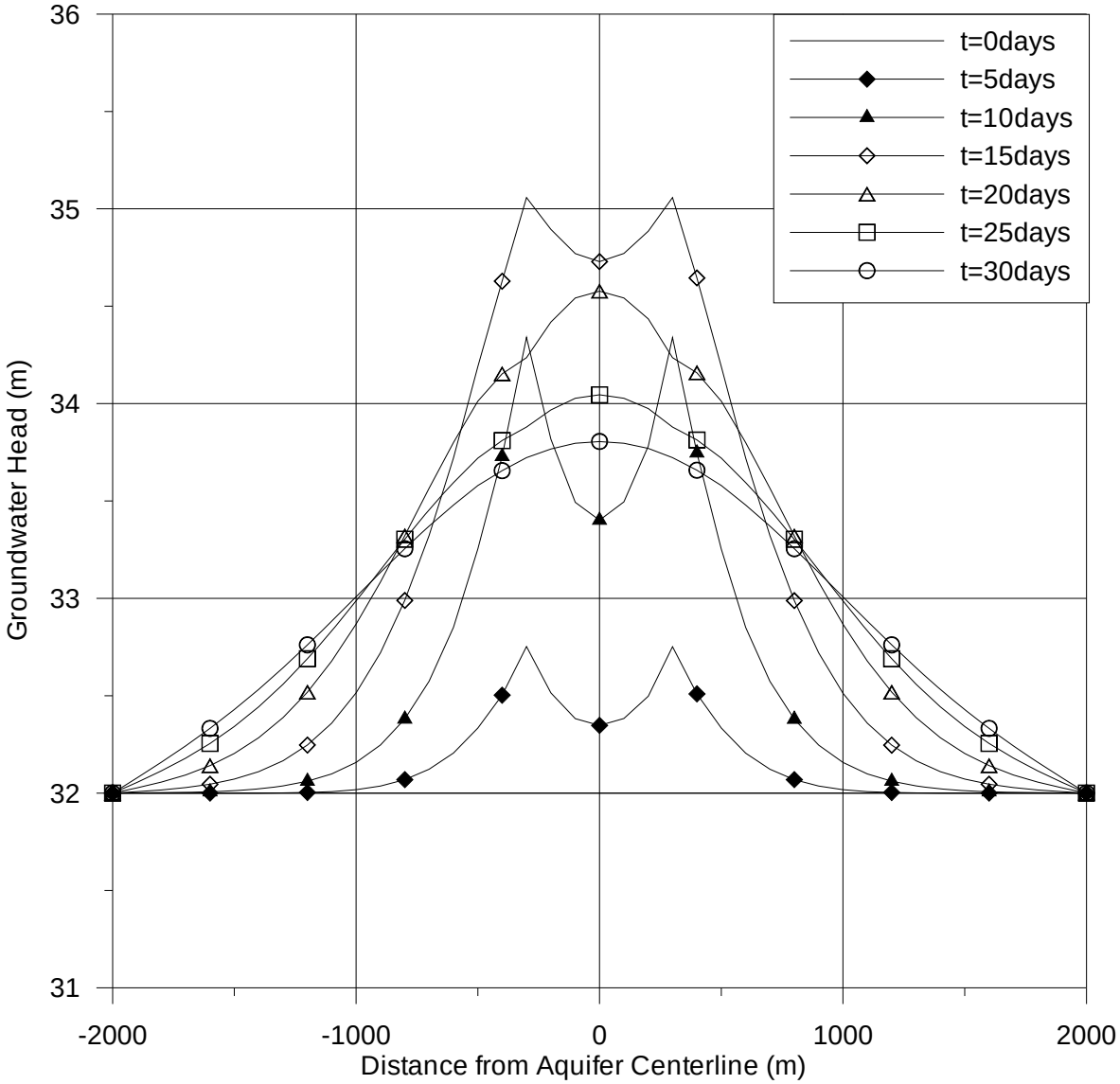

Figure 13. Groundwater head profile at various times along the transect-2 (P2-S1)

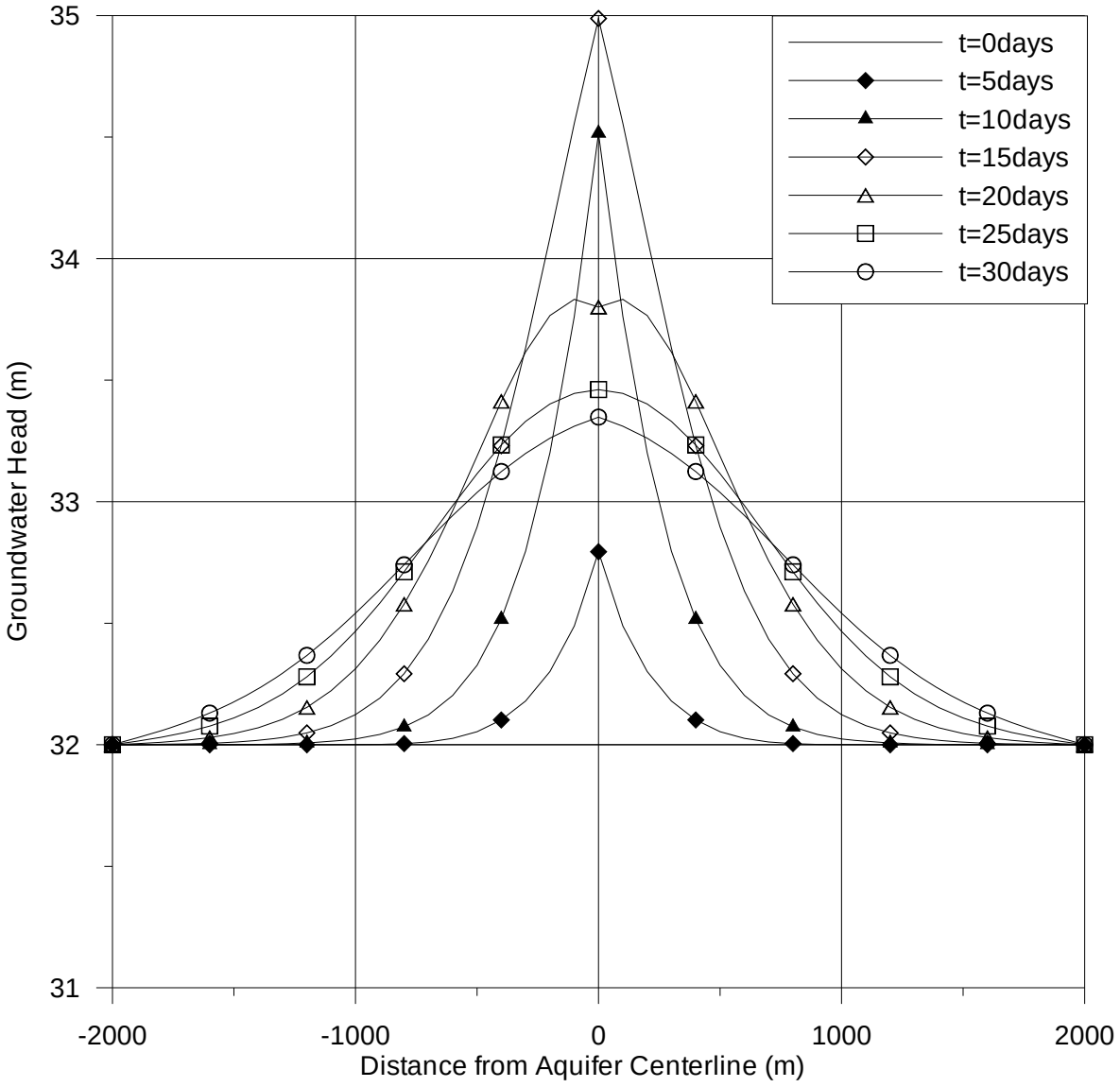

Figure 14. Groundwater head profile at various times along the transect-3 (P2-S1)

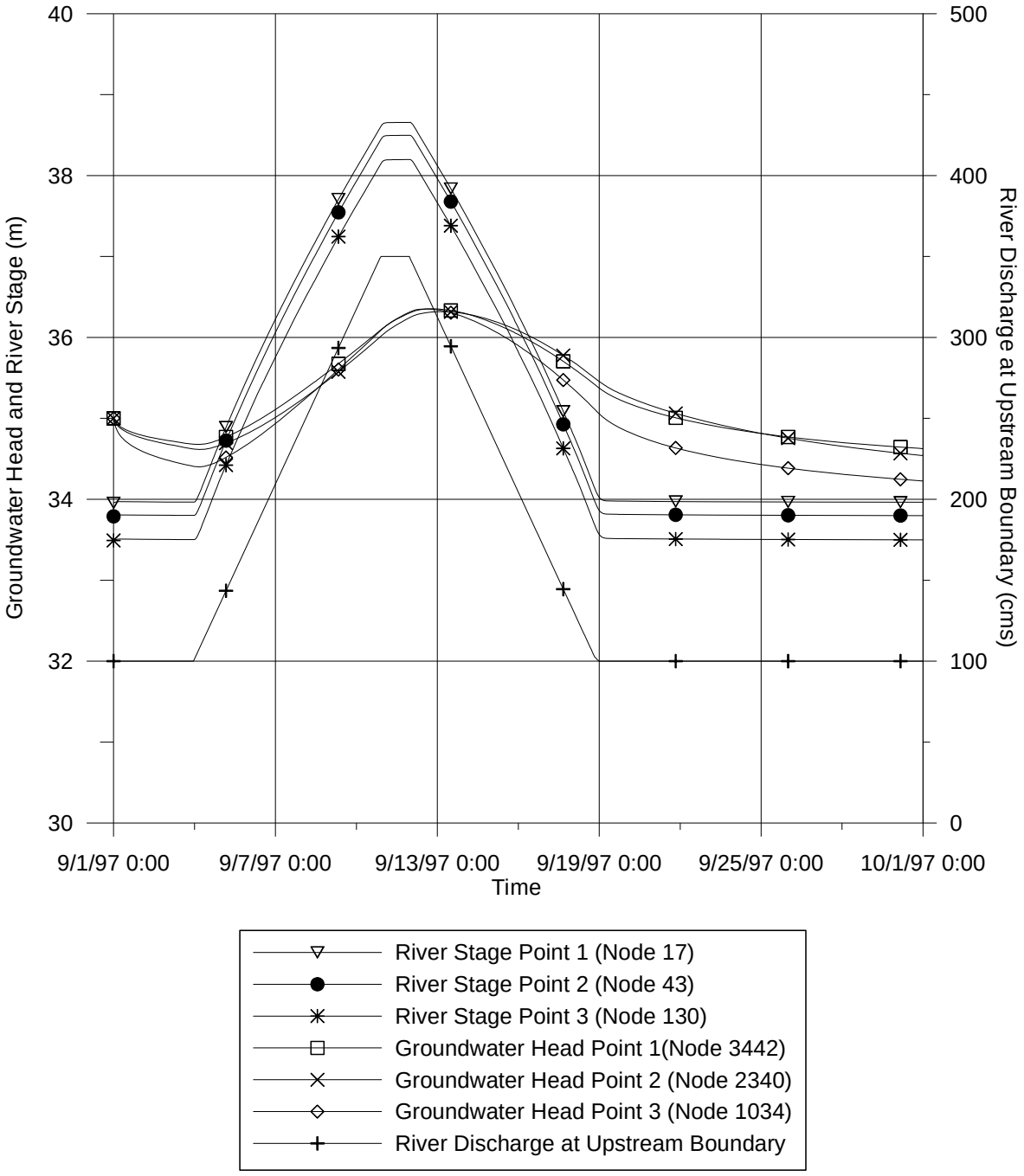

Figure 15. Groundwater head and river stage at various points in domain and river discharge at the upstream boundary (P2-S2)

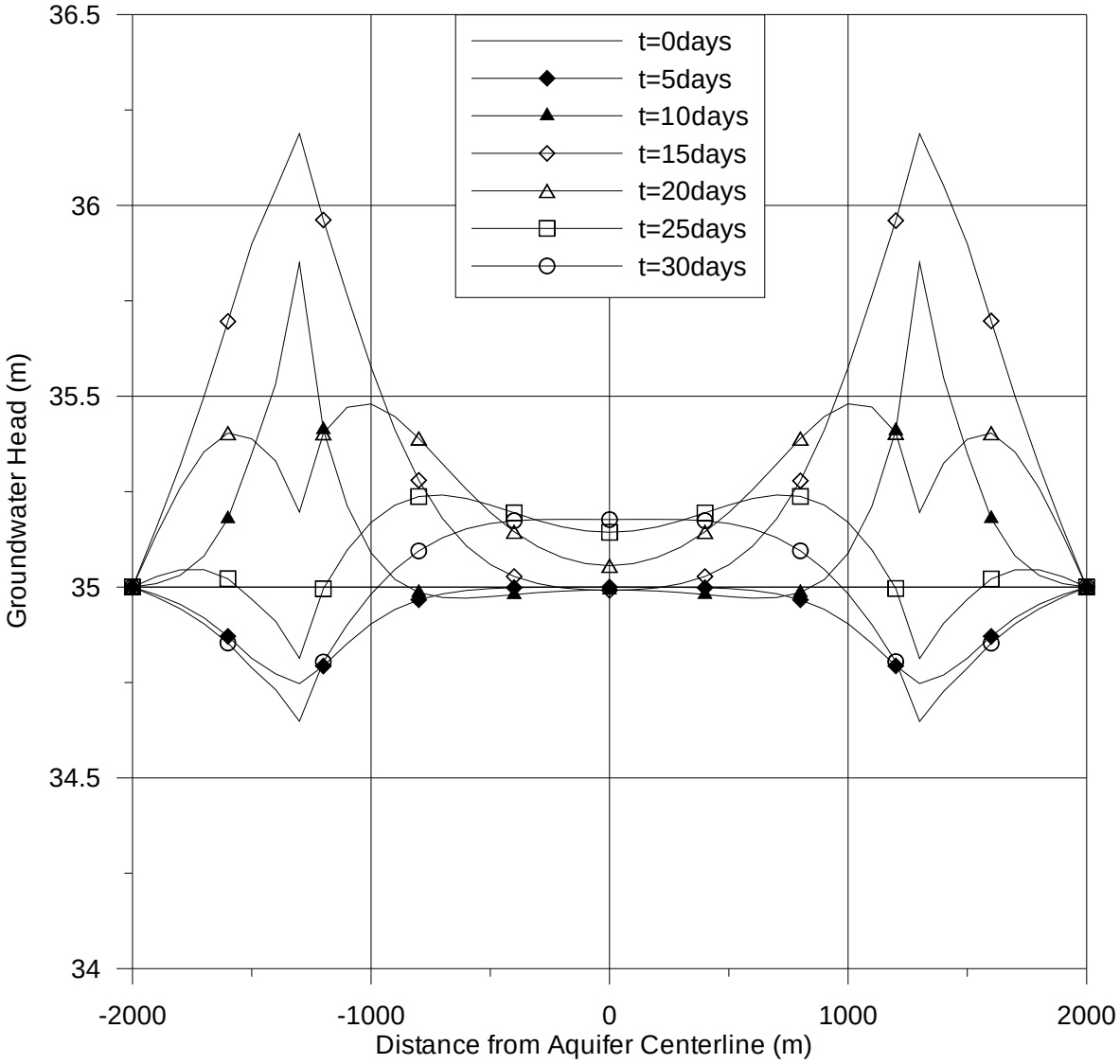

Figure 16. Groundwater head profile at various times along the transect-1 (P2-S2)

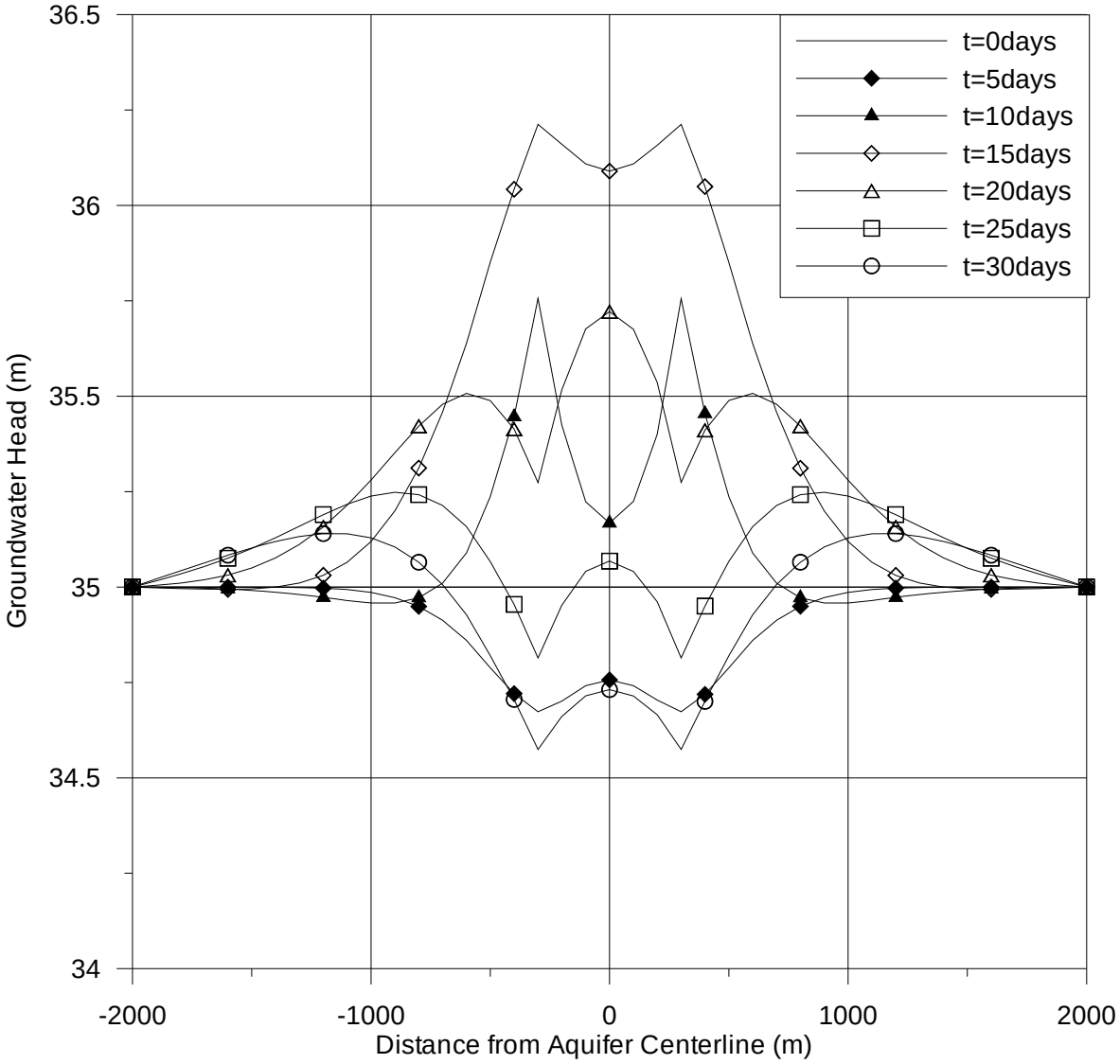

Figure 17. Groundwater head profile at various times along the transect-2 (P2-S2)

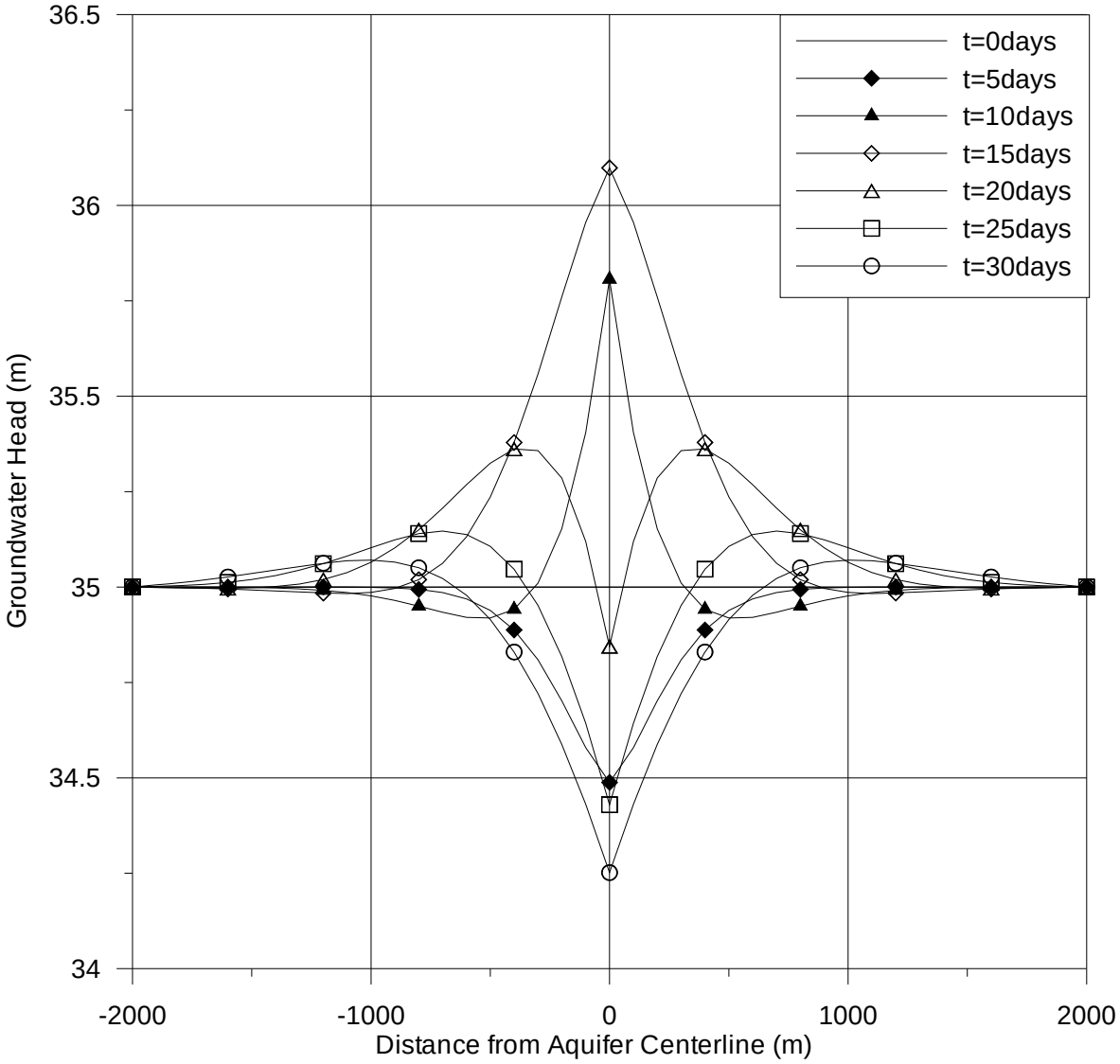

Figure 18. Groundwater head profile at various times along the transect-3 (P2-S2)

4.3. Lower Altamaha Watershed

The proposed model is also applied to the Altamaha River basin in southern Georgia. The modeling domain includes a portion of the Altamaha and Ohoopee rivers. It covers the drainage area bounded by the USGS stream gaging stations at Baxley, Reidsville and Doctortown. This area is discretized by 7,031 nodal points and 6,828 quadrilateral finite elements in the groundwater flow zone and 394 nodal points in the channel flow zone. The average element side length along the river sections varies from 150 m to 400 m and about 1000 m elsewhere. The discretized modeling domain is shown in Figure 19.

An unconfined surfacial aquifer overlying the Upper Floridian aquifer is considered to be present in the entire area, with an average thickness of about 40 m. The aquifer consists primarily of unconsolidated, well sorted sand and silt soils. The soil types in the aquifer were determined using the State Soils Geographic Database (STATSGO) of Georgia developed by the US Department of Agriculture (STATSGO, 1998). The corresponding saturated hydraulic conductivities of these soils are assumed to follow the statistically averaged values provided by Carsel and Parrish (1988). The conductivity values used in the model was 1.25E-6m/s for silt loam soils, 4.05E-5m/s for loamy sand soils and 1.23E-5 m/s for sandy loam soils. In addition, a 0.3m thickness of river sediments is considered to be uniformly present along the channel system with a hydraulic conductivity of 6.94E-7m/s, representing silt material deposited in the channel bottoms. The Altamaha river system is modeled as a head-dependent line source that creates lateral in/out flow to/from the groundwater flow domain according to the relative values of the river and groundwater heads. The natural and artificial lakes and ponds in the basin are modeled as constant-head boundary conditions. Moreover, the external watershed boundary is simulated as a no-flux type boundary condition except for the immediate vicinity of the Altamaha River near Doctortown gage that is mostly characterized as marshland and modeled as a constant head boundary condition.

The cross-sectional areas of computational nodes in the channel flow domain are obtained by using (i) the measurements taken at the gaging stations by USGS; (ii) the profiles of highway bridges along the river channels; and, (iii) the topographic maps of the area. The Manning's roughness coefficients used in simulations vary between 0.020 to 0.030 within the main channel and 0.030 to 0.070 along the floodplain. The simulation period covers a two-month period starting with 09/01/1997 through 11/01/1997 with a common time step of 6 hrs for both the groundwater and the channel flow domains. The discharge hydrographs at Baxley and Reidsville are used as the upstream boundary conditions of the channel model and the stage-discharge rating curve at Doctortown are used as the downstream boundary condition. The discharge hydrographs at Baxley and Reidsville can be seen in Figure 20. The single-valued stage-discharge rating curve at Doctortown is given in Figure 21.

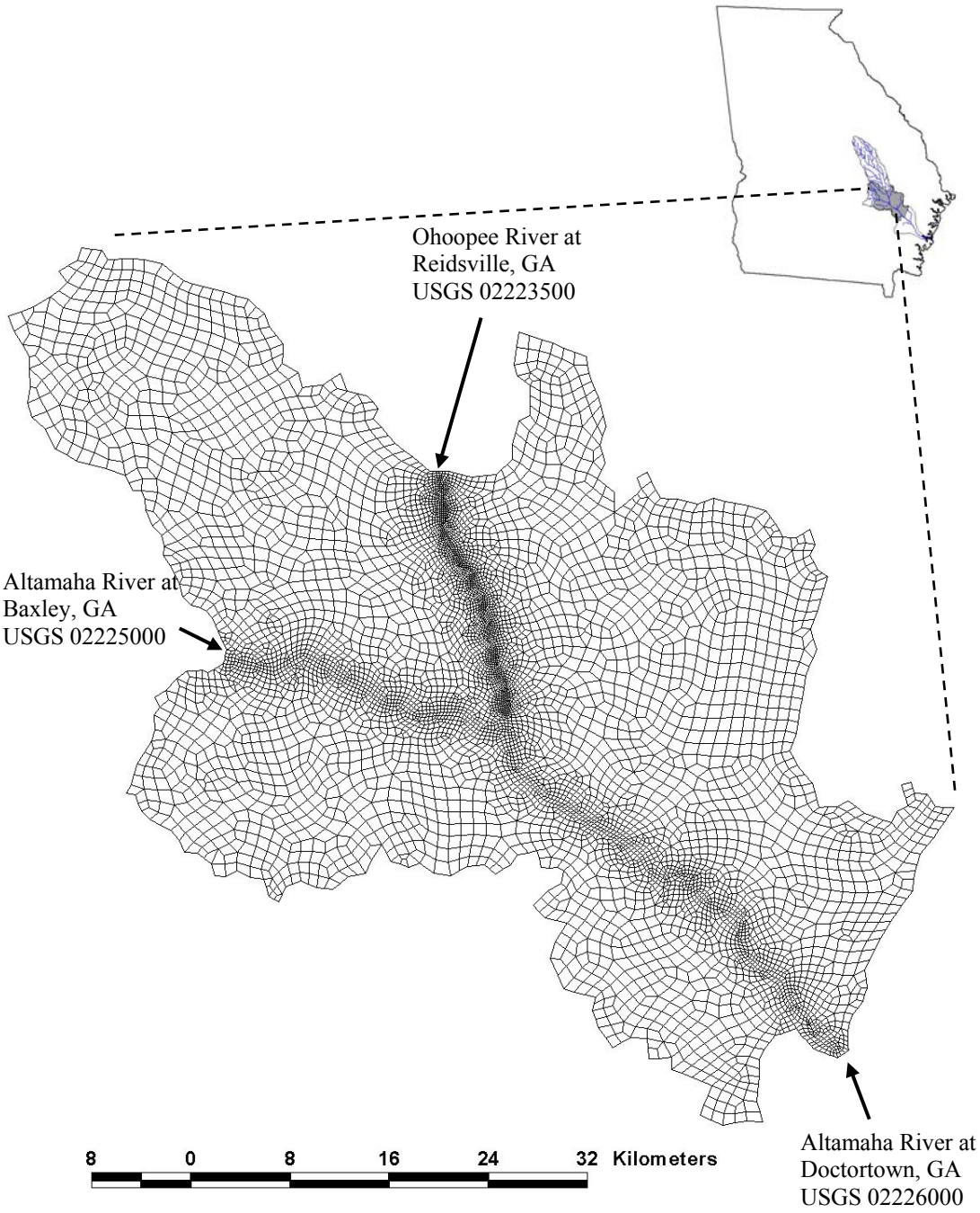

Figure 19. Discretized domain of Lower Altamaha River Basin

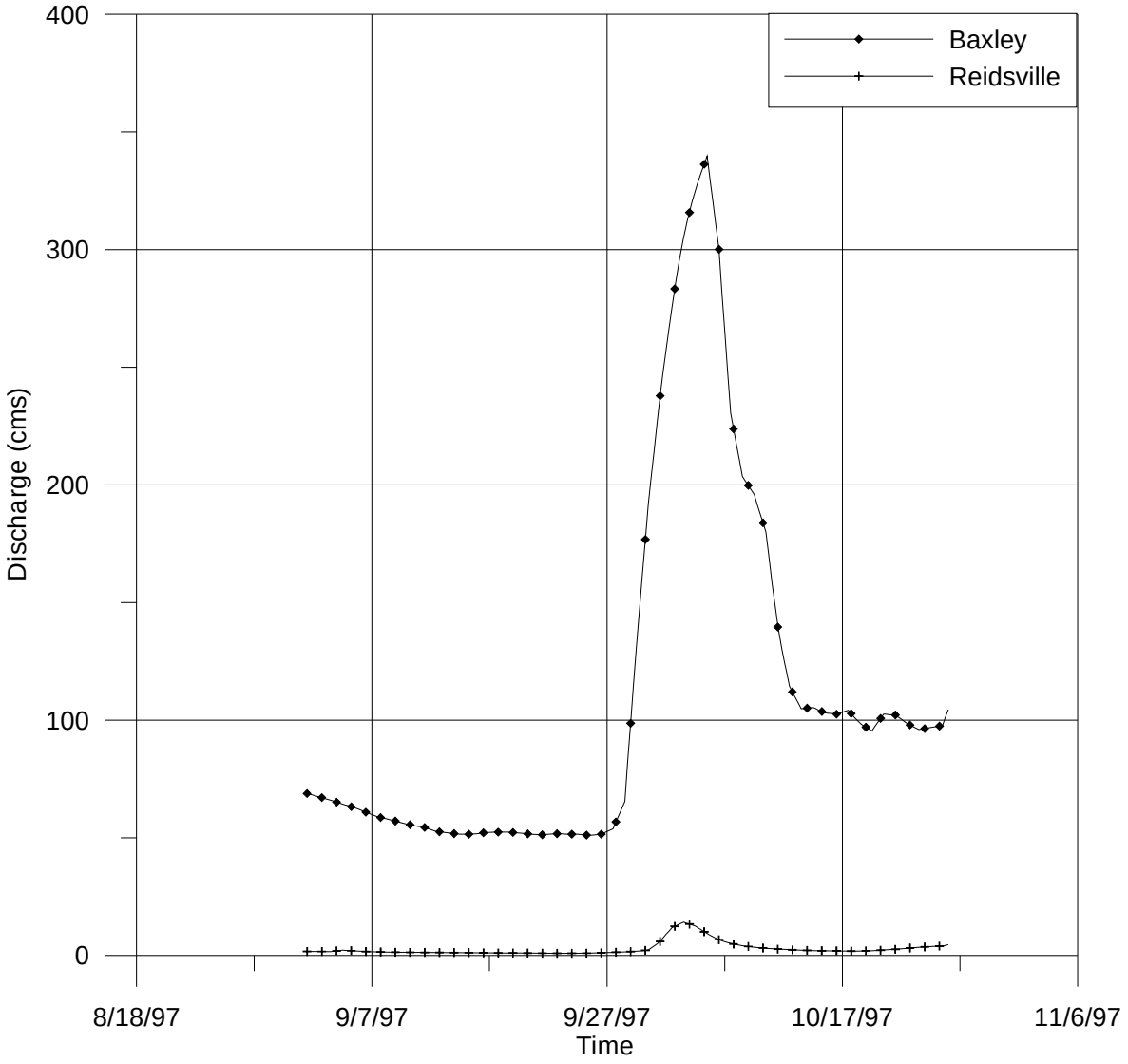

Figure 20. Discharge hydrographs observed in Baxley and Reidsville gaging stations

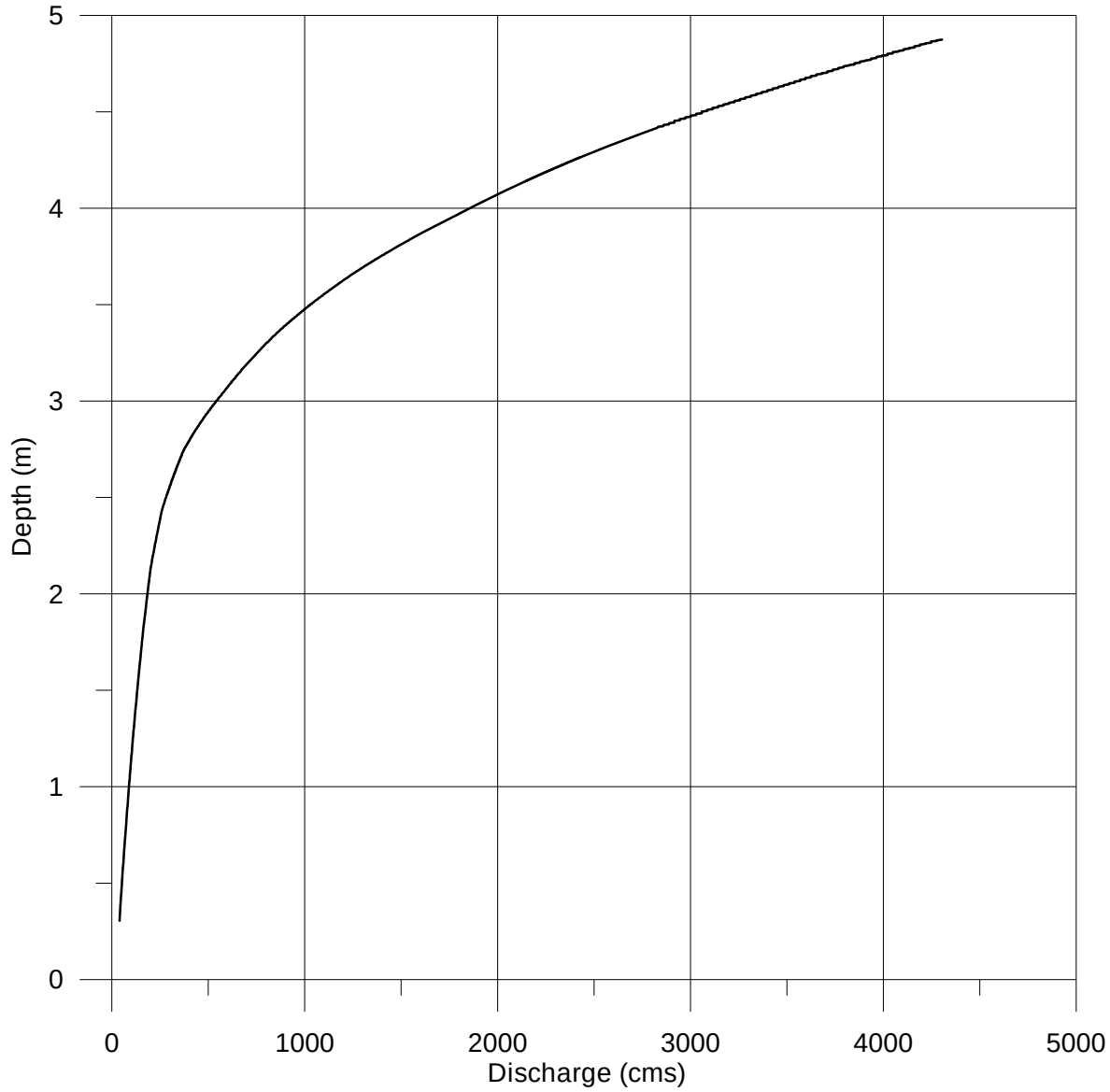

Figure 21. Doctortown gaging station rating curve

The stage and discharge hydrograph recorded at Doctortown is used as the calibration parameter. A comparison of simulation results vs. Doctortown gage measurements are shown in Figure 22 and 23. As seen from the figure, the model simulations are found to be very close to the gage measurements. The maximum error between the measured and simulated stage values is calculated to be 1.2% and the mean error is calculated to be below 1%. Similarly, the maximum error between the measured and simulated discharge values is calculated to be 10% and the mean error is calculated to be below 2%. These values are well below the accepted deviations reported in the literature (Fread, 1985). Part of these errors is associated with the contributions from the tributaries of the Altamaha River between Baxley and Doctortown gages. These are not quantified and not modeled in the simulations. Hence, the discharge in the river is modeled to be less than measured. Another possible source of error can be attributed to the quality of input data used in simulations including the channel cross-sections and river bottom slopes. These datasets are created mostly from the measurements taken at the gaging stations by USGS and the profiles of highway bridges along the river channels; and partly from the topographic maps of the area. Any possible errors in the creation of these datasets are reflected in the modeling results.

The groundwater head contours obtained at the time of peak flood time (i.e., 09/13/1997) are shown in Figure 24. The head contours in the surfacial aquifer mostly follow the surface elevation. The groundwater head contours are consistent with the river positions within the domain. Most of the closed contours are attributed to the natural and artificial ponds and lakes that are included in the simulations as constant head boundary conditions. Along all no-flux boundaries of the domain, the groundwater contours make perfect right angles representing the absence of any flow out of these boundaries. Due to the large nodal spacing used along the channel vicinity (about 300m), small hydraulic conductivity values of the aquifer and the non-symmetric nodal positions in both banks of the river, the entire behavior of the bank-storage effect along the channel is not clearly represented as shown in previous problems.

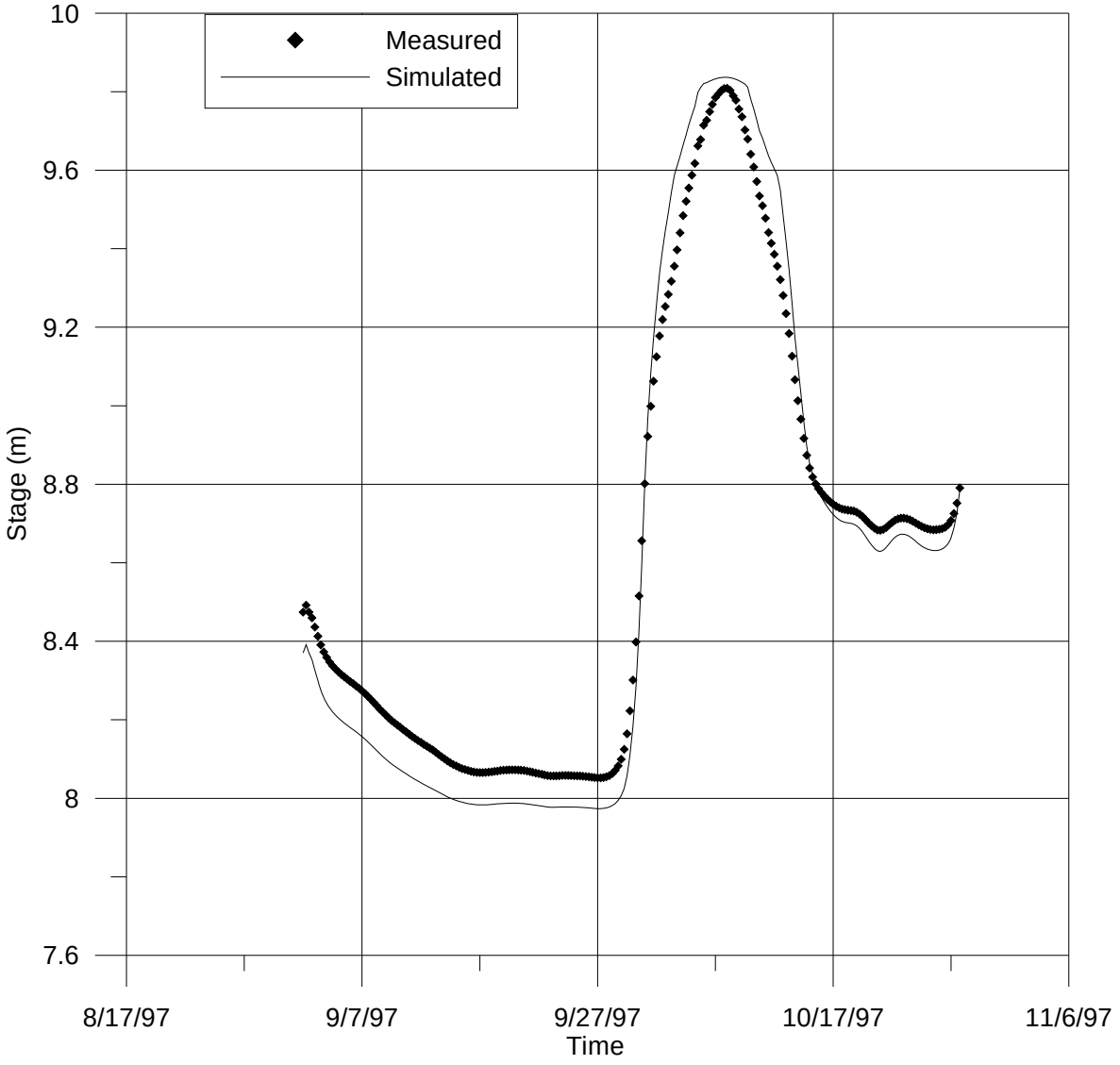

Figure 22. Simulated vs. measured stage values in Doctortown gaging station

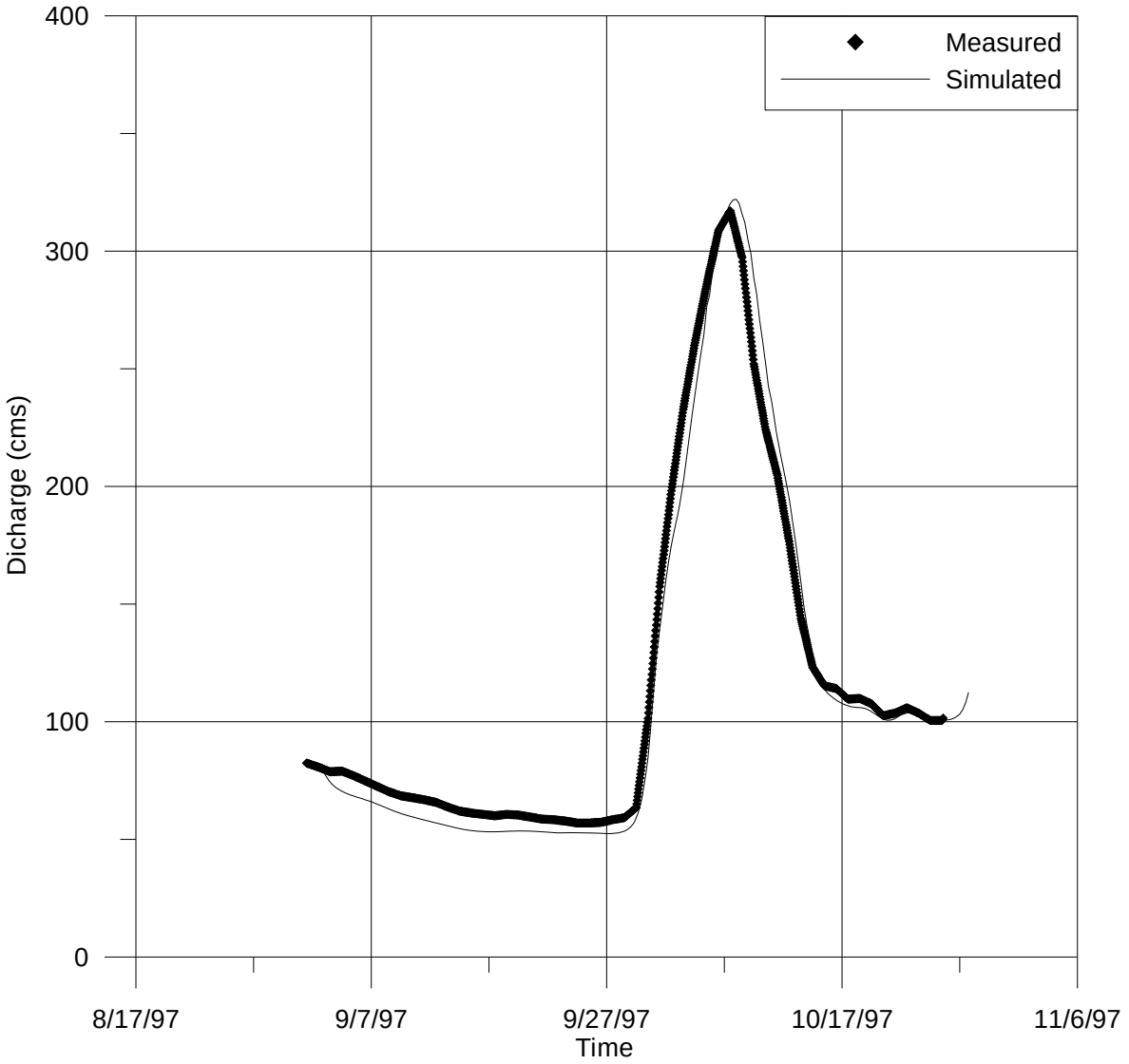

Figure 23. Simulated vs. measured discharge values in Doctortown gaging station

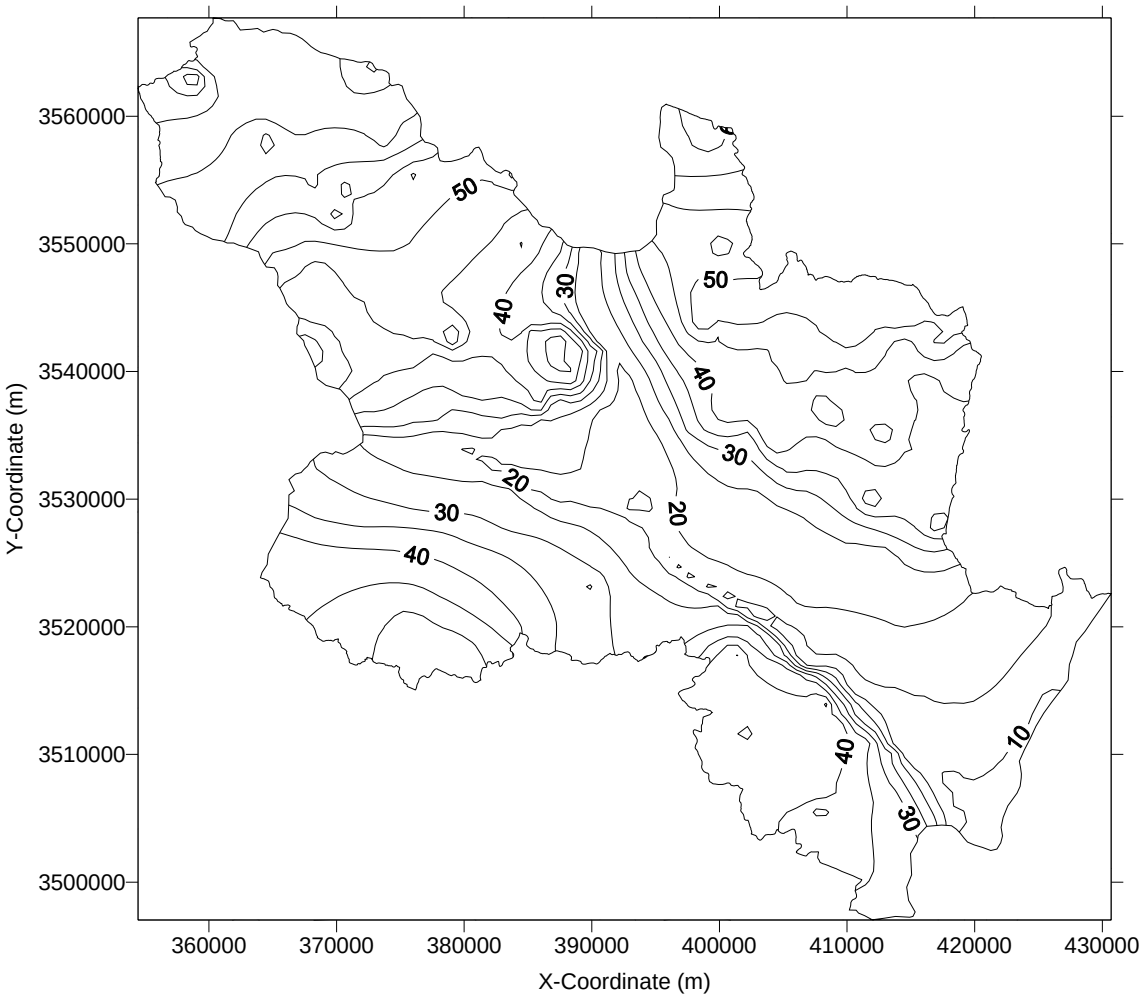

Figure 24. Groundwater head distribution in the project area at 09/13/1997

5. Conclusions

A new solution strategy is proposed to solve surface and subsurface flow systems in a coupled manner. In this regard, a one-dimensional channel flow model is coupled with a two-dimensional vertically-averaged groundwater flow model via the lateral flow interactions beneath the channel bottom. Instead of implementing the commonly applied iterative solution technique, the proposed method is based on the idea of solving the two systems in a simultaneous manner within a single global matrix format. The model is applicable to systems with non-looped channel networks overlying a non-uniform, anisotropic unconfined aquifer. The link between the two domains is provided by the lateral flow term. Three applications of the model are performed on hypothetical and existing systems to test its response characteristics to imaginary systems as well as capabilities to simulate real systems. The model results indicated good predictive capability of combined surface-subsurface systems. Therefore, it is proposed as an alternative tool for analyzing the hydrologic patterns in large watersheds.

References

Akan, A.O. and Yen, B.C. (1981a). "Mathematical model of shallow water flow over porous media." *Journal of the Hydraulics Division, ASCE*, Vol. 107, No. HY4, pp. 479-494.

Akan, A.O. and Yen. B.C. (1981b). "Diffusion-wave flood routing in channel networks". *Journal of the Hydraulics Division, ASCE*, Vol. 107, No. HY 6, pp. 719-732.

Amein, M. and Fang, C. S. (1970). "Implicit flood routing in natural channels." *Journal of the Hydraulics Division, ASCE*, Vol. 96, No. HY 12, pp. 2481-2500.

Aral, M.M. (1990). *Groundwater modeling in multilayer aquifers: Unsteady flow.* Lewis Publishers, Inc. 143p.

Carsel, R. F. and Parrish, R. S., (1988). "Developing joint probability distributions of soil water retention characteristics." *Water Resources Research*, Vol. 24, No. 5, pp. 755-769.

Chaundhry, Y. M. and Contractor, D. N. (1973). "Application of implicit method to surges in channels." *Water Resources Research*, Vol. 9, No. 6, pp. 1605-1612.

Cunningham, A.B. and Sinclair, P.J. (1979). "Application and analysis of a coupled surface and groundwater model." *Journal of Hydrology*, Vol. 43, pp. 129-148.

Fread, D. L. (1974). *Numerical properties of implicit four point finite difference equations of unsteady flow.* NOAA Technical Memo NWS HYDRO-18, U.S. Department of Commerce, National Weather Service, Silver Spring, Maryland.

Fread, D. L. (1985). "Chapter 14: Channel Routing." *Hydrological Forecasting,* ed. M. G. Anderson and T. P. Burt, John Wiley and Sons Ltd, pp. 437-503.

Fread, D.L. (1993). "Flow Routing." *Handbook of Hydrology*, ed. D.R. Maidment, McGraw-Hill, Inc. pp. 10.1-10.36.

Freeze, R.A. (1972). "Role of subsurface flow in generating surface runoff: 1. Base flow contributions to channel flow." *Water Resources Research*, Vol. 8, No. 3, pp. 609-623.

Gunduz, O. and Aral, M.M. (2003). "Simultaneous solution of coupled surface water / groundwater flow systems." *River Basin Management 2003,* pp. 25-33, WIT Press, UK.

Harris, J.W. and Stocker H., 1998. *Handbook of Mathematics and Computational Science*. Springer-Verlag, Inc., New York, 1028p.

Huyakorn, P.S., Springer, E.P., Guvanasen, V. and Wardsworth, T.D. (1986). "A three-dimensional finite element model for simulating water flow in variably-saturated porous media." *Water Resources Research*, Vol. 22, No. 13, pp. 1790-1808.

Jha, R., Herath, S. and Musiake, K. (2000). "River network solution for a distributed hydrological model and applications". *Hydrological Processes*, Vol. 14, pp. 575-592.

McDonald, M.G. and Harbaugh, A.W. (1998). "A modular three-dimensional finite difference groundwater flow model." *U.S. Geological Survey Techniques of Water Resources Investigations,* Book 6, Chapter A1, 586p.

Morita, M. and Yen, B.C. (2002). "Modeling of conjunctive two-dimensional surface-three dimensional subsurface flows." *Journal of Hydraulic Engineering*, ASCE, Vol. 128, No. 2, pp. 184-200.

Pinder, G.F. and Sauer, S.P. (1971). "Numerical simulation of flood wave modification due to bank storage effects." *Water Resources Research*, Vol. 7, No. 1, pp. 63-70.

Preissmann, A. (1961). "Propagation of translatory waves in channels and rivers." *Proceedings of the First Congress of French Association for Computation*, Grenoble, France, pp. 433-442.

Smith, R.E. and Woolhiser, D.A. (1971). "Overland flow on an infiltrating surface." *Water Resources Research*, Vol. 7, No. 4, pp. 899-913.

STATSGO (1998). State soil geographic (STATSGO) database of Georgia. Georgia GIS Data Clearinghouse: http://gis1.state.ga.us

Sturm, T. W. (2001). *Open Channel Hydraulics.* McGraw Hill Inc., 493p.

Swain, E.D. and Wexler, E.J. (1991). "A coupled surface water and groundwater model." *Proceedings of the 1991 National Conference on Irrigation and Drainage, Honolulu, Hawaii,* pp. 330-336.

VanderKwaak, J.E. and Loague, K. (2001). "Hydrologic-response simulations for the R-5 catchment with a comprehensive physics-based model." *Water Resources Research*, Vol. 37, No. 4, pp. 999-1013.

Zienkiewicz, O.C. and Taylor, R.L. (1989). *The Finite Element Method: Volume 1 Basic Formulation and Linear Problems*. McGraw-Hill Book Company, 648p.

Appendix I. Derivation of Finite Difference Equations of Channel Flow

The finite difference equations of continuity, momentum and boundary condition equations of channel flow are derived in this appendix. For each channel of the network, the continuity and momentum equations given in Equations (1) and (2) are discretized in the *x*-*t* plane using the "four-point" weighted difference implicit scheme. Two additional equations are then used to represent the conditions in the upstream and downstream boundaries of the channel. When this procedure is done for all channels, a system of *2N* equations is formed which is then solved to evaluate the unknown discharge and stage at the discretized nodes. The discretized forms of the continuity, momentum and boundary condition equations are given in the following sections.

Channel Network

In order to assist the derivation, the sample network shown in Figure 25 is used in the following discussion. This network contains 5 channels and 2 junctions. The channel numbering scheme starts from the most upstream channel and follows the direction of flow. When a junction is reached, the node numbering continues from the next channel's most upstream node and follows sequentially up to the junction until all inflowing channels are numbered sequentially. When all inflowing channels are numbered for a particular junction, node numbering continues with the most upstream node of the outflowing channel. This procedure is continued until the entire system is numbered.

Discretized forms of continuity and momentum equations

The finite difference discretization of continuity and momentum equations is done for all channels as shown in Figure 26. It can be seen from Figure 26 that the solution plane for channel k is represented by a total of N_k nodes with local node numbers starting from 1 and running through N_k. In the four-point scheme, the approximations of derivatives and constant terms are given in Equations (55), (56) and (57) for a dummy parameter E:

$$\frac{\partial E}{\partial t} = \psi \frac{E_{i+1}^{j+1} - E_{i+1}^{j}}{\Delta t^{j}} + (1-\psi)\frac{E_{i}^{j+1} - E_{i}^{j}}{\Delta t^{j}} \tag{55}$$

$$\frac{\partial E}{\partial x} = \theta \frac{E_{i+1}^{j+1} - E_{i}^{j+1}}{\Delta x_i} + (1-\theta)\frac{E_{i+1}^{j} - E_{i}^{j}}{\Delta x_i} \tag{56}$$

$$E = \theta \frac{E_{i+1}^{j+1} + E_{i}^{j+1}}{2} + (1-\theta)\frac{E_{i+1}^{j} + E_{i}^{j}}{2} \tag{57}$$

where i and j are subscripts for x and t axis, respectively, ψ and θ are weighing factors between 0 and 1, and Δx_i and Δt^j are reach length between nodes i and $i+1$, and time step between timelines j and $j+1$, respectively. It is possible to create different modifications of the scheme using different values for the weighing factors. A θ value of 0.0 and 0.5 corresponded to the "explicit" scheme and "box" scheme, respectively. Similarly, a scheme with a θ value of 1.0 is known as the "fully-implicit" scheme in space. Many researchers preferred using a ψ value of 0.5 and approximated the time derivative at the center of grid between $(j)^{th}$ and $(j+1)^{th}$ time lines (Amein and Fang, 1970; Chaudhry and Contractor, 1973) where as others used varying values depending on the particular application (Fread, 1985).

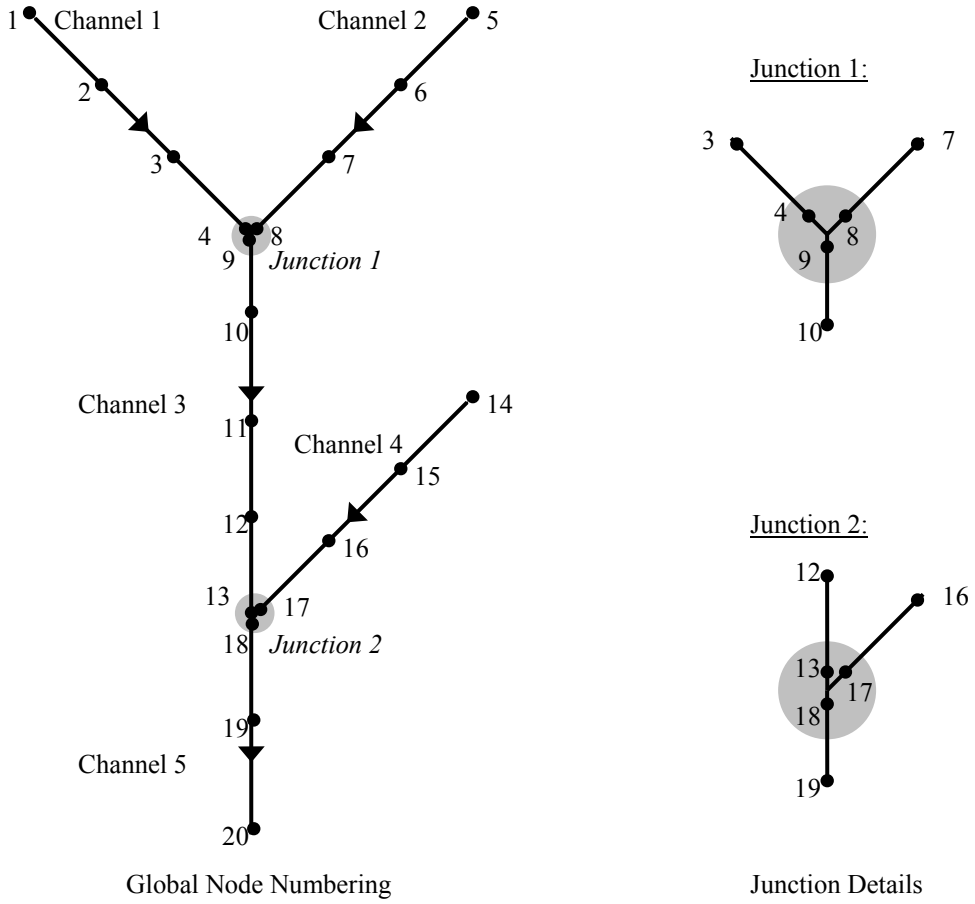

Figure 25. Sample channel network and numbering scheme

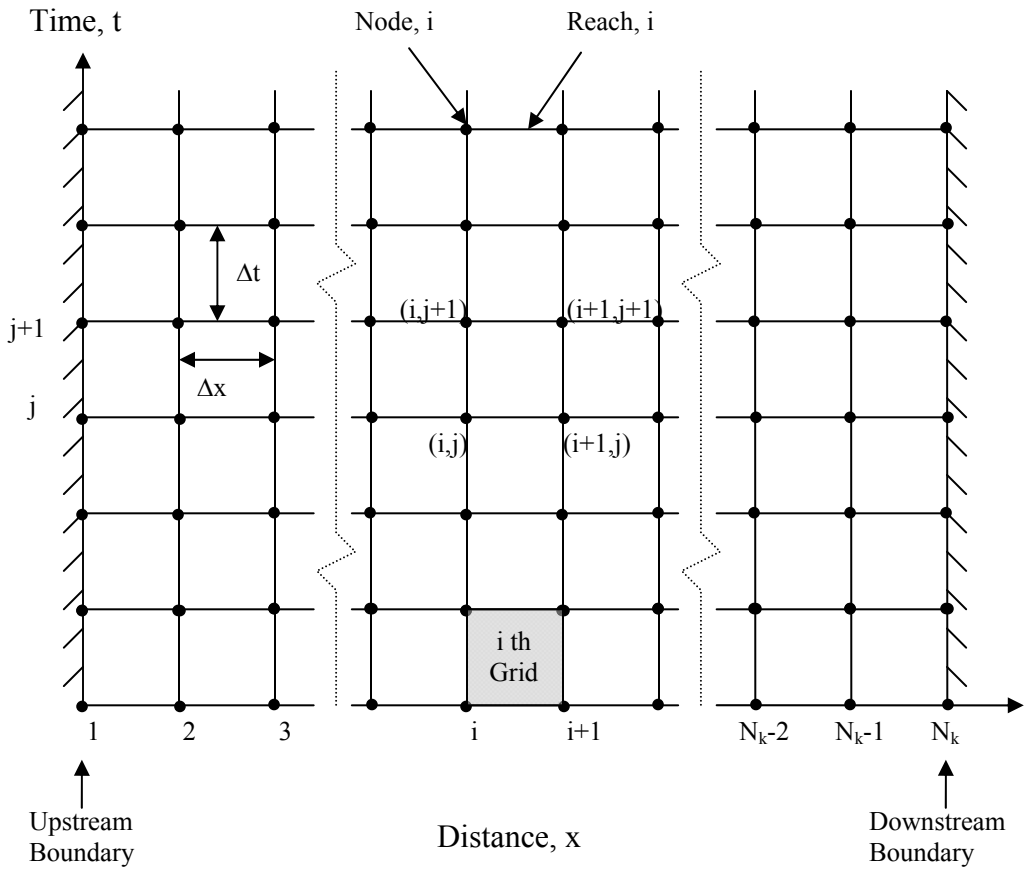

Figure 26. The distance-time grid used to formulate the implicit finite difference scheme for channel *k* (After Fread, 1974)

Fread (1974) has shown that the weighted four-point implicit scheme is unconditionally stable for any time step if the value of θ is selected between 0.5 and 1.0. In addition to stability criteria, he also analyzed the influence of the weighing factor on the accuracy of computations and found out that the accuracy decreases as θ departs from 0.5 and approaches to 1.0. He reported that this effect became more pronounced as the magnitude of the computational time step increased. Furthermore, his analysis revealed that a θ value of between 0.55 and 0.6 provided unconditional stability and good accuracy, which makes this scheme superior compared to the explicit scheme that requires time steps of less than a critical value determined by the Courant condition. With the template given in Equations (55), (56) and (57), the space derivatives in Equations (1) and (2) are approximated as:

$$\frac{\partial Q}{\partial x} = \theta \frac{Q_{i+1}^{j+1} - Q_i^{j+1}}{\Delta x_i} + (1-\theta)\frac{Q_{i+1}^{j} - Q_i^{j}}{\Delta x_i} \tag{58}$$

$$\frac{\partial h_r}{\partial x} = \theta \frac{h_{r\,i+1}^{\,j+1} - h_{r\,i}^{\,j+1}}{\Delta x_i} + (1-\theta)\frac{h_{r\,i+1}^{\,j} - h_{r\,i}^{\,j}}{\Delta x_i} \tag{59}$$

$$\frac{\partial\left(\beta Q^2 / A\right)}{\partial x} = \theta \frac{\left(\beta Q^2 / A\right)_{i+1}^{j+1} - \left(\beta Q^2 / A\right)_{i}^{j+1}}{\Delta x_i} + (1-\theta)\frac{\left(\beta Q^2 / A\right)_{i+1}^{j} - \left(\beta Q^2 / A\right)_{i}^{j}}{\Delta x_i} \tag{60}$$

Similarly, the time derivatives are approximated as:

$$\frac{\partial s_c\left(A + A_o\right)}{\partial t} = \frac{s_{c\,i+1/2}^{\,j+1}\left(A + A_o\right)_{i+1}^{j+1} - s_{c\,i+1/2}^{\,j}\left(A + A_o\right)_{i+1}^{j}}{2\Delta t^{\,j}} + \frac{s_{c\,i+1/2}^{\,j+1}\left(A + A_o\right)_{i}^{j+1} - s_{c\,i+1/2}^{\,j}\left(A + A_o\right)_{i}^{j}}{2\Delta t^{\,j}} \tag{61}$$

$$\frac{\partial s_m Q}{\partial t} = \frac{s_{m\,i+1/2}^{\,j+1} Q_{i+1}^{j+1} - s_{m\,i+1/2}^{\,j} Q_{i+1}^{j}}{2\Delta t^{\,j}} + \frac{s_{m\,i+1/2}^{\,j+1} Q_{i}^{j+1} - s_{m\,i+1/2}^{\,j} Q_{i}^{j}}{2\Delta t^{\,j}} \tag{62}$$

Finally, the constant terms such as q, S_f, S_e, L and A are approximated as:

$$q_L = \theta q_{L\,i+1/2}^{\,j+1} + (1-\theta) q_{L\,i+1/2}^{\,j} \tag{63}$$

$$S_f = \theta S_{f\,i+1/2}^{\,j+1} + (1-\theta) S_{f\,i+1/2}^{\,j} \tag{64}$$

$$S_e = \theta S_{e\,i+1/2}^{\,j+1} + (1-\theta) S_{e\,i+1/2}^{\,j} \tag{65}$$

$$L = \theta L_{i+1/2}^{j+1} + (1-\theta) L_{i+1/2}^{j} \tag{66}$$

$$A = \theta \frac{A_{i+1}^{j+1} + A_i^{j+1}}{2} + (1-\theta)\frac{A_{i+1}^{j} + A_i^{j}}{2} = \theta A_{i+1/2}^{j+1} + (1-\theta) A_{i+1/2}^{j} \tag{67}$$

where the variables with subscripts (i+½) are defined for the reach between nodes (i) and (i+1) as an average of the two nodal values. The following explicit formulations are used to define the above variables:

$$\left(q_L\right)_{i+1/2} = -K_{r\,i+1/2} w_{r\,i+1/2} \frac{h_{r\,i+1/2} - h_{g\,i+1/2}}{m_{r\,i+1/2}} \tag{68}$$

$$\left(S_f\right)_{i+1/2} = \frac{n_{i+1/2}^2 \left|Q_{i+1/2}\right| Q_{i+1/2}}{{c_1}^2 A_{i+1/2}^2 R_{hi+1/2}^{4/3}} = \frac{\left|Q_{i+1/2}\right| Q_{i+1/2}}{K_{i+1/2}^2} \tag{69}$$

$$\left(S_e\right)_{i+1/2} = \frac{K_{eci+1/2}}{2g\Delta x_i}\left[\left(\frac{Q}{A}\right)_{i+1}^2 - \left(\frac{Q}{A}\right)_i^2\right] \tag{70}$$

$$L_{i+1/2} = \frac{Q_{i+1/2} q_{Li+1/2}}{2A_{i+1/2}} \tag{71}$$

$$Q_{i+1/2} = \frac{Q_i + Q_{i+1}}{2} \tag{72}$$

$$R_{hi+1/2} = \frac{A_{i+1/2}}{w_{ri+1/2}} \approx \frac{A_{i+1/2}}{B_{i+1/2}} \tag{73}$$

$$A_{i+1/2} = \frac{A_i + A_{i+1}}{2} \tag{74}$$

$$B_{i+1/2} = \frac{B_i + B_{i+1}}{2} \tag{75}$$

$$K_{i+1/2} = \frac{K_i + K_{i+1}}{2} \tag{76}$$

$$K_{ri+1/2} = \frac{K_{ri} + K_{ri+1}}{2} \tag{77}$$

$$w_{ri+1/2} = \frac{w_{ri} + w_{ri+1}}{2} \approx \frac{B_i + B_{i+1}}{2} \tag{78}$$

$$h_{ri+1/2} = \frac{h_{ri} + h_{ri+1}}{2} \tag{79}$$

$$h_{gi+1/2} = \frac{h_{gi} + h_{gi+1}}{2} \tag{80}$$

The finite difference form of continuity equation is obtained when Equations (58) through (80) are substituted into (1) and rearranged for each channel in the network:

$$\theta\left[Q_{i+1}^{j+1}-Q_i^{j+1}-\Delta x_i\left[\left(-\frac{K_r w_r}{m_r}\right)_{i+1/2}^{j+1}\left(h_{r\,i+1/2}^{\;j+1}-h_{g\,i+1/2}^{\;j+1}\right)\right]\right]+$$

$$(1-\theta)\left[Q_{i+1}^{j}-Q_i^{j}-\Delta x_i\left[\left(-\frac{K_r w_r}{m_r}\right)_{i+1/2}^{j}\left(h_{r\,i+1/2}^{\;j}-h_{g\,i+1/2}^{\;j}\right)\right]\right]+ \qquad (81)$$

$$\frac{\Delta x_i}{2\Delta t^{\,j}}\begin{bmatrix} s_{c\,i+1/2}^{\;j+1}\left(A+A_o\right)_{i+1}^{j+1}+s_{c\,i+1/2}^{\;j+1}\left(A+A_o\right)_i^{j+1} \\ -s_{c\,i+1/2}^{\;j}\left(A+A_o\right)_{i+1}^{j}-s_{c\,i+1/2}^{\;j}\left(A+A_o\right)_i^{j}\end{bmatrix}=0$$

Similarly, the finite difference form of the momentum equation is obtained when Equations (58) through (80) are substituted into (2) and rearranged for each channel in the network (i.e., written for the lateral outflow case):

$$\frac{\Delta x_i}{2\Delta t^{\,j}}\left[s_{m\,i+1/2}^{\;j+1}Q_{i+1}^{j+1}+s_{m\,i+1/2}^{\;j+1}Q_i^{j+1}-s_{m\,i+1/2}^{\;j}Q_{i+1}^{j}-s_{m\,i+1/2}^{\;j}Q_i^{j}\right]+$$

$$\theta\left[\begin{array}{l}\left(\beta Q^2/A\right)_{i+1}^{j+1}-\left(\beta Q^2/A\right)_i^{j+1}+ \\ gA_{i+1/2}^{j+1}\left[h_{r\,i+1}^{\;j+1}-h_{r\,i}^{\;j+1}+\Delta x_i S_{f\,i+1/2}^{\;j+1}+\Delta x_i S_{e\,i+1/2}^{\;j+1}\right]+ \\ \Delta x_i\left(-\dfrac{Q_{i+1/2}^{j+1}}{2A_{i+1/2}^{j+1}}\right)\left[\left(-\dfrac{K_r w_r}{m_r}\right)_{i+1/2}^{j+1}\left(h_{r\,i+1/2}^{\;j+1}-h_{g\,i+1/2}^{\;j+1}\right)\right]\end{array}\right]+$$

$$(1-\theta)\left[\begin{array}{l}\left(\beta Q^2/A\right)_{i+1}^{j}-\left(\beta Q^2/A\right)_i^{j}+ \\ gA_{i+1/2}^{j}\left(h_{r\,i+1}^{\;j}-h_{r\,i}^{\;j}+\Delta x_i S_{f\,i+1/2}^{\;j}+\Delta x_i S_{e\,i+1/2}^{\;j}\right)+ \\ \Delta x_i\left(-\dfrac{Q_{i+1/2}^{j}}{2A_{i+1/2}^{j}}\right)\left[\left(-\dfrac{K_r w_r}{m_r}\right)_{i+1/2}^{j}\left(h_{r\,i+1/2}^{\;j}-h_{g\,i+1/2}^{\;j}\right)\right]\end{array}\right]=0 \qquad (82)$$

Since there is no contribution to momentum for the case of lateral inflow, the last terms inside the second and third brackets drop out.

Discretized forms of external boundary condition equations

At any upstream external boundary of a channel, a discharge or a stage hydrograph can be used as the boundary condition equation. The discretized forms of these equations are given as:

$$Q_m^{j+1} - Q_u(t) = 0 \tag{83}$$

$$h_{r\,m}^{\;j+1} - h_u(t) = 0 \tag{84}$$

where subscript *m* represents the global upstream node number of the channel. For a single channel system, *m* takes the value 1. In the sample network, channels 1, 2 and 4 have external upstream conditions and m takes values 1, 5 and 14, respectively. Since the proposed model does not allow looped networks, only one external downstream boundary condition can be included in the model. The boundary condition at the downstream external boundary can also be defined as a discharge or a stage hydrograph. The discretized forms of these equations are given as:

$$Q_N^{j+1} - Q_d(t) = 0 \tag{85}$$

$$h_{r\,N}^{\;j+1} - h_d(t) = 0 \tag{86}$$

where *N* represents the last node in the entire network. In the case of the sample network shown in Figure 25, *N* takes the value of 20. In addition to the stage and discharge conditions, the external downstream boundary condition can also be specified as a single-valued rating curve, a looped-rating curve and a critical depth section. If a single-valued rating curve is used as the downstream boundary condition, the discretized form becomes:

$$\mathrm{Q}_N^{j+1} - \left[Q^k + \frac{Q^{k+1} - Q^k}{h_r^{k+1} - h_r^k} \left[h_{r\,N}^{\;j+1} - h^k \right] \right] = 0 \tag{87}$$

where subscript *k* represents the values from the rating curve data. If a looped-valued rating curve is used as the downstream boundary condition, the discretized form becomes:

$$Q_N^{j+1} - c_1 \left(\frac{AR_h^{\,2/3}}{n} \right)_N^{j+1} \left(S_f^{1/2} \right)_{N-1/2}^{j+1} = 0 \tag{88}$$

where the friction slope is approximated using the known values of discharge and stage at the downstream reach:

$$\left(S_f\right)_{N-1/2}^{j+1} \approx -\frac{1}{gA_N^j}\left(\frac{Q_N^j - Q_N^{j-1}}{\Delta t^{j-1/2}}\right) - \frac{1}{gA_N^j}\left(\frac{\left(Q^2/A\right)_N^j - \left(Q^2/A\right)_{N-1}^j}{\Delta x_{N-1}}\right) - \left(\frac{h_{r\,N}^{\ j} - h_{r\,N-1}^{\ j}}{\Delta x_{N-1}}\right) \quad (89)$$

Finally, if a critical depth section is used as the downstream boundary condition, the discretized form becomes:

$$Q_N^{j+1} - \sqrt{\frac{g}{B_N^{j+1}}}\left(A^{3/2}\right)_N^{j+1} = 0 \quad (90)$$

Discretized forms of internal boundary condition equations

When the external boundary conditions are implemented, it is observed that certain channels do not have any upstream and downstream boundary condition. These missing conditions occur at the junction points of these channels. Therefore, internal boundary conditions are written to satisfy the mass and momentum balance at these junctions. For any junction with *m* inflowing channels, it is required to specify a total of *m+1* internal boundary condition. These conditions are specified as *m* downstream boundary conditions for each inflowing channel and one upstream boundary condition for the outflowing channel. In this regard, one momentum equation is written for each inflowing channel satisfying the continuity in stages.

$$h_{r\,i}^{\ j+1} - h_{r\,o}^{\ j+1} = 0 \quad (91)$$

where subscript *i* now represent the last node of the particular inflowing channel to the junction and subscript *o* represent the first node of the outflowing channel from the junction. When (91) is written is for all inflowing channels, a total of *m* equations are written for the junction and the missing internal downstream boundary condition of all inflowing channels are completed. Finally, one last condition is specified to get the missing internal upstream boundary condition of the outflowing channel. This condition is satisfied by writing the continuity equation for the junction:

$$\sum_{k=1}^{m} Q_i^{j+1} - Q_o^{j+1} = 0 \quad (92)$$

where *i* represents the last node of channel *k*. For the first junction of the particular network shown in Figure 25, the internal downstream boundary conditions of the inflowing channels 1 and 2 is specified by:

$$h_{r\,4}^{\ j+1} - h_{r\,9}^{\ j+1} = 0 \quad (93)$$

$$h_{r8}^{j+1} - h_{r9}^{j+1} = 0 \tag{94}$$

and the internal upstream boundary condition of the outflowing channel 3 is specified by:

$$Q_4^{j+1} + Q_8^{j+1} - Q_9^{j+1} = 0 \tag{95}$$

Similarly, for the second junction of the particular network shown in Figure 25, the internal downstream boundary conditions of the inflowing channels 3 and 4 is specified by:

$$h_{r13}^{j+1} - h_{r18}^{j+1} = 0 \tag{96}$$

$$h_{r17}^{j+1} - h_{r18}^{j+1} = 0 \tag{97}$$

and the internal upstream boundary condition of the outflowing channel 5 is specified by:

$$Q_{13}^{j+1} + Q_{17}^{j+1} - Q_{18}^{j+1} = 0 \tag{98}$$

Appendix II. Derivation of Partial Derivatives of the Finite Difference Equations of Channel Flow

The Newton-Raphson technique is based on the analytical or numerical differentiation of the continuity and momentum equations to evaluate the partial derivative terms of the Jacobian matrix. The difference forms of continuity and momentum equations given in (25) and (26) are partially differentiated with respect to the unknown terms h_r and Q at the $(j+1)^{th}$ time line for the nodal points (i) and $(i+1)$. In the following derivations, the continuity and momentum equations are represented by the letters "C" and "M", and the external upstream and external downstream boundary condition equations are represented by the letters "UB" and "DB", respectively, for clarity. Similarly, the internal boundary condition equations are represented by the letter "IB".

Partial Derivatives of the Continuity Equation

The partial derivatives of the continuity equation with respect to the unknown terms (i.e., h_i, h_{i+1}, Q_i and Q_{i+1} at $(j+1)^{th}$ time line) are computed as follows:

$$\frac{\partial C}{\partial h_{ri}^{\,j+1}} = -\theta\Delta x_i\left(-\frac{K_r}{m_r}\right)_{i+1/2}^{j+1}\left[\frac{1}{2}B_{i+1/2}^{j+1}+\frac{1}{2}\frac{\Delta B_i^{j+1}}{\Delta h_{ri}^{\,j+1}}\left(h_{ri+1/2}^{\,j+1}-h_{gi+1/2}^{\,j+1}\right)\right] + \frac{\Delta x_i}{2\Delta t^{j}}\left[s_{ci+1/2}^{\,j+1}\left(B+B_o\right)_i^{j+1}\right] \tag{99}$$

$$\frac{\partial C}{\partial h_{ri+1}^{\,j+1}} = -\theta\Delta x_i\left(-\frac{K_r}{m_r}\right)_{i+1/2}^{j+1}\left[\frac{1}{2}B_{i+1/2}^{j+1}+\frac{1}{2}\frac{\Delta B_{i+1}^{j+1}}{\Delta h_{ri+1}^{\,j+1}}\left(h_{ri+1/2}^{\,j+1}-h_{gi+1/2}^{\,j+1}\right)\right] + \frac{\Delta x_i}{2\Delta t^{j}}\left[s_{ci+1/2}^{\,j+1}\left(B+B_o\right)_{i+1}^{j+1}\right] \tag{100}$$

$$\frac{\partial C}{\partial Q_i^{j+1}} = -\theta \tag{101}$$

$$\frac{\partial C}{\partial Q_{i+1}^{j+1}} = \theta \tag{102}$$

Partial Derivatives of the Momentum Equation

The partial derivatives of the momentum equation with respect to unknown terms (i.e., h_i, h_{i+1}, Q_i and Q_{i+1} at $(j+1)^{th}$ time line) are computed as follows:

$$\frac{\partial M}{\partial h_{ri}^{j+1}} = \frac{\partial M}{\partial A_i^{j+1}} \frac{\partial A_i^{j+1}}{\partial h_{ri}^{j+1}}$$

$$= \theta \left[\begin{array}{l} \left(\frac{\beta Q^2 B}{A^2} \right)_i^{j+1} + g A_{i+1/2}^{j+1} \left(-1 + \Delta x_i \frac{\partial S_{f\,i+1/2}^{j+1}}{\partial h_{ri}^{j+1}} + \Delta x_i \frac{\partial S_{e\,i+1/2}^{j+1}}{\partial h_{ri}^{j+1}} \right) \\ + \frac{1}{2} g B_i^{j+1} \left(h_{ri+1}^{j+1} - h_{ri}^{j+1} + S_{f\,i+1/2}^{j+1} \Delta x_i + S_{e\,i+1/2}^{j+1} \Delta x_i \right) + \Delta x_i \frac{\partial L_{i+1/2}^{j+1}}{\partial h_{ri}^{j+1}} \end{array} \right] \quad (103)$$

where:

$$\frac{\partial S_{f\,i+1/2}^{j+1}}{\partial h_{ri}^{j+1}} = S_{f\,i+1/2}^{j+1} \left[\frac{2}{n_{i+1/2}^{j+1}} \frac{\Delta n_{i+1/2}^{j+1}}{\Delta h_{ri}^{j+1}} - \frac{5}{3} \frac{B_i^{j+1}}{A_{i+1/2}^{j+1}} + \frac{2}{3 B_{i+1/2}^{j+1}} \frac{\Delta B_i^{j+1}}{\Delta h_{ri}^{j+1}} \right] \quad (104)$$

$$\frac{\partial S_{e\,i+1/2}^{j+1}}{\partial h_{ri}^{j+1}} = \frac{K_{ec\,i+1/2}^{j+1} \left(Q^2 \right)_i^{j+1} B_i^{j+1}}{g \Delta x_i \left(A^3 \right)_i^{j+1}} \quad (105)$$

$$\frac{\partial L_{i+1/2}^{j+1}}{\partial h_{ri}^{j+1}} = \left\{ \begin{array}{l} 0 \\ - \frac{Q_{i+1/2}^{j+1} q_{L\,i+1/2}^{j+1}}{2 A_{i+1/2}^{j+1}} \left[- \frac{B_i^{j+1}}{2 A_{i+1/2}^{j+1}} + \frac{1}{2 B_{i+1/2}^{j+1}} \frac{\Delta B_i^{j+1}}{\Delta h_{ri}^{j+1}} + \frac{1}{2 \left(h_{ri+1/2}^{j+1} - h_{g\,i+1/2}^{j+1} \right)} \right] \end{array} \right. \quad (106)$$

$$\frac{\partial M}{\partial h_{ri+1}^{j+1}} = \frac{\partial M}{\partial A_{i+1}^{j+1}} \frac{\partial A_{i+1}^{j+1}}{\partial h_{ri+1}^{j+1}}$$

$$= \theta \left[\begin{array}{l} - \left(\frac{\beta Q^2 B}{A^2} \right)_{i+1}^{j+1} + g A_{i+1/2}^{j+1} \left(1 + \Delta x_i \frac{\partial S_{f\,i+1/2}^{j+1}}{\partial h_{ri+1}^{j+1}} + \Delta x_i \frac{\partial S_{e\,i+1/2}^{j+1}}{\partial h_{ri+1}^{j+1}} \right) \\ + \frac{1}{2} g B_{i+1}^{j+1} \left(h_{ri+1}^{j+1} - h_{ri}^{j+1} + S_{f\,i+1/2}^{j+1} \Delta x_i + S_{e\,i+1/2}^{j+1} \Delta x_i \right) + \Delta x_i \frac{\partial L_{i+1/2}^{j+1}}{\partial h_{ri+1}^{j+1}} \end{array} \right] \quad (107)$$

where:

$$\frac{\partial S_{f\,i+1/2}^{j+1}}{\partial h_{ri+1}^{j+1}} = S_{f\,i+1/2}^{j+1} \left[\frac{2}{n_{i+1/2}^{j+1}} \frac{\Delta n_{i+1/2}^{j+1}}{\Delta h_{ri+1}^{j+1}} - \frac{5}{3} \frac{B_{i+1}^{j+1}}{A_{i+1/2}^{j+1}} + \frac{2}{3 B_{i+1/2}^{j+1}} \frac{\Delta B_{i+1}^{j+1}}{\Delta h_{ri+1}^{j+1}} \right] \quad (108)$$

$$\frac{\partial S_{e\,i+1/2}^{\;\;j+1}}{\partial h_{r\,i+1}^{\;\;j+1}} = \frac{K_{ec\,i+1/2}^{\;\;j+1}(Q^2)_{i+1}^{j+1} B_{i+1}^{j+1}}{g\Delta x_i (A^3)_{i+1}^{j+1}} \tag{109}$$

$$\frac{\partial L_{i+1/2}^{j+1}}{\partial h_{r\,i+1}^{\;\;j+1}} = \begin{cases} 0 \\ -\dfrac{Q_{i+1/2}^{j+1} q_{L\,i+1/2}^{\;\;j+1}}{2\overline{A}_i^{j+1}} \left[-\dfrac{B_{i+1}^{j+1}}{2A_{i+1/2}^{j+1}} + \dfrac{1}{2B_{i+1/2}^{j+1}} \dfrac{\Delta B_{i+1}^{j+1}}{\Delta h_{r\,i+1}^{\;\;j+1}} + \dfrac{1}{2\left(h_{r\,i+1/2}^{\;\;j+1} - h_{g\,i+1/2}^{\;\;j+1}\right)} \right] \end{cases} \tag{110}$$

$$\frac{\partial M}{\partial Q_i^{j+1}} = \frac{\Delta x_i}{2\Delta t^{\,j}} s_{m\,i+1/2}^{\;\;j+1} + \theta \left[-\left(\frac{2\beta Q}{A} \right)_i^{j+1} + g A_{i+1/2}^{j+1} \left(\Delta x_i \frac{\partial S_{f\,i+1/2}^{\;\;j+1}}{\partial Q_i^{j+1}} + \Delta x_i \frac{\partial S_{e\,i+1/2}^{\;\;j+1}}{\partial Q_i^{j+1}} \right) + \Delta x_i \frac{\partial L_{i+1/2}^{j+1}}{\partial Q_i^{j+1}} \right] \tag{111}$$

where:

$$\frac{\partial S_{f\,i+1/2}^{\;\;j+1}}{\partial Q_i^{j+1}} = S_{f\,i+1/2}^{\;\;j+1} \left[\frac{1}{n_{i+1/2}^{j+1}} \frac{\Delta n_{i+1/2}^{j+1}}{\Delta Q_{i+1/2}^{j+1}} + \frac{1}{Q_{i+1/2}^{j+1}} \right] \tag{112}$$

$$\frac{\partial S_{e\,i+1/2}^{\;\;j+1}}{\partial Q_i^{j+1}} = \frac{-K_{ec\,i+1/2}^{\;\;j+1} Q_i^{j+1}}{g\Delta x_i (A^2)_i^{j+1}} \tag{113}$$

$$\frac{\partial L_{i+1/2}^{j+1}}{\partial Q_i^{j+1}} = \begin{cases} 0 \\ -\dfrac{q_{L\,i+1/2}^{\;\;j+1}}{4\left(A^2\right)_{i+1/2}^{j+1}} \end{cases} \tag{114}$$

$$\frac{\partial M}{\partial Q_{i+1}^{j+1}} = \frac{\Delta x_{i+1/2}}{2\Delta t^{\,j+1/2}} s_{m\,i+1/2}^{\;\;j+1} + \theta \left[\left(\frac{2\beta Q}{A} \right)_{i+1}^{j+1} + g A_{i+1/2}^{j+1} \left(\Delta x_i \frac{\partial S_{f\,i+1/2}^{\;\;j+1}}{\partial Q_{i+1}^{j+1}} + \Delta x_i \frac{\partial S_{e\,i+1/2}^{\;\;j+1}}{\partial Q_{i+1}^{j+1}} \right) + \Delta x_i \frac{\partial L_{i+1/2}^{j+1}}{\partial Q_{i+1}^{j+1}} \right] \tag{115}$$

where:

$$\frac{\partial S_{f\,i+1/2}^{\;\;j+1}}{\partial Q_{i+1}^{j+1}} = S_{f\,i+1/2}^{\;\;j+1} \left[\frac{1}{n_{i+1/2}^{j+1}} \frac{\Delta n_{i+1/2}^{j+1}}{\Delta Q_{i+1/2}^{j+1}} + \frac{1}{Q_{i+1/2}^{j+1}} \right] \tag{116}$$

$$\frac{\partial S_{e\,i+1/2}^{\,j+1}}{\partial Q_{i+1}^{j+1}} = \frac{-K_{ec\,i+1/2}^{\,j+1} Q_{i+1}^{j+1}}{g\Delta x_i (A^2)_{i+1}^{j+1}} \tag{117}$$

$$\frac{\partial L_{i+1/2}^{j+1}}{\partial Q_i^{j+1}} = \begin{cases} 0 \\ -\dfrac{q_{L\,i+1/2}^{\,j+1}}{4\left(A^2\right)_{i+1/2}^{j+1}} \end{cases} \tag{118}$$

Partial Derivatives of the External Boundary Conditions

At upstream boundaries, a discharge or a stage hydrograph can be implemented as the boundary condition. When a discharge hydrograph is used as the upstream boundary condition, the partial derivatives of Jacobian become:

$$\frac{\partial UB}{\partial Q_i^{j+1}} = 1 \tag{119}$$

$$\frac{\partial UB}{\partial h_{r\,i}^{\,j+1}} = 0 \tag{120}$$

where subscript i represent the upstream node number of the channel. However, if a stage hydrograph is used as the upstream boundary condition, then the partial derivatives become:

$$\frac{\partial UB}{\partial Q_i^{j+1}} = 0 \tag{121}$$

$$\frac{\partial UB}{\partial h_{r\,i}^{\,j+1}} = 1 \tag{122}$$

At the downstream boundary, a discharge hydrograph, a stage hydrograph, a single-valued rating curve, a looped rating curve or a critical depth section can be implemented as the boundary condition. If a discharge hydrograph is used as the downstream boundary condition, the partial derivatives become:

$$\frac{\partial DB}{\partial Q_N^{j+1}} = 1 \tag{123}$$

$$\frac{\partial DB}{\partial h_{r\,N}^{j+1}} = 0 \tag{124}$$

If a stage hydrograph is used as the downstream boundary condition, the partial derivatives become:

$$\frac{\partial DB}{\partial Q_N^{j+1}} = 0 \tag{125}$$

$$\frac{\partial DB}{\partial h_{r\,N}^{j+1}} = 1 \tag{126}$$

For the single-valued rating curve, the partial derivatives can become:

$$\frac{\partial DB}{\partial Q_N^{j+1}} = 1 \tag{127}$$

$$\frac{\partial DB}{\partial h_{r\,N}^{j+1}} = -\left(\frac{Q^{k+1} - Q^k}{h_r^{k+1} - h_r^k} \right) \tag{128}$$

If a looped rating curve is used, the partial derivatives are written as:

$$\frac{\partial DB}{\partial Q_N^{j+1}} = 1 + Q' \left(\frac{1}{n} \frac{\Delta n}{\Delta Q} \right)_N^{j+1} \tag{129}$$

$$\frac{\partial DB}{\partial h_{r\,N}^{j+1}} = Q' \left(\frac{1}{n} \frac{\Delta n}{\Delta h_r} - \frac{5}{3} \frac{B}{A} + \frac{2}{3B} \frac{\Delta B}{\Delta h_r} \right)_N^{j+1} \tag{130}$$

where:

$$Q' = c_1 \left(\frac{A R_h^{\,2/3}}{n} \right)_N^{j+1} \left(S_f^{1/2} \right)_{N-1/2}^{j+1} \tag{131}$$

Finally, if a critical section is used at the downstream boundary, the partial derivatives are written as:

$$\frac{\partial DB}{\partial Q_N^{j+1}} = 1 \tag{132}$$

$$\frac{\partial DB}{\partial h_{r\,N}^{\,j+1}} = Q_{cr}\left(-\frac{3}{2}\frac{B}{A}+\frac{1}{2B}\frac{\Delta B}{\Delta h_r}\right)_N^{j+1} \tag{133}$$

where:

$$Q_{cr} = \sqrt{\frac{g}{B_N^{j+1}}}\left(A^{3/2}\right)_N^{j+1} \tag{134}$$

Partial Derivatives of the Internal Boundary Conditions

At any junction with *m* inflowing channels, a total of *m+1* internal boundary conditions are specified. The partial derivatives of the junction momentum equation shown in Equation (91) written for each inflowing channels become:

$$\frac{\partial IB}{\partial Q_i^{j+1}} = 0 \tag{135}$$

$$\frac{\partial IB}{\partial h_{r\,i}^{\,j+1}} = 1 \tag{136}$$

where subscript *i* represents the last node of the particular inflowing channel to the junction. Similarly, the partial derivatives of the junction momentum equation shown in Equation (91) written for the outflowing channel become:

$$\frac{\partial IB}{\partial Q_o^{j+1}} = 0 \tag{137}$$

$$\frac{\partial IB}{\partial h_{r\,o}^{\,j+1}} = -1 \tag{138}$$

where subscript *o* represents the first node of the outflowing channel from the junction. The partial derivatives of the junction continuity equation shown in Equation (92) written for each inflowing channels become:

$$\frac{\partial IB}{\partial Q_i^{j+1}} = 1 \tag{139}$$

$$\frac{\partial IB}{\partial h_{r\,i}^{\,j+1}} = 0 \tag{140}$$

where subscript *i* again represents the last node of the particular inflowing channel to the junction. Similarly, the partial derivatives of the junction continuity equation shown in Equation (92) written for the outflowing channel become:

$$\frac{\partial IB}{\partial Q_o^{j+1}} = -1 \tag{141}$$

$$\frac{\partial IB}{\partial h_{r\,o}^{\;j+1}} = 0 \tag{142}$$

Appendix III. Interpolating Functions in Galerkin Method

Interpolating (or basis/shape) functions form the core of the finite element analysis. There is a one-to-one relation between basis functions and nodes in the discretized domain. A basis function that is identified at a particular node is zero over any element unless that node is associated with the element of concern.

Theoretically, basis functions can be written in global or local coordinates. However, it is practical to use a local coordinate system with quadrilateral elements to simplify the integrations and differentiations of the basis functions. In this regard, a local coordinate system together with a master element concept is implemented in this study (Figure 27). A direct consequence of this approach is the necessity to formulate a transformation function between global and local coordinates. Unfortunately, this transformation is not linear for an irregular quadrilateral element and hence a numerical integration scheme is normally required to evaluate the integrals in the finite element analysis.

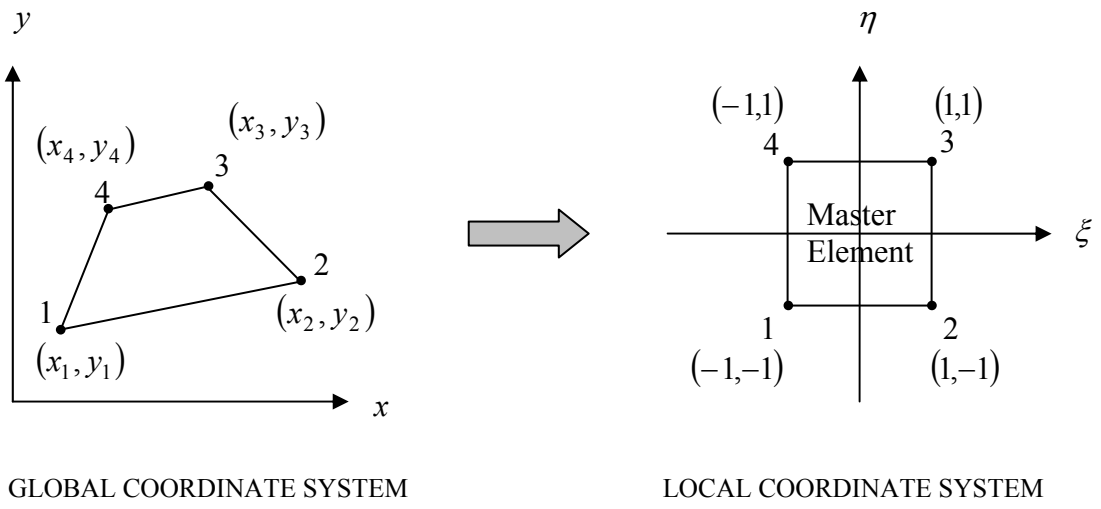

Figure 27. Global and local coordinate systems and the master element concept

In this method, the two dimensional domain is globally discretized using irregular quadrilateral elements. Then, coordinates of the nodes of each element is mapped to a local coordinate system via the master element concept. The master element is a 2X2 square located at the center of the local coordinate axes with nodes at each corner. The corner coordinates of the master element are (-1,-1), (1,-1), (1,1) and (-1,1). Therefore, all the integrations can be done on the master element using the limits $-1 \leq \xi \leq +1$ and $-1 \leq \eta \leq +1$. The general formula for the shape functions of a quadrilateral element can be obtained by taking the tensor product of the two shape functions for the linear line element and given by the expression:

$$N_i(\xi,\eta)=\frac{1}{4}(1+\xi\xi_i)(1+\eta\eta_i) \tag{143}$$

where ξ and η define the local coordinate system used with the master element concept. Using this formula and the local coordinates of the master element, it is possible to write the four shape functions of the quadrilateral element shown in Figure 27:

$$\begin{aligned} N_1(\xi,\eta)&=\frac{1}{4}(1-\xi)(1-\eta)\\ N_2(\xi,\eta)&=\frac{1}{4}(1+\xi)(1-\eta)\\ N_3(\xi,\eta)&=\frac{1}{4}(1+\xi)(1+\eta)\\ N_4(\xi,\eta)&=\frac{1}{4}(1-\xi)(1+\eta) \end{aligned} \tag{144}$$

There are two important modifications that should be done before the master element concept can be used in finite element analysis. The first one of these modifications is to transform the derivatives of the integrands to local coordinates. In order to implement this transformation from global to local coordinates, derivatives of these shape functions with respect to local coordinates are evaluated using the chain rule of differentiation:

$$\begin{aligned} \frac{\partial N_i}{\partial x}&=\frac{\partial N_i}{\partial \xi}\frac{\partial \xi}{\partial x}+\frac{\partial N_i}{\partial \eta}\frac{\partial \eta}{\partial x}\\ \frac{\partial N_i}{\partial y}&=\frac{\partial N_i}{\partial \xi}\frac{\partial \xi}{\partial y}+\frac{\partial N_i}{\partial \eta}\frac{\partial \eta}{\partial y} \end{aligned} \tag{145}$$

which can be represented in matrix form as:

$$\begin{bmatrix} \dfrac{\partial N_i}{\partial x}\\ \dfrac{\partial N_i}{\partial y} \end{bmatrix}=\begin{bmatrix} \dfrac{\partial \xi}{\partial x} & \dfrac{\partial \eta}{\partial x}\\ \dfrac{\partial \xi}{\partial y} & \dfrac{\partial \eta}{\partial y} \end{bmatrix}\begin{bmatrix} \dfrac{\partial N_i}{\partial \xi}\\ \dfrac{\partial N_i}{\partial \eta} \end{bmatrix} \tag{146}$$

The derivatives of the shape functions with respect to local coordinates can easily be computed as follows:

$$\begin{aligned}
\frac{\partial N_1}{\partial \xi} &= -\frac{1}{4}(1-\eta) & \frac{\partial N_1}{\partial \eta} &= -\frac{1}{4}(1-\xi) \\
\frac{\partial N_2}{\partial \xi} &= +\frac{1}{4}(1-\eta) & \frac{\partial N_2}{\partial \eta} &= -\frac{1}{4}(1+\xi) \\
\frac{\partial N_3}{\partial \xi} &= +\frac{1}{4}(1+\eta) & \frac{\partial N_3}{\partial \eta} &= +\frac{1}{4}(1+\xi) \\
\frac{\partial N_4}{\partial \xi} &= -\frac{1}{4}(1+\eta) & \frac{\partial N_4}{\partial \eta} &= +\frac{1}{4}(1-\xi)
\end{aligned} \tag{147}$$

The coefficient matrix, however, requires a functional relationship that maps the global coordinates to local coordinates. This transformation from global to local coordinates is obtained by using shape functions to interpolate the global coordinates. Hence, one can write:

$$\begin{aligned}
x &= x(\xi,\eta) = \sum_{i=1}^{4} x_i N_i(\xi,\eta) \\
y &= y(\xi,\eta) = \sum_{i=1}^{4} y_i N_i(\xi,\eta)
\end{aligned} \tag{148}$$

If the derivatives of these expressions are taken with respect to the local coordinates, one would obtain a 2X2 matrix that is commonly known as the Jacobian matrix:

$$[J] = \begin{bmatrix} \frac{\partial x}{\partial \xi} & \frac{\partial x}{\partial \eta} \\ \frac{\partial y}{\partial \xi} & \frac{\partial y}{\partial \eta} \end{bmatrix} = \begin{bmatrix} \sum_{i=1}^{4} x_i \frac{\partial N_i}{\partial \xi} & \sum_{i=1}^{4} x_i \frac{\partial N_i}{\partial \eta} \\ \sum_{i=1}^{4} y_i \frac{\partial N_i}{\partial \xi} & \sum_{i=1}^{4} y_i \frac{\partial N_i}{\partial \eta} \end{bmatrix} \tag{149}$$

The determinant of the Jacobian is an important quantity and is extensively used in the master element integrations using local coordinates.

$$\det[J] = |J| = \left(\sum_{i=1}^{4} x_i \frac{\partial N_i}{\partial \xi}\right)\left(\sum_{i=1}^{4} y_i \frac{\partial N_i}{\partial \eta}\right) - \left(\sum_{i=1}^{4} x_i \frac{\partial N_i}{\partial \eta}\right)\left(\sum_{i=1}^{4} y_i \frac{\partial N_i}{\partial \xi}\right) \tag{150}$$

It should be noted, however, that the matrix required to transform the derivatives in global coordinates to derivatives in local coordinates is not exactly the Jacobian matrix given above. The link between these two matrices can be established if an identity matrix is written such that:

$$\begin{bmatrix} 1 & 0 \\ 0 & 1 \end{bmatrix} = \begin{bmatrix} \frac{\partial \xi}{\partial x} & \frac{\partial \eta}{\partial x} \\ \frac{\partial \xi}{\partial y} & \frac{\partial \eta}{\partial y} \end{bmatrix} \begin{bmatrix} \frac{\partial x}{\partial \xi} & \frac{\partial y}{\partial \xi} \\ \frac{\partial x}{\partial \eta} & \frac{\partial y}{\partial \eta} \end{bmatrix} \tag{151}$$

In the above equation, the second matrix is simply the transpose of the Jacobian matrix. Since the identity matrix is obtained by multiplying a matrix and its inverse, the first matrix then becomes the inverse of the Jacobian transpose.

$$\begin{bmatrix} \frac{\partial \xi}{\partial x} & \frac{\partial \eta}{\partial x} \\ \frac{\partial \xi}{\partial y} & \frac{\partial \eta}{\partial y} \end{bmatrix} = \left[J^T\right]^{-1} = \frac{1}{|J|} \begin{bmatrix} \sum_{i=1}^{4} y_i \frac{\partial N_i}{\partial \eta} & -\sum_{i=1}^{4} y_i \frac{\partial N_i}{\partial \xi} \\ -\sum_{i=1}^{4} x_i \frac{\partial N_i}{\partial \eta} & \sum_{i=1}^{4} x_i \frac{\partial N_i}{\partial \xi} \end{bmatrix} \tag{152}$$

It is now possible to complete the transformation of the shape function derivatives by using this matrix and the derivatives of the shape functions with respect to local coordinates. The second modification that is required to use the master element concept in finite element analysis is to convert the integration variables to local coordinates. The basic formula for a change of integration variables is given as:

$$\iint_{\substack{master \\ element}} f(x,y)dxdy = \iint_{\substack{master \\ element}} f\left(x(\xi,\eta), y(\xi,\eta)\right)|J|d\xi d\eta \tag{153}$$

where the determinant of the Jacobian is used explicitly. It should be noted that this change in integration variables does not pose any extra difficulty as long as the determinant of the Jacobian is a constant. For non-linear coordinate transformations, such as the one used in quadrilateral elements, the Jacobian is not a constant and the above integration can only be done using a numerical integration scheme.

Appendix IV. Derivation of Galerkin Form of Groundwater Flow Equation

The first step of the derivation of the weak form is to approximate the unknown function over the domain using interpolating functions, N_j, of the form:

$$h_g(x,y,t) \approx \hat{h}_g(x,y,t) = \sum_{j=1}^{N} h_j(t) N_j(x,y) \tag{154}$$

where $\hat{h}_g$ is the approximate value of the hydraulic head and N is the total number of nodes in the two dimensional groundwater flow domain. In essence, the temporal and spatial discretization is separated from each other in the approximate solution. The nodal values, $h_j(t)$, becomes only a function of time and the shape function, $N_j(x,y)$, is now only a function of space. It is also important to note that the shape functions are defined only its corresponding node and neighboring elements. They are zero elsewhere. Since the solution is only approximate, it does not satisfy the differential equation exactly and a residual, R, occurs. The Galerkin method states that the weighted average of this residual over the whole domain becomes zero. Furthermore, the weighing functions are taken to be the basis functions. If the approximate solution is substituted in the differential equation, one can write the total residual as:

$$\begin{aligned} R(x,y,t) = & \frac{\partial}{\partial x}\left[\left(\hat{h}_g - z_b\right)K_{xx}\frac{\partial \hat{h}_g}{\partial x} + \left(\hat{h}_g - z_b\right)K_{xy}\frac{\partial \hat{h}_g}{\partial y}\right] \\ & + \frac{\partial}{\partial y}\left[\left(\hat{h}_g - z_b\right)K_{yx}\frac{\partial \hat{h}_g}{\partial x} + \left(\hat{h}_g - z_b\right)K_{yy}\frac{\partial \hat{h}_g}{\partial y}\right] \\ & + \sum_{k=1}^{n_w}\left[Q_{w_k}(x,y,t)\delta(x-x_k)\delta(y-y_k)\right] \\ & + \sum_{m=1}^{n_r}\left[\int_0^1 q_{Lm}(x,y,t)\sqrt{\left(\frac{dg_{xm}}{dt}\right)^2 + \left(\frac{dg_{ym}}{dt}\right)^2}\,\delta\left(x - g_{xm}(t)\right)\delta\left(y - g_{ym}(t)\right)dt\right] \\ & + I - S_y\frac{\partial \hat{h}_g}{\partial t} \end{aligned} \tag{155}$$

The Galerkin finite element method is based on weighing this residual over the whole domain using interpolating functions as the weighing functions:

$$\iint_{\Omega} R(x,y,t) N_i(x,y)\, d\Omega = 0 \tag{156}$$

where i runs from *1* through N. When the expression for the residual is substituted in Equation (156) and the square root expression is written simply as the norm of the gradient of parametric vector equation $\mathbf{g} = g_x\mathbf{i} + g_y\mathbf{j}$, the integral simplifies to:

$$\iint_{\Omega}\left\{\begin{array}{l}\dfrac{\partial}{\partial x}\left[\left(\hat{h}_g - z_b\right)K_{xx}\dfrac{\partial \hat{h}_g}{\partial x} + \left(\hat{h}_g - z_b\right)K_{xy}\dfrac{\partial \hat{h}_g}{\partial y}\right] \\ + \dfrac{\partial}{\partial y}\left[\left(\hat{h}_g - z_b\right)K_{yx}\dfrac{\partial \hat{h}_g}{\partial x} + \left(\hat{h}_g - z_b\right)K_{yy}\dfrac{\partial \hat{h}_g}{\partial y}\right] \\ + \sum_{k=1}^{n_w}\left[Q_{w_k}(x,y,t)\delta(x - x_k)\delta(y - y_k)\right] \\ + \sum_{m=1}^{n_r}\left[\int_0^1 q_{Lm}(x,y,t)|\nabla \mathbf{g}|\delta\left(x - g_{xm}(t)\right)\delta\left(y - g_{ym}(t)\right)dt\right] \\ + I - S_y\dfrac{\partial \hat{h}_g}{\partial t}\end{array}\right\}N_i\,d\Omega = 0 \tag{157}$$

The integration by parts is now applied to the second order derivative terms in the above integral to reduce them to first order and incorporate the natural boundary conditions:

$$\begin{aligned}&\iint_{\Omega}\left\{\frac{\partial}{\partial x}\left[\left(\hat{h}_g - z_b\right)K_{xx}\frac{\partial \hat{h}_g}{\partial x} + \left(\hat{h}_g - z_b\right)K_{xy}\frac{\partial \hat{h}_g}{\partial y}\right]\right\}N_i\,d\Omega = \\ &-\iint_{\Omega}\left(\hat{h}_g - z_b\right)\left[K_{xx}\frac{\partial \hat{h}_g}{\partial x} + K_{xy}\frac{\partial \hat{h}_g}{\partial y}\right]\frac{\partial N_i}{\partial x}\,d\Omega + \int_{\Gamma}\left(\hat{h}_g - z_b\right)\left[K_{xx}\frac{\partial \hat{h}_g}{\partial x} + K_{xy}\frac{\partial \hat{h}_g}{\partial y}\right]N_i n_x\,d\Gamma\end{aligned} \tag{158}$$

$$\begin{aligned}&\iint_{\Omega}\left\{\frac{\partial}{\partial y}\left[\left(\hat{h}_g - z_b\right)K_{yx}\frac{\partial \hat{h}_g}{\partial x} + \left(\hat{h}_g - z_b\right)K_{yy}\frac{\partial \hat{h}_g}{\partial y}\right]\right\}N_i\,d\Omega = \\ &-\iint_{\Omega}\left(\hat{h}_g - z_b\right)\left[K_{yx}\frac{\partial \hat{h}_g}{\partial x} + K_{yy}\frac{\partial \hat{h}_g}{\partial y}\right]\frac{\partial N_i}{\partial y}\,d\Omega + \int_{\Gamma}\left(\hat{h}_g - z_b\right)\left[K_{yx}\frac{\partial \hat{h}_g}{\partial x} + K_{yy}\frac{\partial \hat{h}_g}{\partial y}\right]N_i n_y\,d\Gamma\end{aligned} \tag{159}$$

where n_x and n_y represent the x and y components of unit normal vector. Substituting these expressions and rearranging gives:

$$\int_{\Gamma}\left(\hat{h}_g - z_b\right)\left\{\left[K_{xx}\frac{\partial \hat{h}_g}{\partial x} + K_{xy}\frac{\partial \hat{h}_g}{\partial y}\right]N_i n_x + \left[K_{yx}\frac{\partial \hat{h}_g}{\partial x} + K_{yy}\frac{\partial \hat{h}_g}{\partial y}\right]N_i n_y\right\}d\Gamma$$
$$-\iint_{\Omega}\left(\hat{h}_g - z_b\right)\left\{\left[K_{xx}\frac{\partial \hat{h}_g}{\partial x} + K_{xy}\frac{\partial \hat{h}_g}{\partial y}\right]\frac{\partial N_i}{\partial x} + \left[K_{yx}\frac{\partial \hat{h}_g}{\partial x} + K_{yy}\frac{\partial \hat{h}_g}{\partial y}\right]\frac{\partial N_i}{\partial y}\right\}d\Omega$$
$$+\iint_{\Omega}\left\{\sum_{k=1}^{n_w}\left[Q_{w_k}(x,y,t)\delta(x-x_k)\delta(y-y_k)\right]\right\}N_i d\Omega \tag{160}$$
$$+\iint_{\Omega}\left\{\sum_{m=1}^{n_r}\left[\int_0^1 q_{Lm}(x,y,t)|\nabla \mathbf{g}|\delta\left(x-g_{x_m}(t)\right)\delta\left(y-g_{y_m}(t)\right)dt\right]\right\}N_i d\Omega$$
$$+\iint_{\Omega} IN_i d\Omega - \iint_{\Omega} S_y\frac{\partial \hat{h}_g}{\partial t}N_i d\Omega = 0$$

In the above form, the boundary integral can be split in to three parts, according to the boundary conditions, Γ_1, Γ_2 and Γ_3:

$$\int_{\Gamma}(...)N_i d\Gamma = \int_{\Gamma_1}(...)N_i d\Gamma_1 + \int_{\Gamma_2}(...)N_i d\Gamma_2 + \int_{\Gamma_3}(...)N_i d\Gamma_3 \tag{161}$$

In this format, the first boundary integral represents the essential boundary conditions and the others correspond to the natural boundary conditions. If the assumed solution is required to satisfy the essential boundary conditions, then the weighing functions become zero over the first boundary, Γ_1. Hence, the first integral vanishes. The expressions in the specified flux and head dependent boundary conditions can be substituted in the remaining integrals to obtain the following simplified form for the boundary integrals:

$$\int_{\Gamma}\left(\hat{h}_g - z_b\right)\left\{\left[K_{xx}\frac{\partial \hat{h}_g}{\partial x} + K_{xy}\frac{\partial \hat{h}_g}{\partial y}\right]N_i n_x + \left[K_{yx}\frac{\partial \hat{h}_g}{\partial x} + K_{yy}\frac{\partial \hat{h}_g}{\partial y}\right]N_i n_y\right\}d\Gamma = -\int_{\Gamma_2} q_N N_i d\Gamma_2 - \int_{\Gamma_3} q_C N_i d\Gamma_3 \tag{162}$$

It is also possible to write the head-dependent boundary integral using the flux expression between the river and the aquifer when the hydraulic head is greater than river bottom sediment lower elevation (z_r - m_r):

$$\int_{\Gamma_3} q_C N_i d\Gamma_3 = -\int_{\Gamma_3} K_r w_r \frac{h_r - \hat{h}_g}{m_r}N_i d\Gamma_3 = -\int_{\Gamma_3}\frac{K_r w_r h_r}{m_r}N_i d\Gamma_3 + \int_{\Gamma_3}\frac{K_r w_r}{m_r}\hat{h}_g N_i d\Gamma_3 \tag{163}$$

Otherwise, the flux is no longer head dependent and is treated as a constant flux integral. From this point on, the derivation is based on the case where a head-dependent flux exists and does not collapse to a constant flux. With these modifications, the equation simplifies to:

$$
\begin{aligned}
&-\int_{\Gamma_2} q_N N_i d\Gamma_2 + \int_{\Gamma_3} \frac{K_r w_r h_r}{m_r} N_i d\Gamma_3 - \int_{\Gamma_3} \frac{K_r w_r}{m_r} \hat{h}_g N_i d\Gamma_3 \\
&-\iint_{\Omega} \left(\hat{h}_g - z_b\right) \left[K_{xx} \frac{\partial \hat{h}_g}{\partial x} \frac{\partial N_i}{\partial x} + K_{xy} \frac{\partial \hat{h}_g}{\partial y} \frac{\partial N_i}{\partial x} + K_{yx} \frac{\partial \hat{h}_g}{\partial x} \frac{\partial N_i}{\partial y} + K_{yy} \frac{\partial \hat{h}_g}{\partial y} \frac{\partial N_i}{\partial y} \right] d\Omega \\
&+\iint_{\Omega} \left\{ \sum_{k=1}^{n_w} \left[Q_{w_k}(x,y,t) \delta(x - x_k) \delta(y - y_k) \right] \right\} N_i d\Omega \\
&+\iint_{\Omega} \left\{ \sum_{m=1}^{n_r} \left[\int_0^1 q_{L\,m}(x,y,t) |\nabla \mathbf{g}| \delta\left(x - g_{x\,m}(t)\right) \delta\left(y - g_{y\,m}(t)\right) dt \right] \right\} N_i d\Omega \\
&+\iint_{\Omega} I N_i d\Omega - \iint_{\Omega} S_y \frac{\partial \hat{h}_g}{\partial t} N_i d\Omega = 0
\end{aligned}
\tag{164}
$$

The domain integral of point source term associated with wells can be simplified using the sifting property of the Dirac-δ function. After implementing the property for each delta function, one would obtain:

$$
\iint_{\Omega} \sum_{k=1}^{n_w} \left[Q_{w_k}(x,y,t) \delta(x - x_k) \delta(y - y_k) \right] N_i d\Omega = \sum_{k=1}^{n_w} Q_{w_k}(x_k, y_k) N(x_k, y_k) \tag{165}
$$

Since the interpolating function takes the value of 1 at the particular node, the expression simplifies to:

$$
\iint_{\Omega} \sum_{k=1}^{n_w} \left[Q_{w_k}(x,y,t) \delta(x - x_k) \delta(y - y_k) \right] N_i d\Omega = \sum_{k=1}^{n_w} Q_{w_k}(x_k, y_k) \tag{166}
$$

After substituting this expression and writing the lateral flow according to the first condition of Equation (6), one would obtain:

$$
\begin{aligned}
&-\int_{\Gamma_2} q_N N_i d\Gamma_2 + \int_{\Gamma_3} \frac{K_r w_r h_r}{m_r} N_i d\Gamma_3 - \int_{\Gamma_3} \frac{K_r w_r}{m_r} \hat{h}_g N_i d\Gamma_3 \\
&-\iint_{\Omega} \left(\hat{h}_g - z_b\right) \left[K_{xx} \frac{\partial \hat{h}_g}{\partial x} \frac{\partial N_i}{\partial x} + K_{xy} \frac{\partial \hat{h}_g}{\partial y} \frac{\partial N_i}{\partial x} + K_{yx} \frac{\partial \hat{h}_g}{\partial x} \frac{\partial N_i}{\partial y} + K_{yy} \frac{\partial \hat{h}_g}{\partial y} \frac{\partial N_i}{\partial y} \right] d\Omega \\
&+\iint_{\Omega} \left\{ \sum_{m=1}^{n_r} \left[\int_0^1 \left(-K_r w_r \frac{h_r - \hat{h}_g}{m_r} \right)_m |\nabla \mathbf{g}| \delta\left(x - g_{x\,m}(t)\right) \delta\left(y - g_{y\,m}(t)\right) dt \right] \right\} N_i d\Omega \\
&+\sum_{k=1}^{n_w} Q_{w_k}(x,y,t) + \iint_{\Omega} I N_i d\Omega - \iint_{\Omega} S_y \frac{\partial \hat{h}_g}{\partial t} N_i d\Omega = 0
\end{aligned}
\tag{167}
$$

It is seen that this boundary value problem is non-linear due to the term ($\hat{h}_g$-z_b). Therefore, it is required to use an iterative solution technique and a suitable convergence criterion. In the proposed model, this term is treated as a constant by using an element average value for each iteration step. Hence, it is possible to write this term as:

$$
\left(\hat{h}_g - z_b\right) \approx \left(\left(\hat{h}_g\right)_{avg} - z_b\right) \tag{168}
$$

With this simplification, we obtain the following expression when the approximate solution in (154) is substituted in the weak from:

$$
\begin{aligned}
&-\int_{\Gamma_2} q_N N_i d\Gamma_2 + \int_{\Gamma_3} \frac{K_r w_r h_r}{m_r} N_i d\Gamma_3 - \int_{\Gamma_3} \frac{K_r w_r}{m_r} \left[\sum_{j=1}^{N} \left(\hat{h}_g\right)_j N_j \right] N_i d\Gamma_3 \\
&-\iint_{\Omega} \left(\left(\hat{h}_g\right)_{avg} - z_b\right) \left[\begin{array}{l} K_{xx} \dfrac{\partial}{\partial x} \left[\sum_{j=1}^{N} \left(\hat{h}_g\right)_j N_j \right] \dfrac{\partial N_i}{\partial x} + K_{xy} \dfrac{\partial}{\partial y} \left[\sum_{j=1}^{N} \left(\hat{h}_g\right)_j N_j \right] \dfrac{\partial N_i}{\partial x} \\ + K_{yx} \dfrac{\partial}{\partial x} \left[\sum_{j=1}^{N} \left(\hat{h}_g\right)_j N_j \right] \dfrac{\partial N_i}{\partial y} + K_{yy} \dfrac{\partial}{\partial y} \left[\sum_{j=1}^{N} \left(\hat{h}_g\right)_j N_j \right] \dfrac{\partial N_i}{\partial y} \end{array} \right] d\Omega \\
&+\iint_{\Omega} \left\{ \sum_{m=1}^{n_r} \left[\int_0^1 \left(-\frac{K_r w_r}{m_r} \right)_m \left(h_r - \sum_{j=1}^{N} \left(\hat{h}_g\right)_j N_j \right)_m |\nabla \mathbf{g}| \delta\left(x - g_{x\,m}(t)\right) \delta\left(y - g_{y\,m}(t)\right) dt \right] \right\} N_i d\Omega \\
&+\sum_{k=1}^{n_w} Q_{w_k}(x,y,t) + \iint_{\Omega} I N_i d\Omega - \iint_{\Omega} S_y \frac{\partial}{\partial t} \left[\sum_{j=1}^{N} \left(\hat{h}_g\right)_j N_j \right] N_i d\Omega = 0
\end{aligned}
\tag{169}
$$

Since the nodal values are only a function of time and the shape function is only a function of space, the above expression can be simplified by taking some of the terms out of the derivatives:

$$
\begin{aligned}
&-\int_{\Gamma_2} q_N N_i d\Gamma_2 + \int_{\Gamma_3} \frac{K_r w_r h_r}{m_r} N_i d\Gamma_3 - \int_{\Gamma_3} \frac{K_r w_r}{m_r} \left[\sum_{j=1}^{N} \left(\hat{h}_g\right)_j N_j \right] N_i d\Gamma_3 \\
&-\iint_{\Omega} \left(\left(\hat{h}_g\right)_{avg} - z_b \right) \begin{bmatrix} K_{xx} \sum_{j=1}^{N} \left(\hat{h}_g\right)_j \frac{\partial N_j}{\partial x} \frac{\partial N_i}{\partial x} + K_{xy} \sum_{j=1}^{N} \left(\hat{h}_g\right)_j \frac{\partial N_j}{\partial y} \frac{\partial N_i}{\partial x} \\ + K_{yx} \sum_{j=1}^{N} \left(\hat{h}_g\right)_j \frac{\partial N_j}{\partial x} \frac{\partial N_i}{\partial y} + K_{yy} \sum_{j=1}^{N} \left(\hat{h}_g\right)_j \frac{\partial N_j}{\partial y} \frac{\partial N_i}{\partial y} \end{bmatrix} d\Omega \\
&+\iint_{\Omega} \left\{ \sum_{m=1}^{n_r} \left[\int_0^1 \left(-\frac{K_r w_r}{m_r} \right)_m \left(h_r - \sum_{j=1}^{N} \left(\hat{h}_g\right)_j N_j \right)_m |\nabla \mathbf{g}| \delta\left(x - g_{x\,m}(t)\right) \delta\left(y - g_{y\,m}(t)\right) dt \right] \right\} N_i d\Omega \\
&+\sum_{k=1}^{n_w} Q_{w_k}(x, y, t) + \iint_{\Omega} I N_i d\Omega - \iint_{\Omega} S_y \sum_{j=1}^{N} N_j \frac{\partial \left(\hat{h}_g\right)_j}{\partial t} N_i d\Omega = 0
\end{aligned}
\tag{170}
$$

Simplifying further, we obtain:

$$
\begin{aligned}
&-\int_{\Gamma_2} q_N N_i d\Gamma_2 + \int_{\Gamma_3} \frac{K_r w_r h_r}{m_r} N_i d\Gamma_3 - \int_{\Gamma_3} \left\{ \sum_{j=1}^{N} \frac{K_r w_r}{m_r} \left(\hat{h}_g\right)_j N_j N_i \right\} d\Gamma_3 \\
&-\iint_{\Omega} \left\{ \sum_{j=1}^{N} \left(\hat{h}_g\right)_j \left(\left(\hat{h}_g\right)_{avg} - z_b \right) \begin{bmatrix} K_{xx} \frac{\partial N_j}{\partial x} \frac{\partial N_i}{\partial x} + K_{xy} \frac{\partial N_j}{\partial y} \frac{\partial N_i}{\partial x} \\ + K_{yx} \frac{\partial N_j}{\partial x} \frac{\partial N_i}{\partial y} + K_{yy} \frac{\partial N_j}{\partial y} \frac{\partial N_i}{\partial y} \end{bmatrix} \right\} d\Omega \\
&+\iint_{\Omega} \left\{ \sum_{m=1}^{n_r} \left[\int_0^1 \left(-\frac{K_r w_r}{m_r} \right)_m \left(h_r - \sum_{j=1}^{N} \left(\hat{h}_g\right)_j N_j \right)_m |\nabla \mathbf{g}| \delta\left(x - g_{x\,m}(t)\right) \delta\left(y - g_{y\,m}(t)\right) dt \right] \right\} N_i d\Omega \\
&+\sum_{k=1}^{n_w} Q_{w_k}(x_k, y_k) + \iint_{\Omega} I N_i d\Omega - \iint_{\Omega} \sum_{j=1}^{N} N_j S_y \frac{\partial \left(\hat{h}_g\right)_j}{\partial t} N_i d\Omega = 0
\end{aligned}
\tag{171}
$$

Since N_i is defined such that it is non-zero only over elements adjacent to node i, the integrations may be performed piecewise over each element and subsequently summed.

$$
\begin{aligned}
&-\sum_{e=1}^{n_e}\left[\int_{\Gamma_2^e} q_N N_i d\Gamma_2^e\right]+\sum_{e=1}^{n_e}\left[\int_{\Gamma_3^e}\frac{K_r w_r h_r}{m_r} N_i d\Gamma_3^e\right]-\sum_{e=1}^{n_e}\left[\int_{\Gamma_3^e}\left\{\sum_{j=1}^{N}\frac{K_r w_r}{m_r}\left(\hat{h}_g\right)_j N_j N_i\right\} d\Gamma_3^e\right] \\
&-\sum_{e=1}^{n_e}\left[\iint_{\Omega^e}\left\{\sum_{j=1}^{N}\left(\hat{h}_g\right)_j\left(\left(\hat{h}_g\right)_{avg}-z_b\right)\begin{bmatrix} K_{xx}\dfrac{\partial N_j}{\partial x}\dfrac{\partial N_i}{\partial x}+K_{xy}\dfrac{\partial N_j}{\partial y}\dfrac{\partial N_i}{\partial x} \\ +K_{yx}\dfrac{\partial N_j}{\partial x}\dfrac{\partial N_i}{\partial y}+K_{yy}\dfrac{\partial N_j}{\partial y}\dfrac{\partial N_i}{\partial y}\end{bmatrix}\right\} d\Omega^e\right] \\
&+\sum_{e=1}^{n_e}\left[\iint_{\Omega^e}\sum_{m=1}^{n_r}\left[\int_0^1\left(-\frac{K_r w_r}{m_r}\right)_m\left(h_r-\sum_{j=1}^{N}\left(\hat{h}_g\right)_j N_j\right)_m |\nabla\mathbf{g}|\delta\left(x-g_{x\,m}(t)\right)\delta\left(y-g_{y\,m}(t)\right)dt\right] N_i d\Omega^e\right] \\
&+\sum_{k=1}^{n_w} Q_{w_k}(x_k,y_k)+\sum_{e=1}^{n_e}\left[\iint_{\Omega^e} IN_i d\Omega^e\right]-\sum_{e=1}^{n_e}\left[\iint_{\Omega^e}\sum_{j=1}^{N} N_j S_y\frac{\partial\left(\hat{h}_g\right)_j}{\partial t} N_i d\Omega^e\right]=0
\end{aligned}
\tag{172}
$$

When linear quadrilateral elements are used to discretize the domain, the sides of the element are straight lines between two nodal points. Therefore, the river (i.e., the line source) becomes a combination of several straight line segments. Each of these segments is defined by the two end points such that the parametric equation of each line segment is written as:

$$
\begin{aligned}
x &= g_x(t) = x_A + (x_B - x_A)t \\
y &= g_y(t) = y_A + (y_B - y_A)t
\end{aligned}
\tag{173}
$$

where points $A(x_A,y_A)$ and $B(x_B,y_B)$ define the global coordinates of the end points of a line segment. For a straight line, the gradient of parametric vector equation **g** is evaluated to be the length of the line segment:

$$
|\nabla\mathbf{g}| = \sqrt{\left(\frac{dg_x}{dt}\right)^2+\left(\frac{dg_y}{dt}\right)^2} = \sqrt{(x_B-x_A)^2+(y_B-y_A)^2} = L_{AB} \tag{174}
$$

It is assumed that the lateral flow associated with each line segment is constant along the segment and is not a function of the parameter t. Therefore, both the gradient term and the lateral flow term can be taken out of the integral with respect to *t* such that the line source integral becomes:

$$\sum_{m=1}^{n_r}\left[\sum_{e=1}^{n_e}\iint_{\Omega^e}\left[L_{AB,e,m}\left(-\frac{K_r w_r}{m_r}\right)_{e,m}\left(h_r-\sum_{j=1}^{N}\left(\hat{h}_g\right)_j N_j\right)_{e,m}\left[\int_0^1\delta\left(x-g_{x\,e,m}(t)\right)\delta\left(y-g_{y_{e,m}}(t)\right)dt\right]\right]N_i d\Omega^e\right] \tag{175}$$

The integration with respect to t can now be performed using any one of the Dirac-δ function expressions. After substituting the expressions for g_x and g_y given in Equation (173), the integral becomes:

$$\int_0^1\delta\left(x-x_{A,e,m}+\left(x_{A,e,m}-x_{B,e,m}\right)t\right)\delta\left(y-y_{A,e,m}+\left(y_{A,e,m}-y_{B,e,m}\right)t\right)dt \tag{176}$$

If the x-component is selected to perform the integration, the y-component of the Dirac-δ function can be written as some function $h(t)$ such that the integral becomes:

$$\int_0^1 h(t)\delta\left(x-x_{A,e,m}+\left(x_{A,e,m}-x_{B,e,m}\right)t\right)dt \tag{177}$$

The expression in the Dirac-δ function can now be rearranged to give:

$$\delta\left(x-x_{A,e,m}+\left(x_{A,e,m}-x_{B,e,m}\right)t\right)=\delta\left(\left(x_{A,e,m}-x_{B,e,m}\right)\left[\frac{x-x_{A,e,m}}{x_{A,e,m}-x_{B,e,m}}+t\right]\right) \tag{178}$$

Since the term ($x_{A,e,m}$-$x_{B,e,m}$) is a constant, it can be written as:

$$\delta\left(x-x_{A,e,m}+\left(x_{A,e,m}-x_{B,e,m}\right)t\right)=\frac{1}{\left|x_{A,e,m}-x_{B,e,m}\right|}\delta\left(\left[\frac{x-x_{A,e,m}}{x_{A,e,m}-x_{B,e,m}}+t\right]\right) \tag{179}$$

Rewriting the Dirac-δ function gives:

$$\delta\left(x-x_{A,e,m}+\left(x_{A,e,m}-x_{B,e,m}\right)t\right)=\frac{1}{\left|x_{A,e,m}-x_{B,e,m}\right|}\delta\left(t-\frac{x-x_{A,e,m}}{x_{B,e,m}-x_{A,e,m}}\right) \tag{180}$$

Since the derivative of the Dirac-δ function is the Heaviside step function by using the sifting property (Harris and Stocker, 1998), the integration over t yields:

$$\int_0^1 h(t)\frac{1}{\left|x_{A,e,m}-x_{B,e,m}\right|}\delta\left(t-\frac{x-x_{A,e,m}}{x_{B,e,m}-x_{A,e,m}}\right)dt = \frac{1}{\left|x_{A,e,m}-x_{B,e,m}\right|}h\left(\frac{x-x_{A,e,m}}{x_{B,e,m}-x_{A,e,m}}\right)H\left(t-\frac{x-x_{A,e,m}}{x_{B,e,m}-x_{A,e,m}}\right)\Bigg|_{t=0}^{t=1} \quad (181)$$

where H is the Heaviside step function. Evaluating this function at two points gives:

$$H\left(t-\frac{x-x_{A,e,m}}{x_{B,e,m}-x_{A,e,m}}\right)\Bigg|_{t=0}^{t=1} = H\left(\frac{x_{B,e,m}-x}{x_{B,e,m}-x_{A,e,m}}\right)-H\left(\frac{x-x_{A,e,m}}{x_{B,e,m}-x_{A,e,m}}\right) \quad (182)$$

Along the line where $x_{A,e,m} \le x \le x_{B,e,m}$, the Heaviside function expression above is calculated to be 1 and 0 elsewhere. After evaluating the function *h(t)* and substituting, the integral with respect to parameter *t* simplifies to:

$$\int_0^1 \delta\left(x-x_{A,e,m}+\left(x_{A,e,m}-x_{B,e,m}\right)t\right)\delta\left(y-y_{A,e,m}+\left(y_{A,e,m}-y_{B,e,m}\right)t\right)dt = \frac{1}{\left|x_{A,e,m}-x_{B,e,m}\right|}\delta\left(y-y_{A,e,m}+\left(y_{A,e,m}-y_{B,e,m}\right)\left(\frac{x-x_{A,e,m}}{x_{B,e,m}-x_{A,e,m}}\right)\right) \quad (183)$$

This term can now be substituted back in the general line source term to give:

$$\sum_{m=1}^{n_r}\left[\sum_{e=1}^{n_e}\iint_{\Omega^e}\left[\begin{array}{l} L_{AB,e,m}\left(-\frac{K_r w_r}{m_r}\right)_{e,m}\left(h_r-\sum_{j=1}^{N}\left(\hat{h}_g\right)_j N_j\right)_{e,m} \\ \left[\frac{1}{\left|x_{A,e,m}-x_{B,e,m}\right|}\delta\left(y-y_{A,e,m}+\left(y_{A,e,m}-y_{B,e,m}\right)\left(\frac{x-x_{A,e,m}}{x_{B,e,m}-x_{A,e,m}}\right)\right)\right]\end{array}\right]N_i d\Omega^e\right] \quad (184)$$

Taking the constant terms out of the domain integral gives:

$$\sum_{m=1}^{n_r}\left[\sum_{e=1}^{n_e}\frac{L_{AB,e,m}}{\left|x_{A,e,m}-x_{B,e,m}\right|}\iint_{\Omega^e}\left[\begin{array}{l} \left(-\frac{K_r w_r}{m_r}\right)_{e,m}\left(h_r-\sum_{j=1}^{N}\left(\hat{h}_g\right)_j N_j\right)_{e,m} \\ \left[\delta\left(y-y_{A,e,m}+\left(y_{A,e,m}-y_{B,e,m}\right)\left(\frac{x-x_{A,e,m}}{x_{B,e,m}-x_{A,e,m}}\right)\right)\right]\end{array}\right]N_i d\Omega^e\right] \quad (185)$$

The domain integral can now be isolated from the summations such that:

$$\iint_{\Omega^e}\left[\left(-\frac{K_r w_r}{m_r}\left(h_r-\sum_{j=1}^{N}\left(\hat{h}_g\right)_j N_j\right)\right)_{e,m}\delta\left(y-y_{A,e,m}+\left(y_{A,e,m}-y_{B,e,m}\right)\left(\frac{x-x_{A,e,m}}{x_{B,e,m}-x_{A,e,m}}\right)\right)\right]N_i d\Omega^e \tag{186}$$

The expression in front of the Dirac-δ function is treated as a function and the element integral can be evaluated using the sifting property and the Heaviside function:

$$\begin{aligned}&\iint_{\Omega^e}\left[\left(-\frac{K_r w_r}{m_r}\left(h_r-\sum_{j=1}^{N}\left(\hat{h}_g\right)_j N_j\right)\right)_{e,m}\delta\left(y-y_{A,e,m}+\left(y_{A,e,m}-y_{B,e,m}\right)\left(\frac{x-x_{A,e,m}}{x_{B,e,m}-x_{A,e,m}}\right)\right)\right]N_i d\Omega^e\\ &=\int_{x^e}\left[\begin{array}{l}\left(-\frac{K_r w_r}{m_r}\left(h_r-\sum_{j=1}^{N}\left(\hat{h}_g\right)_j N_j\right)\right)_{e,m}\left(x,y_{A,e,m}+\left(y_{B,e,m}-y_{A,e,m}\right)\left(\frac{x-x_{A,e,m}}{x_{B,e,m}-x_{A,e,m}}\right)\right)\\ N_i\left(x,y_{A,e,m}+\left(y_{B,e,m}-y_{A,e,m}\right)\left(\frac{x-x_{A,e,m}}{x_{B,e,m}-x_{A,e,m}}\right)\right)\end{array}\right]dx^e\end{aligned} \tag{187}$$

In this equation, both the shape function and the expressions in front of them are reduced to a single variable valid along the line segment. Therefore, the integral with respect to x will be performed between the two end points of the line segment. Dropping out the functional parenthesis for simplicity and substituting this expression in the line source term yields:

$$\sum_{m=1}^{n_r}\left[\sum_{e=1}^{n_e}\frac{L_{AB,e,m}}{\left|x_{A,e,m}-x_{B,e,m}\right|}\int_{x^e}\left[\left(-\frac{K_r w_r}{m_r}\left(h_r-\sum_{j=1}^{N}\left(\hat{h}_g\right)_j N_j\right)\right)_{e,m}N_i\right]dx^e\right] \tag{188}$$

It is important to note that the shape functional and the expression in front of the shape function are evaluated along the line segment. The general equation now becomes:

$$
\begin{aligned}
&-\sum_{e=1}^{n_e}\left[\int_{\Gamma_2^e} q_N N_i d\Gamma_2^e\right]+\sum_{e=1}^{n_e}\left[\int_{\Gamma_3^e}\frac{K_r w_r h_r}{m_r}N_i d\Gamma_3^e\right]-\sum_{e=1}^{n_e}\left[\int_{\Gamma_3^e}\left\{\sum_{j=1}^{N}\frac{K_r w_r}{m_r}\left(\hat{h}_g\right)_j N_j N_i\right\}d\Gamma_3^e\right]\\
&-\sum_{e=1}^{n_e}\left[\iint_{\Omega^e}\left\{\sum_{j=1}^{N}\left(\hat{h}_g\right)_j\left(\left(\hat{h}_g\right)_{avg}-z_b\right)\begin{bmatrix}K_{xx}\dfrac{\partial N_j}{\partial x}\dfrac{\partial N_i}{\partial x}+K_{xy}\dfrac{\partial N_j}{\partial y}\dfrac{\partial N_i}{\partial x}\\ +K_{yx}\dfrac{\partial N_j}{\partial x}\dfrac{\partial N_i}{\partial y}+K_{yy}\dfrac{\partial N_j}{\partial y}\dfrac{\partial N_i}{\partial y}\end{bmatrix}\right\}d\Omega^e\right]\\
&+\sum_{m=1}^{n_r}\left[\sum_{e=1}^{n_e}\frac{L_{AB,e,m}}{\left|x_{A,e,m}-x_{B,e,m}\right|}\int_{x^e}\left[\left(-\frac{K_r w_r}{m_r}\left(h_r-\sum_{j=1}^{N}\left(\hat{h}_g\right)_j N_j\right)\right)_{e,m}N_i\right]dx^e\right]\\
&+\sum_{k=1}^{n_w}Q_{w_k}\left(x_k,y_k\right)+\sum_{e=1}^{n_e}\left[\iint_{\Omega^e} IN_i d\Omega^e\right]-\sum_{e=1}^{n_e}\left[\iint_{\Omega^e}\sum_{j=1}^{N}N_j S_y\frac{\partial\left(\hat{h}_g\right)_j}{\partial t}N_i d\Omega^e\right]=0
\end{aligned}
\tag{189}
$$

If the entire equation is multiplied by -1, one would obtain the weak form of the governing equation:

$$
\begin{aligned}
&\sum_{e=1}^{n_e}\left[\int_{\Gamma_2^e} q_N N_i d\Gamma_2^e\right]-\sum_{e=1}^{n_e}\left[\int_{\Gamma_3^e}\frac{K_r w_r h_r}{m_r}N_i d\Gamma_3^e\right]+\sum_{e=1}^{n_e}\left[\int_{\Gamma_3^e}\left\{\sum_{j=1}^{N}\frac{K_r w_r}{m_r}\left(\hat{h}_g\right)_j N_j N_i\right\}d\Gamma_3^e\right]\\
&+\sum_{e=1}^{n_e}\left[\iint_{\Omega^e}\left\{\sum_{j=1}^{N}\left(\hat{h}_g\right)_j\left(\left(\hat{h}_g\right)_{avg}-z_b\right)\begin{bmatrix}K_{xx}\dfrac{\partial N_j}{\partial x}\dfrac{\partial N_i}{\partial x}+K_{xy}\dfrac{\partial N_j}{\partial y}\dfrac{\partial N_i}{\partial x}\\ +K_{yx}\dfrac{\partial N_j}{\partial x}\dfrac{\partial N_i}{\partial y}+K_{yy}\dfrac{\partial N_j}{\partial y}\dfrac{\partial N_i}{\partial y}\end{bmatrix}\right\}d\Omega^e\right]\\
&+\sum_{m=1}^{n_r}\left[\sum_{e=1}^{n_e}\frac{L_{AB,e,m}}{\left|x_{A,e,m}-x_{B,e,m}\right|}\int_{x^e}\left[\left(\frac{K_r w_r}{m_r}\left(h_r-\sum_{j=1}^{N}\left(\hat{h}_g\right)_j N_j\right)\right)_{e,m}N_i\right]dx^e\right]\\
&-\sum_{k=1}^{n_w}Q_{w_k}\left(x_k,y_k\right)-\sum_{e=1}^{n_e}\left[\iint_{\Omega^e} IN_i d\Omega^e\right]+\sum_{e=1}^{n_e}\left[\iint_{\Omega^e}\sum_{j=1}^{N}N_j S_y\frac{\partial\left(\hat{h}_g\right)_j}{\partial t}N_i d\Omega^e\right]=0
\end{aligned}
\tag{190}
$$

Combining terms under the element summation:

$$
\begin{aligned}
&\sum_{e=1}^{n_e}\left[\int_{\Gamma_2^e} q_N N_i d\Gamma_2^e - \int_{\Gamma_3^e} \frac{K_r w_r h_r}{m_r} N_i d\Gamma_3^e + \int_{\Gamma_3^e}\left\{\sum_{j=1}^{N}\frac{K_r w_r}{m_r}\left(\hat{h}_g\right)_j N_j N_i\right\} d\Gamma_3^e\right] \\
&+\sum_{e=1}^{n_e}\left[\begin{array}{l}\iint_{\Omega^e}\left\{\sum_{j=1}^{N}\left(\hat{h}_g\right)_j\left(\left(\hat{h}_g\right)_{avg} - z_b\right)\left[\begin{array}{l}K_{xx}\dfrac{\partial N_j}{\partial x}\dfrac{\partial N_i}{\partial x} + K_{xy}\dfrac{\partial N_j}{\partial y}\dfrac{\partial N_i}{\partial x} \\ + K_{yx}\dfrac{\partial N_j}{\partial x}\dfrac{\partial N_i}{\partial y} + K_{yy}\dfrac{\partial N_j}{\partial y}\dfrac{\partial N_i}{\partial y}\end{array}\right]\right\} d\Omega^e \\ -\iint_{\Omega^e} IN_i d\Omega^e + \iint_{\Omega^e}\sum_{j=1}^{N} N_j S_y \dfrac{\partial\left(\hat{h}_g\right)_j}{\partial t} N_i d\Omega^e\end{array}\right] \\
&+\sum_{m=1}^{n_r}\left[\sum_{e=1}^{n_e}\frac{L_{AB,e,m}}{\left|x_{A,e,m} - x_{B,e,m}\right|}\int_{x^e}\left[\left(\frac{K_r w_r}{m_r}\left(h_r - \sum_{j=1}^{N}\left(\hat{h}_g\right)_j N_j\right)\right)_{e,m} N_i\right] dx^e\right] \\
&-\sum_{k=1}^{n_w} Q_{w_k}\left(x_k, y_k\right) = 0
\end{aligned}
\tag{191}
$$

The element integrals can be written in matrix form:

$$
\mathbf{S^e}\cdot\hat{\mathbf{h}}_\mathbf{g} + \mathbf{M^e}\cdot\frac{d\,\hat{\mathbf{h}}_\mathbf{g}}{dt} = \mathbf{F^e} \tag{192}
$$

where $\hat{\mathbf{h}}_\mathbf{g}$ is the unknown vector and $\mathbf{S^e}$, $\mathbf{M^e}$ and $\mathbf{F^e}$ are element matrices and vectors defined as follows:

$$\mathbf{S^e} = \iint_{\Omega^e} \left\{ \left(\left(\hat{h}_g \right)_{avg} - z_b \right) \begin{bmatrix} K_{xx} \dfrac{\partial N_j}{\partial x} \dfrac{\partial N_i}{\partial x} + K_{xy} \dfrac{\partial N_j}{\partial y} \dfrac{\partial N_i}{\partial x} + \\ K_{yx} \dfrac{\partial N_j}{\partial x} \dfrac{\partial N_i}{\partial y} + K_{yy} \dfrac{\partial N_j}{\partial y} \dfrac{\partial N_i}{\partial y} \end{bmatrix} \right\} d\Omega^e + \int_{\Gamma_3^e} \frac{K_r w_r}{m_r} N_j N_i d\Gamma_3^e$$
$$- \sum_{m=1}^{n_r} \left[\sum_{e=1}^{n_e} \frac{L_{AB,e,m}}{\left| x_{A,e,m} - x_{B,e,m} \right|} \int_{x^e} \left[\left(\frac{K_r w_r}{m_r} \right)_{e,m} N_j N_i \right] dx^e \right]$$

$$\mathbf{F^e} = - \int_{\Gamma_2^e} q_N N_i d\Gamma_2^e + \int_{\Gamma_3^e} \frac{K_r w_r h_r}{m_r} N_i d\Gamma_3^e + \iint_{\Omega^e} I N_i d\Omega^e + \sum_{k=1}^{n_w} Q_{w_k} \left(x_k, y_k \right)$$
$$- \sum_{m=1}^{n_r} \left[\sum_{e=1}^{n_e} \frac{L_{AB,e,m}}{\left| x_{A,e,m} - x_{B,e,m} \right|} \int_{x^e} \left[\left(\frac{K_r w_r}{m_r} h_r \right)_{e,m} N_i \right] dx^e \right]$$

$$\mathbf{M^e} = \iint_{\Omega^e} S_y N_j N_i d\Omega^e \tag{193}$$

Finally, the global assembly of these matrices would yield the following matrix equation:

$$\mathbf{S} \cdot \hat{\mathbf{h}}_\mathbf{g} + \mathbf{M} \cdot \frac{d \hat{\mathbf{h}}_\mathbf{g}}{dt} = \mathbf{F} \tag{194}$$

where **S**, **M** and **F** is generally known as stiffness matrix, mass matrix and load vector, respectively, from the structural mechanics analogy.

Appendix V. Derivation of Element Integrals

The key point in finite element analysis is the derivation of element matrices and vectors. In the proposed model, the element matrices and vectors will be 4X4 and 4X1 systems, respectively, since four-noded linear quadrilateral elements are selected as the element shape. The main advantage of using element matrices and vectors is that the complex integrations can be performed on the element level and then the resultant element matrices could be assembled sequentially to obtain the global system. In the following sections, derivation of element integrals is presented for inner and boundary elements of the analysis domain. It should be noted that each component of the weak form shown in Appendix 4 are analyzed separately in the following discussion.

Derivation of Element Matrices and Vectors within the Domain

For all elements within the domain, a series of two dimensional integrals are evaluated to obtain the members of the 4X4 element matrix. Hence, in what follows, the subscripts *i* and *j* run from 1 to 4.

- $\iint_{\Omega^e} \left(\left(\hat{h}_g \right)_{avg} - z_b \right) K_{xx} \frac{\partial N_j}{\partial x} \frac{\partial N_i}{\partial x} d\Omega^e$

This integral is associated with the flux term in x-direction due to the change in hydraulic head in x-direction. The basic assumption is that the hydraulic conductivity K_{xx} and the average hydraulic head are taken to be constant values over the element. Therefore, both of these terms can be taken out of the integral.

$$\iint_{\Omega^e} \left(\left(\hat{h}_g \right)_{avg} - z_b \right) K_{xx} \frac{\partial N_j}{\partial x} \frac{\partial N_i}{\partial x} d\Omega^e = \left(\left(\hat{h}_g \right)_{avg} - z_b \right) K_{xx} \iint_{\Omega^e} \frac{\partial N_j}{\partial x} \frac{\partial N_i}{\partial x} d\Omega^e \tag{195}$$

Furthermore, the integral is written in local coordinates using the determinant of the Jacobian matrix and the master element concept. At this stage, it is important to transform the partial derivatives with respect to the global coordinates to the partial derivatives with respect to the local coordinates. Using the chain rule of differentiation and the transformation matrix, the partial derivatives of the shape functions are written as:

$$\begin{aligned} \frac{\partial N_i}{\partial x} &= \frac{1}{|J|} \left[\left(\sum_{k=1}^{4} y_k \frac{\partial N_k}{\partial \eta} \right) \frac{\partial N_i}{\partial \xi} - \left(\sum_{k=1}^{4} y_k \frac{\partial N_k}{\partial \xi} \right) \frac{\partial N_i}{\partial \eta} \right] \\ \frac{\partial N_j}{\partial x} &= \frac{1}{|J|} \left[\left(\sum_{k=1}^{4} y_k \frac{\partial N_k}{\partial \eta} \right) \frac{\partial N_j}{\partial \xi} - \left(\sum_{k=1}^{4} y_k \frac{\partial N_k}{\partial \xi} \right) \frac{\partial N_j}{\partial \eta} \right] \end{aligned} \tag{196}$$

In these two equations, all the derivatives are simple partials of the shape functions with respect to local coordinates and can be computed easily. Substituting these two derivatives and writing the integral in terms of local coordinates, one would obtain:

$$\iint_{\Omega^e} \frac{\partial N_j}{\partial x}\frac{\partial N_i}{\partial x} d\Omega^e = \int_{-1}^{1}\int_{-1}^{1} \left\{ \begin{array}{l} \frac{1}{|J|}\left[\left(\sum_{k=1}^{4} y_k \frac{\partial N_k}{\partial \eta}\right)\frac{\partial N_i}{\partial \xi} - \left(\sum_{k=1}^{4} y_k \frac{\partial N_k}{\partial \xi}\right)\frac{\partial N_i}{\partial \eta}\right] * \\ \frac{1}{|J|}\left[\left(\sum_{k=1}^{4} y_k \frac{\partial N_k}{\partial \eta}\right)\frac{\partial N_j}{\partial \xi} - \left(\sum_{k=1}^{4} y_k \frac{\partial N_k}{\partial \xi}\right)\frac{\partial N_j}{\partial \eta}\right] \end{array} \right\} |J| d\xi d\eta \qquad (197)$$

If the whole expression inside the integral is simplified and written as:

$$f(\xi,\eta) = \frac{1}{|J|}\left[\left(\sum_{k=1}^{4} y_k \frac{\partial N_k}{\partial \eta}\right)\frac{\partial N_i}{\partial \xi} - \left(\sum_{k=1}^{4} y_k \frac{\partial N_k}{\partial \xi}\right)\frac{\partial N_i}{\partial \eta}\right] * \left[\left(\sum_{k=1}^{4} y_k \frac{\partial N_k}{\partial \eta}\right)\frac{\partial N_j}{\partial \xi} - \left(\sum_{k=1}^{4} y_k \frac{\partial N_k}{\partial \xi}\right)\frac{\partial N_j}{\partial \eta}\right] \qquad (198)$$

then the integral simplifies to:

$$\iint_{\Omega^e} \frac{\partial N_j}{\partial x}\frac{\partial N_i}{\partial x} d\Omega^e = \int_{-1}^{1}\int_{-1}^{1} f(\xi,\eta) d\xi d\eta \qquad (199)$$

and evaluated using the Gaussian quadrature:

$$\int_{-1}^{1}\int_{-1}^{1} f(\xi,\eta) d\xi d\eta = \sum_{l=1}^{NSP}\sum_{m=1}^{NSP} w_l w_m f(\xi_m, \eta_l) \qquad (200)$$

Finally, the element matrix is written using the above formula and substituting the derivatives of the corresponding shape functions for each node of the element. The final outcome of the integral is a 4X4 element matrix.

- $\iint_{\Omega^e} \left(\left(\hat{h}_g\right)_{avg} - z_b\right) K_{xy} \frac{\partial N_j}{\partial y}\frac{\partial N_i}{\partial x} d\Omega^e$

This integral is associated with the flux term in x-direction due to the change in hydraulic head in y-direction. The basic assumption is that the hydraulic conductivity K_{xy} and the average hydraulic head are taken to be constant values over the element. Therefore, both of these terms can be taken out of the integral.

$$\iint_{\Omega^e}\left(\left(\hat{h}_g\right)_{avg}-z_b\right)K_{xy}\frac{\partial N_j}{\partial y}\frac{\partial N_i}{\partial x}d\Omega^e=\left(\left(\hat{h}_g\right)_{avg}-z_b\right)K_{xy}\iint_{\Omega^e}\frac{\partial N_j}{\partial y}\frac{\partial N_i}{\partial x}d\Omega^e \tag{201}$$

Furthermore, the integral is written in local coordinates using the determinant of the Jacobian matrix and the master element concept. At this stage, it is important to transform the partial derivatives with respect to the global coordinates to the partial derivatives with respect to the local coordinates. Using the chain rule of differentiation and the transformation matrix, the partial derivatives of the shape functions are written as:

$$\begin{aligned}\frac{\partial N_i}{\partial x}&=\frac{1}{|J|}\left[\left(\sum_{k=1}^{4}y_k\frac{\partial N_k}{\partial \eta}\right)\frac{\partial N_i}{\partial \xi}-\left(\sum_{k=1}^{4}y_k\frac{\partial N_k}{\partial \xi}\right)\frac{\partial N_i}{\partial \eta}\right]\\ \frac{\partial N_j}{\partial y}&=\frac{1}{|J|}\left[-\left(\sum_{k=1}^{4}x_k\frac{\partial N_k}{\partial \eta}\right)\frac{\partial N_j}{\partial \xi}+\left(\sum_{k=1}^{4}x_k\frac{\partial N_k}{\partial \xi}\right)\frac{\partial N_j}{\partial \eta}\right]\end{aligned} \tag{202}$$

In these two equations, all the derivatives are simple partials of the shape functions with respect to local coordinates and can be computed easily. Substituting these two derivatives and writing the integral in terms of local coordinates, one would obtain:

$$\iint_{\Omega^e}\frac{\partial N_j}{\partial y}\frac{\partial N_i}{\partial x}d\Omega^e=\int_{-1}^{1}\int_{-1}^{1}\left\{\begin{array}{l}\frac{1}{|J|}\left[-\left(\sum_{k=1}^{4}x_k\frac{\partial N_k}{\partial \eta}\right)\frac{\partial N_j}{\partial \xi}+\left(\sum_{k=1}^{4}x_k\frac{\partial N_k}{\partial \xi}\right)\frac{\partial N_j}{\partial \eta}\right]*\\ \frac{1}{|J|}\left[\left(\sum_{k=1}^{4}y_k\frac{\partial N_k}{\partial \eta}\right)\frac{\partial N_i}{\partial \xi}-\left(\sum_{k=1}^{4}y_k\frac{\partial N_k}{\partial \xi}\right)\frac{\partial N_i}{\partial \eta}\right]\end{array}\right\}|J|d\xi d\eta \tag{203}$$

If the whole expression inside the integral is simplified and written as:

$$\begin{aligned}f(\xi,\eta)=\frac{1}{|J|}&\left[-\left(\sum_{k=1}^{4}x_k\frac{\partial N_k}{\partial \eta}\right)\frac{\partial N_j}{\partial \xi}+\left(\sum_{k=1}^{4}x_k\frac{\partial N_k}{\partial \xi}\right)\frac{\partial N_j}{\partial \eta}\right]*\\ &\left[\left(\sum_{k=1}^{4}y_k\frac{\partial N_k}{\partial \eta}\right)\frac{\partial N_i}{\partial \xi}-\left(\sum_{k=1}^{4}y_k\frac{\partial N_k}{\partial \xi}\right)\frac{\partial N_i}{\partial \eta}\right]\end{aligned} \tag{204}$$

then the integral simplifies to:

$$\iint_{\Omega^e}\frac{\partial N_j}{\partial y}\frac{\partial N_i}{\partial x}d\Omega^e=\int_{-1}^{1}\int_{-1}^{1}f(\xi,\eta)d\xi d\eta \tag{205}$$

and evaluated using the Gaussian quadrature:

$$\int_{-1}^{1}\int_{-1}^{1} f(\xi,\eta)d\xi d\eta = \sum_{l=1}^{NSP}\sum_{m=1}^{NSP} w_l w_m f(\xi_m,\eta_l) \tag{206}$$

Finally, the element matrix is written using the above formula and substituting the derivatives of the corresponding shape functions for each node of the element. The final outcome of the integral is a 4X4 element matrix.

- $\iint_{\Omega^e}\left(\left(\hat{h}_g\right)_{avg} - z_b\right)K_{yx}\frac{\partial N_j}{\partial x}\frac{\partial N_i}{\partial y}d\Omega^e$

This integral is associated with the flux term in y-direction due to the change in hydraulic head in x-direction. The basic assumption is that the hydraulic conductivity K_{yx} and the average hydraulic head are taken to be constant values over the element. Therefore, both of these terms can be taken out of the integral.

$$\iint_{\Omega^e}\left(\left(\hat{h}_g\right)_{avg} - z_b\right)K_{yx}\frac{\partial N_j}{\partial x}\frac{\partial N_i}{\partial y}d\Omega^e = \left(\left(\hat{h}_g\right)_{avg} - z_b\right)K_{yx}\iint_{\Omega^e}\frac{\partial N_j}{\partial x}\frac{\partial N_i}{\partial y}d\Omega^e \tag{207}$$

Furthermore, the integral is written in local coordinates using the determinant of the Jacobian matrix and the master element concept. At this stage, it is important to transform the partial derivatives with respect to the global coordinates to the partial derivatives with respect to the local coordinates. Using the chain rule of differentiation and the transformation matrix, the partial derivatives of the shape functions are written as:

$$\begin{aligned}
\frac{\partial N_j}{\partial x} &= \frac{1}{|J|}\left[\left(\sum_{k=1}^{4} y_k\frac{\partial N_k}{\partial \eta}\right)\frac{\partial N_j}{\partial \xi} - \left(\sum_{k=1}^{4} y_k\frac{\partial N_k}{\partial \xi}\right)\frac{\partial N_j}{\partial \eta}\right] \\
\frac{\partial N_i}{\partial y} &= \frac{1}{|J|}\left[-\left(\sum_{k=1}^{4} x_k\frac{\partial N_k}{\partial \eta}\right)\frac{\partial N_i}{\partial \xi} + \left(\sum_{k=1}^{4} x_k\frac{\partial N_k}{\partial \xi}\right)\frac{\partial N_i}{\partial \eta}\right]
\end{aligned} \tag{208}$$

In these two equations, all the derivatives are simple partials of the shape functions with respect to local coordinates and can be computed easily. Substituting these two derivatives and writing the integral in terms of local coordinates, one would obtain:

$$\iint_{\Omega^e}\frac{\partial N_j}{\partial x}\frac{\partial N_i}{\partial y}d\Omega^e = \int_{-1}^{1}\int_{-1}^{1}\left\{\begin{array}{l}\frac{1}{|J|}\left[\left(\sum_{k=1}^{4} y_k\frac{\partial N_k}{\partial \eta}\right)\frac{\partial N_j}{\partial \xi} - \left(\sum_{k=1}^{4} y_k\frac{\partial N_k}{\partial \xi}\right)\frac{\partial N_j}{\partial \eta}\right] * \\ \frac{1}{|J|}\left[-\left(\sum_{k=1}^{4} x_k\frac{\partial N_k}{\partial \eta}\right)\frac{\partial N_i}{\partial \xi} + \left(\sum_{k=1}^{4} x_k\frac{\partial N_k}{\partial \xi}\right)\frac{\partial N_i}{\partial \eta}\right]\end{array}\right\}|J|d\xi d\eta \tag{209}$$

If the whole expression inside the integral is simplified and written as:

$$f(\xi,\eta)=\frac{1}{|J|}\left[\left(\sum_{k=1}^{4}y_k\frac{\partial N_k}{\partial \eta}\right)\frac{\partial N_j}{\partial \xi}-\left(\sum_{k=1}^{4}y_k\frac{\partial N_k}{\partial \xi}\right)\frac{\partial N_j}{\partial \eta}\right]* \left[-\left(\sum_{k=1}^{4}x_k\frac{\partial N_k}{\partial \eta}\right)\frac{\partial N_i}{\partial \xi}+\left(\sum_{k=1}^{4}x_k\frac{\partial N_k}{\partial \xi}\right)\frac{\partial N_i}{\partial \eta}\right] \tag{210}$$

then the integral simplifies to:

$$\iint_{\Omega^e}\frac{\partial N_j}{\partial x}\frac{\partial N_i}{\partial y}d\Omega^e=\int_{-1}^{1}\int_{-1}^{1}f(\xi,\eta)d\xi d\eta \tag{211}$$

and evaluated using the Gaussian quadrature:

$$\int_{-1}^{1}\int_{-1}^{1}f(\xi,\eta)d\xi d\eta=\sum_{l=1}^{NSP}\sum_{m=1}^{NSP}w_l w_m f(\xi_m,\eta_l) \tag{212}$$

Finally, the element matrix is written using the above formula and substituting the derivatives of the corresponding shape functions for each node of the element. The final outcome of the integral is a 4X4 element matrix.

- $$\iint_{\Omega^e}\left(\left(\hat{h}_g\right)_{avg}-z_b\right)K_{yy}\frac{\partial N_j}{\partial y}\frac{\partial N_i}{\partial y}d\Omega^e$$

This integral is associated with the flux term in y-direction due to the change in hydraulic head in y-direction. The basic assumption is that the hydraulic conductivity K_{yy} and the average hydraulic head are taken to be constant values over the element. Therefore, both of these terms can be taken out of the integral.

$$\iint_{\Omega^e}\left(\left(\hat{h}_g\right)_{avg}-z_b\right)K_{yy}\frac{\partial N_j}{\partial y}\frac{\partial N_i}{\partial y}d\Omega^e=\left(\left(\hat{h}_g\right)_{avg}-z_b\right)K_{yy}\iint_{\Omega^e}\frac{\partial N_j}{\partial y}\frac{\partial N_i}{\partial y}d\Omega^e \tag{213}$$

Furthermore, the integral is written in local coordinates using the determinant of the Jacobian matrix and the master element concept. At this stage, it is important to transform the partial derivatives with respect to the global coordinates to the partial derivatives with respect to the local coordinates. Using the chain rule of differentiation and the transformation matrix, the partial derivatives of the shape functions are written as:

$$\frac{\partial N_j}{\partial y} = \frac{1}{|J|}\left[-\left(\sum_{k=1}^{4} x_k \frac{\partial N_k}{\partial \eta}\right)\frac{\partial N_j}{\partial \xi} + \left(\sum_{k=1}^{4} x_k \frac{\partial N_k}{\partial \xi}\right)\frac{\partial N_j}{\partial \eta}\right]$$
$$\frac{\partial N_i}{\partial y} = \frac{1}{|J|}\left[-\left(\sum_{k=1}^{4} x_k \frac{\partial N_k}{\partial \eta}\right)\frac{\partial N_i}{\partial \xi} + \left(\sum_{k=1}^{4} x_k \frac{\partial N_k}{\partial \xi}\right)\frac{\partial N_i}{\partial \eta}\right] \tag{214}$$

In these two equations, all the derivatives are simple partials of the shape functions with respect to local coordinates and can be computed easily. Substituting these two derivatives and writing the integral in terms of local coordinates, one would obtain:

$$\iint_{\Omega^e} \frac{\partial N_j}{\partial y}\frac{\partial N_i}{\partial y} d\Omega^e = \int_{-1}^{1}\int_{-1}^{1} \left\{ \begin{array}{l} \frac{1}{|J|}\left[-\left(\sum_{k=1}^{4} x_k \frac{\partial N_k}{\partial \eta}\right)\frac{\partial N_j}{\partial \xi} + \left(\sum_{k=1}^{4} x_k \frac{\partial N_k}{\partial \xi}\right)\frac{\partial N_j}{\partial \eta}\right] * \\ \frac{1}{|J|}\left[-\left(\sum_{k=1}^{4} x_k \frac{\partial N_k}{\partial \eta}\right)\frac{\partial N_i}{\partial \xi} + \left(\sum_{k=1}^{4} x_k \frac{\partial N_k}{\partial \xi}\right)\frac{\partial N_i}{\partial \eta}\right] \end{array} \right\} |J| d\xi d\eta \tag{215}$$

If the whole expression inside the integral is simplified and written as:

$$f(\xi,\eta) = \frac{1}{|J|}\left[-\left(\sum_{k=1}^{4} x_k \frac{\partial N_k}{\partial \eta}\right)\frac{\partial N_j}{\partial \xi} + \left(\sum_{k=1}^{4} x_k \frac{\partial N_k}{\partial \xi}\right)\frac{\partial N_j}{\partial \eta}\right] * \left[-\left(\sum_{k=1}^{4} x_k \frac{\partial N_k}{\partial \eta}\right)\frac{\partial N_i}{\partial \xi} + \left(\sum_{k=1}^{4} x_k \frac{\partial N_k}{\partial \xi}\right)\frac{\partial N_i}{\partial \eta}\right] \tag{216}$$

then the integral simplifies to:

$$\iint_{\Omega^e} \frac{\partial N_j}{\partial y}\frac{\partial N_i}{\partial y} d\Omega^e = \int_{-1}^{1}\int_{-1}^{1} f(\xi,\eta) d\xi d\eta \tag{217}$$

and evaluated using the Gaussian quadrature:

$$\int_{-1}^{1}\int_{-1}^{1} f(\xi,\eta) d\xi d\eta = \sum_{l=1}^{NSP}\sum_{m=1}^{NSP} w_l w_m f(\xi_m, \eta_l) \tag{218}$$

Finally, the element matrix is written using the above formula and substituting the derivatives of the corresponding shape functions for each node of the element. The final outcome of the integral is a 4X4 element matrix.

- $\iint_{\Omega^e} S_y N_j N_i d\Omega^e$

This integral is associated with the time rate of change of the hydraulic heads over an element. The basic assumption is that the specific yield is a time independent constant value over an element. Therefore, this term can be taken out of the integral. Furthermore, the integral is written in local coordinates using the determinant of the Jacobian matrix and the master element concept.

$$\iint_{\Omega^e} S_y N_j N_i d\Omega^e = S_y \iint_{\Omega^e} N_j N_i d\Omega^e = S_y \int_{-1}^{1}\int_{-1}^{1} N_j(\xi,\eta) N_i(\xi,\eta) |J| d\xi d\eta \tag{219}$$

If the integral is evaluated using the Gaussian quadrature, one would obtain:

$$\int_{-1}^{1}\int_{-1}^{1} N_j(\xi,\eta) N_i(\xi,\eta) |J| d\xi d\eta = \sum_{l=1}^{NSP}\sum_{m=1}^{NSP} w_l w_m N_j(\xi_m,\eta_l) N_i(\xi_m,\eta_n) |J(\xi_m,\eta_l)| \tag{220}$$

Finally, the element matrix is written using the above formula and substituting the corresponding shape functions for each node of the element. The final outcome of the integral is a 4X4 matrix from each element.

- $\iint_{\Omega^e} I N_i d\Omega^e$

This integral represents the contribution of infiltration over an element. The basic assumption is that infiltration is taken to be a constant value over an element. Therefore, the *I* term can be taken out of the integral. Furthermore, the integral is written in local coordinates using the determinant of the Jacobian matrix and the master element concept.

$$\iint_{\Omega^e} I N_i d\Omega^e = I \iint_{\Omega^e} N_i d\Omega^e = I \int_{-1}^{1}\int_{-1}^{1} N_i(\xi,\eta) |J| d\xi d\eta \tag{221}$$

If the integral is evaluated using the Gaussian quadrature, one would obtain:

$$\int_{-1}^{1}\int_{-1}^{1} N_i(\xi,\eta) |J| d\xi d\eta = \sum_{l=1}^{NSP}\sum_{m=1}^{NSP} w_l w_m N_i(\xi_m,\eta_l) |J(\xi_m,\eta_l)| \tag{222}$$

Finally, the element vector is written using the above formula and substituting the corresponding shape function term for each node of the element. The final outcome of the integral is a 4X1 vector from each element.

- $\sum_{k=1}^{n_w} Q_{w_k}\left(x_{w_k}, y_{w_k}\right)$

This term represents the contribution of discharge/recharge wells in the domain. The basic assumption is that well locations coincide with the nodal points. For each well, the corresponding flow rate is included in the load vector.

- $\sum_{m=1}^{n_r}\left[\sum_{e=1}^{n_e}\frac{L_{AB,e,m}}{\left|x_{A,e,m}-x_{B,e,m}\right|}\int_{x^e}\left[\left(\frac{K_r w_r}{m_r}\right)_{e,m} N_j N_i\right]dx^e\right]$

This integral represents the contribution of head-dependent part of the line source. The basic assumption is that lateral flow is constant along each segment. Therefore, the integral reduces to:

$$\int_{x^e} N_j N_i dx^e = \int_{x_{A,e,m}}^{x_{B,e,m}} N_j N_i dx^e \tag{223}$$

The integration of the shape functions along the line can be done using global coordinates or local coordinates. The result is a 2X2 matrix. Below, the integration is shown for the (1,1) position such that:

$$\int_{x_{A,e,m}}^{x_{B,e,m}} N_j N_i dx^e = \int_{x_{A,e,m}}^{x_{B,e,m}}\left(\frac{x-x_{A,e,m}}{x_{B,e,m}-x_{A,e,m}}\right)\left(\frac{x-x_{A,e,m}}{x_{B,e,m}-x_{A,e,m}}\right)dx^e = \frac{1}{3}\left(x_{B,e,m}-x_{A,e,m}\right) \tag{224}$$

The other positions follow the same idea. When the result of the integration is substituted in the original term, one would obtain:

$$\left(\frac{K_r w_r}{m_r}\right)_{e,m}\frac{L_{AB,e,m}}{3} \tag{225}$$

The coefficient of the length of the line changes for other positions such that it is 1/3 for positions i = j and 1/6 for i ≠ j.

- $$\sum_{m=1}^{n_r}\left[\sum_{e=1}^{n_e}\frac{L_{AB,e,m}}{\left|x_{A,e,m}-x_{B,e,m}\right|}\int_{x^e}\left[\left(\frac{K_r w_r}{m_r}h_r\right)_{e,m}N_i\right]dx^e\right]$$

This integral represents the contribution of constant part of the line source. The basic assumption is that lateral flow is constant along each segment. Therefore, the integral reduces to:

$$\int_{x^e} N_i dx^e = \int_{x_{A,e,m}}^{x_{B,e,m}} N_i dx^e \tag{226}$$

The integration of the shape functions along the line can be done using global coordinates or local coordinates. The result is a 2X1 vector. Below, the integration is shown for the (1,1) position such that:

$$\int_{x_{A,e,m}}^{x_{B,e,m}} N_i dx^e = \int_{x_{A,e,m}}^{x_{B,e,m}}\left(\frac{x-x_{A,e,m}}{x_{B,e,m}-x_{A,e,m}}\right)dx^e = \frac{1}{2}\left(x_{B,e,m}-x_{A,e,m}\right) \tag{227}$$

The other positions follow the same idea. When the result of the integration is substituted in the original term, one would obtain:

$$\left(\frac{K_r w_r}{m_r}h_r\right)_{e,m}\frac{L_{AB,e,m}}{2} \tag{228}$$

The result is the same for the other position (2,1).

Derivation of Element Matrices and Vectors along the Boundaries

Elements involving a boundary where a natural boundary condition (i.e., Neumann or Cauchy type) is specified require the computation of the three boundary integrals shown in Appendix 4. In these integrals, the integration is performed over the global boundary coordinate $d\Gamma^e$ along the boundary of the element that must be written explicitly. Moreover, the integrands of these integrals must be written on the master element using the local coordinate system and must also be specified for a particular side of the element, which in turn requires that the shape functions are expressed for the particular boundary side of the element. As seen in Figure 28, the boundary of the element can be any side of the quadrilateral depending on its position in the analysis domain. In order to write the shape

functions along each side, appropriate values of ξ and η are substituted for the general shape function formulae.

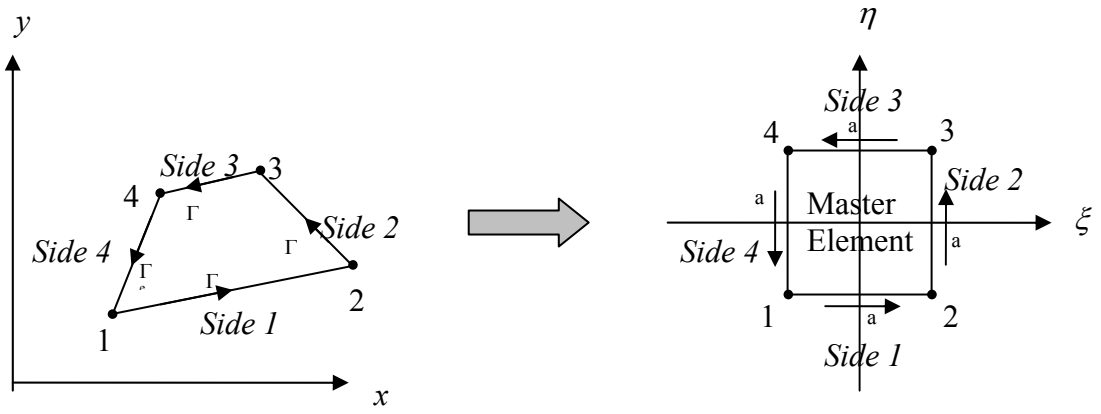

Figure 28. Boundary coordinates on the master and actual element

The global boundary coordinate Γ is mapped to a local boundary coordinate a ($-1 \le a \le 1$) for each side as shown in Figure 28. The local coordinates holds the values ξ = a, η = -1 for side 1, ξ = 1, η = a for side 2, ξ = -a, η = 1 for side 3 and ξ = -1, η = -a for side 4. Using these values, one would obtain the following four shape functions for each side of the element:

$$\begin{aligned} SIDE\ \ 1: &\quad \left[\frac{1-a}{2}, \frac{1+a}{2}, 0, 0\right] \\ SIDE\ \ 2: &\quad \left[0, \frac{1-a}{2}, \frac{1+a}{2}, 0\right] \\ SIDE\ \ 3: &\quad \left[0, 0, \frac{1-a}{2}, \frac{1+a}{2}\right] \\ SIDE\ \ 4: &\quad \left[\frac{1+a}{2}, 0, 0, \frac{1-a}{2}\right] \end{aligned} \tag{229}$$

If the values of -1 and +1 are substituted for a in the above formulae, one would indeed obtain the fact that shape functions are equal to 1 at the node it is written for and 0 at all other nodes of the element. The integral over the element in global coordinates must also be transformed to an integral over the master element in local coordinates. This transformation introduces the determinant of the Jacobian between global boundary and local boundary coordinates.

$$\int_{\Gamma^e} f(B)d\Gamma^e = \int_{-1}^{1} f(a)|J_a|da \tag{230}$$

where J_a is the Jacobian of the boundary and the incremental boundary coordinate in global coordinate system, $d\Gamma$, can be written as follows according to the Figure 29:

$$d\Gamma = \sqrt{(dx)^2 + (dy)^2} \tag{231}$$

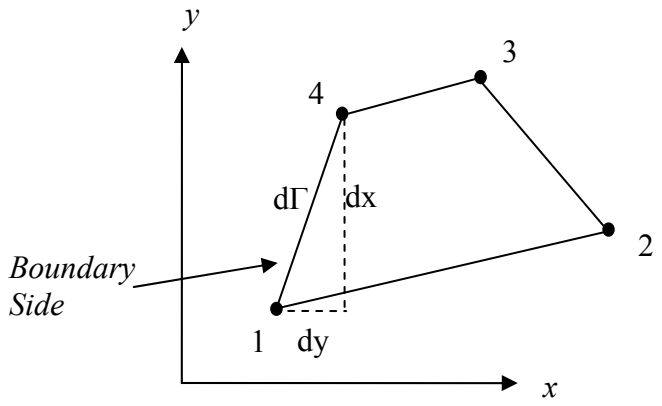

Figure 29. Relationship between boundary coordinate with global coordinates

Dividing both sides of this relationship with differential length, *da*, would give the following relationship between the global and local boundary coordinate:

$$\frac{d\Gamma}{da} = \sqrt{\left(\frac{dx}{da}\right)^2 + \left(\frac{dy}{da}\right)^2} \qquad \Rightarrow \qquad d\Gamma = J_a da \tag{232}$$

Therefore, the Jacobian of the boundary is written as:

$$J_a = \sqrt{\left(\frac{dx}{da}\right)^2 + \left(\frac{dy}{da}\right)^2} \tag{233}$$

where *da* will always take the value of 2 since it is the length of any side on the master element. Using these fundamental concepts, the boundary integrals can be evaluated as follows:

- $\int_{\Gamma_2^e} q_N N_i d\Gamma_2^e$

This integral represents the contribution of Neumann boundary condition. The basic assumption is that flux is taken to be a constant over the boundary side of the element. Therefore, the q_N term can be taken out of the integral.

$$\int_{\Gamma_2^e} q_N N_i d\Gamma_2^e = q_N \int_{\Gamma_2^e} N_i d\Gamma_2^e \tag{234}$$

Furthermore, the integral is written in local coordinates using the determinant of the Jacobian matrix and the master element concept. At this stage, it is important to transform the shape functions with respect to the global coordinates to the shape function with respect to the local coordinates.

$$\int_{\Gamma_2^e} N_i d\Gamma_2^e = \int_{-1}^{1} N_i \left|J_a\right| da \tag{235}$$

and can further be simplified since the Jacobian is simply one half the length of the boundary side.

$$\int_{\Gamma_2^e} N_i d\Gamma_2^e = \frac{L_e}{2} \int_{-1}^{1} N_i da \tag{236}$$

It is important to note that this integral is simple and does not need numerical integration. It can be integrated exactly to obtain 1 regardless of the side and the associated nodes of the element. Therefore, the final outcome of this boundary integral is a 2X1 vector from each boundary element.

- $\int_{\Gamma_3^e} \frac{K_r w_r h_r}{m_r} N_i d\Gamma_3^e$

This integral represents the contribution of head dependent boundary condition due to the constant term. The basic assumption is that the $K_r w_r h_r / m_r$ term is taken to be a constant over the boundary side of the element. Therefore, it can be taken out of the integral to yield:

$$\int_{\Gamma_3^e} \frac{K_r w_r h_r}{m_r} N_i d\Gamma_3^e = \frac{K_r w_r h_r}{m_r} \int_{\Gamma_3^e} N_i d\Gamma_3^e \tag{237}$$

Furthermore, the integral is written in local coordinates using the determinant of the Jacobian matrix and the master element concept. At this stage, it is important to transform the shape functions with respect to the global coordinates to the shape function with respect to the local coordinates.

$$\int_{\Gamma_3^e} N_i d\Gamma_3^e = \int_{-1}^{1} N_i |J_a| da \tag{238}$$

and can further be simplified since the Jacobian is simply one half the length of the boundary side.

$$\int_{\Gamma_3^e} N_i d\Gamma_2^e = \frac{L_e}{2} \int_{-1}^{1} N_i da \tag{239}$$

As before, this integral is simple and does not need numerical integration. It can be integrated exactly to obtain 1 regardless of the side and the associated nodes of the element. Therefore, the final outcome of this boundary integral is a 2X1 vector from each boundary element.

- $\int_{\Gamma_3^e} \frac{K_r w_r}{m_r} N_j N_i d\Gamma_3^e$

This integral represents the contribution of head dependent boundary condition due to the variable groundwater head. It must be noted, however, that this term might also reduce to a constant flux term if the hydraulic head is below the bottom elevation of the river sediments. In such a case, the integral is evaluated as an added contribution to the constant flux integral. Otherwise, this integral is treated as a head-dependent boundary condition. Here, the basic assumption is that the $K_r w_r / m_r$ term is taken to be a constant over the boundary side of the element. Therefore, it can be taken out of the integral to yield:

$$\int_{\Gamma_3^e} \frac{K_r w_r}{m_r} N_j N_i d\Gamma_3^e = \frac{K_r w_r}{m_r} \int_{\Gamma_3^e} N_j N_i d\Gamma_3^e \tag{240}$$

Furthermore, the integral is written in local coordinates using the determinant of the Jacobian matrix and the master element concept. At this stage, it is important to transform the shape functions with respect to the global coordinates to the shape function with respect to the local coordinates.

$$\int_{\Gamma_3^e} N_j N_i d\Gamma_3^e = \int_{-1}^{1} N_j N_i |J_a| da \tag{241}$$

and can further be simplified since the Jacobian is simply one half the length of the boundary side.

$$\int_{\Gamma_3^e} N_j N_i d\Gamma_2^e = \frac{L_e}{2} \int_{-1}^{1} N_j N_i da \tag{242}$$

As before, this integral is simple and does not need numerical integration. It can be integrated exactly using the non-zero shape functions to obtain 2/6 for i = j and 1/6 for i ≠ j, regardless of the side and the associated nodes of the element. Therefore, the final outcome of this boundary integral is a 2X2 vector from each boundary element.

Appendix VI. Numerical Integration of Element Integrals

Element integrals obtained after transformation to local coordinates are generally not evaluated by analytic integration since the integrands are very complicated non-linear functions of local coordinates due to the presence of non-constant Jacobian and its inverse. Particularly for irregular quadrilateral elements, a numerical integration scheme involving various numbers of integration points and corresponding weights is the only viable method of integration. The most common numerical integration scheme is the Gauss quadrature formula. In a one-dimensional setup, this formula takes the following form:

$$\int_{-1}^{1} f(\xi)d\xi = \sum_{j=1}^{NSP} f(a_j)w_j \tag{243}$$

where *NSP* is the total number of sampling locations, $f(a_j)$ is any function evaluated at sampling location a_j and w_j is the corresponding weighing constant. The sampling locations and corresponding weighing coefficients in Gauss quadrature formula are given in Table 1 for the commonly applied schemes of less than six points.

Table 1. Integration Points and Weighing Coefficients in Gauss Quadrature Formula (after Zienkiewicz and Taylor, 1989)

Number of Sampling Point (NSP)	Sampling Location (a)	Weighing Coefficient (w)
1	0.000 000 000 000 000	2.000 000 000 000 000
2	± 0.577 350 269 189 626	1.000 000 000 000 000
3	± 0.774 596 669 241 483 0.000 000 000 000 000	0.555 555 555 555 556 0.888 888 888 888 889
4	± 0.861 136 311 594 953 ± 0.339 981 043 584 856	0.347 854 845 137 454 0.652 145 154 862 546
5	± 0.906 179 845 938 664 ± 0.538 469 310 105 683 0.000 000 000 000 000	0.236 926 885 056 189 0.478 628 670 499 366 0.568 888 888 888 889
6	± 0.932 469 514 203 152 ± 0.661 209 386 466 265 ± 0.238 619 186 083 197	0.171 324 492 379 170 0.360 761 573 048 139 0.467 913 934 572 691

In general, a one-dimensional Gauss quadrature scheme with *NSP* sampling locations integrates any polynomial of *2*NSP-1* order exactly on the interval [-1,1]. Therefore, a two-point scheme will integrate a 3rd order polynomial exactly. Integration in two-dimensions is done based on the same analogy according to the following formula:

$$\int_{-1}^{1}\int_{-1}^{1} f(\xi,\eta)d\xi d\eta = \sum_{i=1}^{NSP}\sum_{j=1}^{NSP} w_i w_j f(\xi_j,\eta_i) \tag{244}$$

The inner integral is evaluated first by taking the η variable constant. The evaluated expression is then integrated with respect to the ξ variable. Generally, the same number of sampling points is used in both integration directions. In the proposed coupled model, the numerical integration is performed by using a three-point Gaussian quadrature formula.